PERFORMANCE-BASED SEISMIC DESIGN OF NONLINEAR STEEL STRUCTURES USING A NOVEL RELIABILITY TECHNIQUE

by

Jose Ramon Gaxiola Camacho

A Dissertation Submitted to the Faculty of the

DEPARTMENT OF CIVIL ENGINEERING AND ENGINEERING MECHANICS

In Partial Fulfillment of the Requirements
For the Degree of

DOCTOR OF PHILOSOPHY

In the Graduate College

THE UNIVERSITY OF ARIZONA

2 0 1 7

THE UNIVERSITY OF ARIZONA
GRADUATE COLLEGE

As members of the Dissertation Committee, we certify that we have read the dissertation prepared by Jose Ramon Gaxiola Camacho, titled Performance-Based Seismic Design of Nonlinear Steel Structures Using a Novel Reliability Technique and recommend that it be accepted as fulfilling the dissertation requirement for the Degree of Doctor of Philosophy.

____ Date: (04/12/2017)
Dr. Achintya Haldar

____ Date: (04/12/2017)
Dr. Tribikram Kundu

____ Date: (04/12/2017)
Dr. Robert B. Fleischman

____ Date: (04/12/2017)
Dr. Hongki Jo

Final approval and acceptance of this dissertation is contingent upon the candidate's submission of the final copies of the dissertation to the Graduate College.

I hereby certify that I have read this dissertation prepared under my direction and recommend that it be accepted as fulfilling the dissertation requirement.

____ Date: (04/12/2017)
Dissertation Director: Dr. Achintya Haldar

STATEMENT BY AUTHOR

SIGNED: _Jose Ramon Gaxiola Camacho_

ACKNOWLEDGEMENTS

I would like to deeply express my sincere gratitude to Prof. Achintya Haldar for his guidance and advice during five years of graduate education at the University of Arizona. Prof. Haldar always helped me to achieve all the necessary objectives to complete my research on time and to write this dissertation. Particularly, I would like to thank Prof. Haldar for his encouragement and support to explore together the research area of performance-based seismic design of steel structures. In addition, I would like to thank Prof. Tribikram Kundu, Prof. Robert B. Fleischman, and Prof. Hongki Jo for being part of my dissertation committee and for their recommendations.

I would like to thank Prof. Alfredo Reyes-Salazar, Prof. Juan I. Velazquez-Dimas†, Prof. Jorge H. Gonzalez-Cuevas, Dr. A. Omar Vazquez H., Dr. Victor Antonio Corrales-Burgueño, and Blanca Lopez. I would like to acknowledge all my dear friends from the Civil Engineering and Engineering Mechanics Department at the University of Arizona: Dr. Abdullah Al-Hussein, Dr. Umar Amjad, Baha, Andisheh, Ulina, Sourav, Anshul, Zhi, Luis, Victor, Karen, Rasoul, Mohammad, Felipe, Hamoon, Francisco, and Moshen.

I am also very grateful with all my friends who I met in Tucson during these five years: Fernanda, Daniela, Lucia, Adrian, Omar, Tania, Ricardo, David S., Vahid, Ali, David P., Jeff, Nadia, Molly, Sam, and Elizabeth. All the support received from my friends from Culiacan Edgar Hernandez, Lino Manjarrez, and Martin Reyes is so much appreciated.

So many thanks are given to my parents and brothers: Eladio Gaxiola, Lorena Camacho, Ivan Gaxiola, and Daniel Gaxiola. In addition, I would like to thank to my family in Mexico for the support and love during my PhD studies.

My gratitude is also expressed to several institutions of Mexico that funded my work: *Consejo Nacional de Ciencia y Tecnología* (CONACYT), *Universidad Autónoma de Sinaloa* (UAS), and *Dirección General de Relaciones Internacionales de la Secretaria de Educación Pública* (DGRI-SEP).

DEDICATIONS

"Sursum Versus, Per Aspera Ad Astra"

Dedicated to:

My Mother: Lorena Camacho

My Father: Eladio Gaxiola

My Brother: Ivan Gaxiola

My Brother: Daniel Gaxiola

My Grandparents: Ramon Camacho†, Emma Lopez, Francisco Gaxiola†, and Juana Camacho

My Country: MEXICO!

TABLE OF CONTENTS

Page

TABLE OF CONTENTS - *Continued*

Page

TABLE OF CONTENTS - ***Continued***

Page

LIST OF FIGURES

Page

LIST OF FIGURES - *Continued*

Page

LIST OF TABLES

Page

LIST OF TABLES - *Continued*

Page

ABSTRACT

A unified performance-based seismic design procedure is proposed and successfully implemented in this dissertation. It provides an alternative to the currently used life safety design requirement. To successfully develop the concept, structures are represented by finite elements and excited by the seismic loading in time domain. To implement the performance-based seismic design concept, a novel reliability evaluation technique is proposed, integrating the finite element method, first order reliability method, the response surface method, and advanced factorial design concept, producing compounding beneficial effects.

Following the 1994 Northridge earthquake, several improved connections in steel buildings were proposed to eliminate brittle fractures in welds. Making connections more flexible was considered to be an attractive option. One type of flexible connection considered in this study is expected to be economical and improve the behavior of steel structures, making them more seismic load-tolerant. However, the partial rigidities of connections need to be considered. To consider rigidities of connections, the 4-parameters Richard model is incorporated in the finite element algorithm.

The accuracy of the procedure is demonstrated by comparing it with respect to Monte Carlo Simulation. The efficiency and robustness are verified with the help of several steel structures of different height. Performances are defined in terms of immediate occupancy, life safety, and collapse prevention. The corresponding risks are evaluated by exciting steel structures designed by experts satisfying all post-Northridge seismic design requirements. In order to incorporate uncertainties in frequency contents of ground motions, the structures are excited by 20 earthquake time histories for each performance level, and the corresponding reliability indexes and probabilities of failure are estimated. Only hundreds

of deterministic finite element analysis are required for extracting the corresponding risk. The superiority in extracting reliability information is demonstrated with respect to Monte Carlo Simulation, which requires thousands or millions of deterministic finite element analysis.

The study confirms the benefits of multiple deterministic analyses suggested in recent design guidelines. The behavior of post-Northridge design is demonstrated to be superior to that of the pre-Northridge design, as expected. The performance criteria suggested by the Federal Emergency Management Agency appear to be reasonable and are expected to satisfy the intent of the performance-based design concept.

Several other advantages of the novel reliability technique are presented in terms of corresponding risk of steel structures excited by simulated ground motions. A broadband platform developed by the Southern California Earthquake Center is used for the artificial generation of time histories. Then, the structural risk is calculated using simulated ground motions.

Designing a structure using multiple time histories, as suggested in recent design guidelines, is a step in the right direction. Based on the results and the observations documented in this dissertation, a robust, efficient, and accurate reliability technique is proposed, and its implementation potential for the performance-based seismic design of steel structures is demonstrated.

CHAPTER 1
INTRODUCTION

1.1 Background and Motivation

The enormous amount of property damages caused by the 1994 Northridge Earthquake prompted the profession to find an alternative to the currently accepted design criteria of life safety. Although life safety was not compromised during this earthquake, structural damage was enormous. Several beam-to-column connections in steel structures fractured in a brittle manner, making buildings unusable following the earthquake, indicating major deficiencies in the current prescriptive design guidelines to protect life. To address the situation, under the sponsorship of the Federal Emergency Management Agency (FEMA), SAC [a joint venture of the Structural Engineers Association of California (SEAOC), Applied Technology Council (ATC), and California Universities for Research in Earthquake Engineering (CUREE)] was funded in the late nineties. The main objective of this joint venture was to develop recommendations for more robust design and construction of steel structures and to propose an alternative design criterion considering adverse economic consequences. The major findings were published in a series of reports (FEMA-350, 2000; FEMA-351, 2000; FEMA-352, 2000; FEMA-353, 2000; FEMA-355C, 2000; FEMA-355F, 2000). One of the major outcomes of the SAC study was the introduction of a new design concept, commonly known as Performance-Based Seismic Design (PBSD). This is an alternative to the life safety design concept currently practiced.

The seismic loading is very unpredictable at a particular site. The dynamic responses of a structure containing many other sources of uncertainties excited by the unpredictable seismic loading are extremely difficult to predict. The SAC study observed that since the sources of uncertainty cannot be eliminated in seismic design, the complete safety of a structure cannot be assured, advocating that the associated risk needs to be managed appropriately. To achieve this objective, SAC proposed to correlate different performance levels with the corresponding risks and let the designers and/or owners decide the level of underlying risk they are willing to accept. FEMA-350 (2000) defined a performance level as, “the intended post-earthquake condition of a building; a well-defined point on a scale measuring how much loss is caused by earthquake damage”. Generally, performance levels range from immediate occupancy (a performance state of very low structural damage) to collapse prevention (a state of extreme structural damage). In order to implement PBSD, it is necessary to estimate the corresponding risk by applying the seismic loading in time domain in the presence of multiple sources of nonlinearity and uncertainty. Unfortunately, SAC did not recommend any specific procedure for the risk estimation.

PBSD involves a set of procedures by which a structural system is designed in a controlled manner. The concept can be implemented by following five sequential steps: (1) select performance objectives, (2) develop preliminary design, (3) assess performance capability, (4) check performance capability with allowable values, in terms of the associated risks, and (5) if risks are not acceptable, revise the initial design. The available literature on PBSD is limited. FEMA-355F (2000) identified six important items that need to be incorporated in the formulation: (1) to account for uncertainty in performance associated with unanticipated events, (2) to set realistic expectations for performance, (3) to assess performance variables in similar buildings located nearby, (4) to develop a reliability framework, (5) to set representative performance levels for various seismic hazards, and (6) to quantify local and global structural behaviors leading to collapse. The above general requirements support the implementation of upgraded PBSD approaches as an alternative to the current practice.

There are several important issues in implementing PBSD. The selection of performance levels and the appropriate mathematical models to represent structural behavior could be very complicated. When seismic loading is applied in time domain, the structure is expected to develop various sources of nonlinearities, and the mathematical model to capture such behavior could be very demanding. To study such nonlinear behavior, the structure is generally represented by Finite Elements (FEs). Considering accuracy and efficiency, representing real, large, and complicated structural systems by FEs could be very difficult. To capture the dynamic application of the seismic loading, several methods with various degrees of sophistication are suggested in the current design guidelines, including pseudo-static to time domain application of the excitation (ASCE/SEI 7-10, 2010). The most sophisticated analysis will require a structure to be represented by nonlinear FEs and the dynamic seismic loading must be applied in time domain. The proper application of seismic loading in time domain depends on the selection of ground motions. Such ground motions represent the seismic hazard of the zone where the structure will be located. Commonly used construction codes recommend the use of seven or more ground motions to perform time domain analysis (ASCE/SEI 7-10, 2010). Ground motions can be recorded (real) or simulated (artificial), depending on the availability of records. Once the ground motions are selected, time domain analysis can be performed following the recommendations reported in building codes (ASCE/SEI 7-10, 2010). However, the main challenge in the profession remains in the explicit quantification of the vulnerability (reliability) of structures to future seismic loading. In addition, commonly used analytical models of nonlinear steel structures are too idealized and may not satisfy the underling physics. For example, joints and support conditions in steel structures are rarely Fully Restrained (FR); they are essentially Partially Restrained (PR) with different rigidities (Chen and Kishi, 1989; Colson, 1991; El-Salti, 1992; Reyes-Salazar and Haldar, 2000; Reyes-Salazar and Haldar, 2001; Reyes-Salazar et al., 2008). Beam-to-column connections introduce nonlinearity in the structural response even when the seismic loading is very small. The structural dynamic properties (stiffness, damping, frequency, mode shape, etc.) are expected to be quite different if the connection conditions are modeled realistically. The major point is that the above desirable performance-enhancing features must be incorporated in developing PBSD.

The most important knowledge gap in implementing PBSD is the risk evaluation, considering all major sources of nonlinearity and uncertainty, and applying the seismic loading in time domain. At present, the risk is generally estimated using the First Order Reliability Method (FORM) (Haldar and Mahadevan, 2000a). It is relatively simple to implement if a required Limit State Function (LSF) can be expressed in an explicit form and the derivatives of it with respect to the design variables are readily available. In the context of PBSD, the performance requirements are suggested by the owner and/or engineers according to the risk they are willing to take and accept the corresponding economic consequences. Thus, a structure is expected to satisfy different performance requirements at specified risk levels. To implement PBSD and satisfy its basic intent, LSFs are expected to be implicit, and the implementation of FORM can be difficult and tedious. As an alternative, Monte Carlo Simulation (MCS) can be used for the risk estimation. However, it is demonstrated that MCS may not be implementable for the time domain seismic analysis of structures. It requires an excessive amount of computational time even after using many sophisticated space reduction techniques (Haldar and Mahadevan, 2000b). A novel reliability technique must be proposed to fill the professional knowledge gap in implementing PBSD. This would help in the improvement of seismic risk evaluation, advancing the current state of the art in seismic-resistant structural design.

1.2 Objectives of the Research

As mentioned in the previous section, a relatively new design concept, commonly referred to as PBSD, has been introduced. It is still being developed. Because of its newness, it is necessary to comprehensively evaluate the concept, identify all the advanced features incorporated in it, document features that may hinder or obstruct its implementation potential, remove some of these deficiencies, and finally showcase its application potential using case studies so that engineers can use it in every day practice. These tasks are undertaken with the help of the following five objectives:

- Objective 1: Address the major weakness of currently available PBSD, develop a new reliability analysis technique for implicit limit state functions considering major sources of nonlinearity and uncertainty and applying the seismic loading in time domain.
- Objective 2: Evaluate the appropriateness of the proposed reliability technique to study three currently used performance levels of immediate occupancy, life safety, and collapse prevention, especially for steel structures.
- Objective 3: Incorporate performance enhancing features like the rigidities of connections in steel frame structures in the proposed reliability evaluation method.

- Objective 4: Generate multiple site-specific ground motions in time domain to address unpredictability in the intensity and the frequency contents of the design earthquake.
- Objective 5: Showcase the implementation potential of the updated PBSD method with a new reliability evaluation technique with the help of several case studies.

1.3 Organization

This dissertation is presented and organized in seven chapters as follows.

Chapter 1 introduces the background of PBSD. The current knowledge gap in the profession about appropriate reliability techniques for implementing PBSD is discussed. Motivation, objectives, and organization of this dissertation are also covered in Chapter 1.

Chapter 2 presents a literature review about PBSD. Numerous subjects are discussed as professional perception, challenges, and limitations in PBSD. The nonlinear deterministic and probabilistic analyses of steel structures are reviewed. Several issues and weaknesses related to the available reliability techniques are discussed. Finally, available literatures on PBSD are reviewed and summarized.

Chapter 3 contains a discussion about the deterministic finite element analysis for steel structures used in this research. The mathematical formulation, solution strategy, and consideration of nonlinearities in the algorithm are explained. The incorporation of beam-to-column connection rigidities in the finite element algorithm is presented. Several partially restrained connection models are discussed. At the end, the 4-Parameter Richard model is selected for the incorporation of connection rigidities in the finite element method. The formulation of the behavior of partially restrained connections is clarified.

Chapter 4 covers a comprehensive discussion about the response surface method. Procedures to represent a response surface by a polynomial are discussed. Several experimental designs concepts for the proper generation of response surfaces are introduced.

Chapter 5 presents a novel reliability technique for implementation of PBSD. It is based on technical discussions made in the previous chapters. An integrated approach by combining several experimental designs concepts, finite element analysis, response surface method, and first order reliability method is presented. Verifications of the novel reliability technique are presented with the help of several steel structures. The corresponding seismic risks of steel structures are calculated using the proposed approach and Monte Carlo Simulation technique. The reliability of three steel structures: 3-, 9-, and 20-story, is estimated using the proposed method. Rigidities in the beam-to-column connections and three performance levels: immediate occupancy, life safety, and collapse prevention, are considered.

Chapter 6 presents an evaluation of seismic risk of steel structures using simulated ground motions.

Chapter 7 summarizes the contributions, findings, conclusions, and recommendations for future studies.

CHAPTER 2
LITERATURE REVIEW

2.1 Introduction

Performance-Based Seismic Design (PBSD) is a relatively new concept to evaluate performance of existing building structures excited by seismic loading. However, this approach is now equally applicable to new buildings, and is a paradigm shift in seismic engineering design, moving away from the prescriptive code approach (Hamburger et al., 2009). This chapter presents a comprehensive literature review of works on PBSD and related areas. The professional perception of PBSD is documented, making some emphasis on building codes, recommendations, and guidelines. The sequence of PBSD and the required performance levels to evaluate a structure are presented. Challenges faced by the profession about PBSD and limitations of reliability approaches to implement it are discussed. A basic review of the state of the art on simulating ground motions for PBSD applications is documented. Research related to nonlinear deterministic and probabilistic seismic analyses of structures is reviewed. At the end of this chapter, the necessity of a unified time-domain reliability technique for implementing PBSD is justified.

2.2 Professional Perception of PBSD

PBSD is an evolving methodology that is becoming popular among professional engineers. However, the main difficulties are to arrive at globally acceptable precise definitions of performance objectives, to quantify performance levels, and to estimate risk applying seismic loading in time domain. The recent drive of the use of PBSD for design as well as assessment of building structures has led to rapid developments to enhance the attractiveness of this analytical approach (Hamburger and Hooper, 2011). The basic idea of PBSD is to design a structure so that it will perform well when subjected to different earthquake ground motions, satisfying various performance levels. In a professional perspective, PBSD has two principal objectives. One is to couple the structural requirements with performance expectations to guarantee that hazards are treated consistently. The other is to assure financial losses associated with the damages to the implied expectations. One of the major challenges of PBSD is the unavailability of required computational tools for the proper performance assessment of structures to evaluate the seismic risk (Ghobarah, 2001).

2.2.1 Building Codes, Recommendations, and Guidelines

Currently, two most important codes for structural design used in the United States are the *Minimum Design Loads for Buildings and Other Structures* (ASCE/SEI 7-10, 2010), and the *International Building Code* (IBC, 2012). However, in PBSD perception, the above building codes are prescriptive in nature and fail to guarantee the real seismic performance of structures (Hamburger and Hooper, 2011). As a result of increasing knowledge about PBSD, several guidelines and recommendations are available in the literature. Some of them are: *An Alternative Procedure for Seismic Analysis and Design of Tall Buildings Located in the Los Angeles Region* (LATBSDC, 2011), *Guidelines for Performance-Based Seismic Design of Tall Buildings* (TBI, 2010), *Seismic Provisions for Structural Steel Buildings* (AISC 341-10, 2010), *Seismic Performance Assessment of Buildings* (FEMA P-58, 2012), *NEHRP Recommended Seismic Provisions: Design Examples* (FEMA P-751, 2012), and *Seismic Evaluation and Retrofit of Existing Buildings* (ASCE/SEI 41-13, 2014).

In the context of PBSD of steel structures, after the 1994 Northridge earthquake, FEMA funded the Applied Technology Council (ATC), the Building Seismic Safety Council (BSSC) and the American Society of Civil Engineers (ASCE) to develop consensus guidelines for seismic rehabilitation of existing buildings. The major findings were published in FEMA-273 (1997). A few years later, since most of the steel structures did not perform well during the 1994 Northridge earthquake, FEMA funded SAC [a joint venture of the Structural Engineers Association of California (SEAOC), Applied Technology Council (ATC), and California Universities for Research in Earthquake Engineering (CUREE)]. SAC joint venture was aimed to the PBSD of steel structures. As a result, a series of reports were published in 2000 (FEMA-350, 2000; FEMA-351, 2000; FEMA-352, 2000; FEMA-353, 2000; FEMA-355C, 2000; FEMA-355F, 2000).

The codes, recommendations, and guidelines document a considerable advancement in PBSD. However, they cannot be completely used to satisfy the major objective of the study proposed here. The available computational tools failed to estimate seismic risk considering major sources of nonlinearities and uncertainties, applying seismic loading in time domain.

2.2.2 Performance Levels

FEMA 350 (2000) recommends three performance levels for PBSD for steel structures: Immediate Occupancy (IO), Life Safety (LS), and Collapse Prevention (CP). They are described in Table 2.1. A great amount of resources and time have been spent in developing PBSD approaches (FEMA-350, 2000; FEMA-351, 2000; FEMA-352, 2000; FEMA-353, 2000; FEMA-355C, 2000; FEMA-355F, 2000). However, there are several challenges that motivate the study presented in this report. This study is expected to advance the state-of-the-art in implementing the PBSD guidelines.

Table 2.1 – Performance levels based on PBSD.

Performance Level	Description
IO	The structure has sustained minimal or no damage to its structural elements and only minor damage to its nonstructural components.
LS	Represents a state of extensive damage to structural and nonstructural components. While the risk to life is low, repairs may be required before re-occupancy can occur.
CP	The building has reached a state of impeding partial or total collapse.

2.2.3 Sequence of PBSD

The main task of PBSD is to design structures that properly achieve different performance levels. PBSD process works in a sequential order as shown in Figure 2.1, generally following five basic steps (ASCE/SEI 41-13, 2014). They are: (1) select performance objectives, (2) develop preliminary design, (3) assess performance capability, (4) check if performance objectives are met, and (5) revise the design if performance objectives are not met.

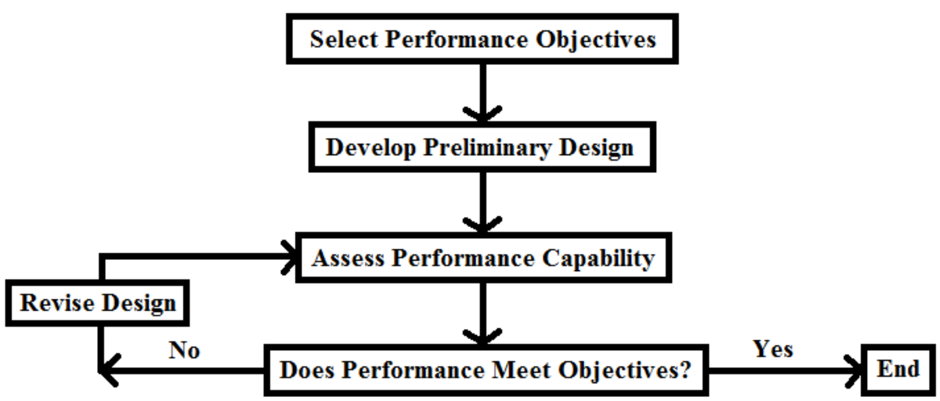

Figure 2.1 – Sequence of PBSD.

However, the major knowledge gap in implementing PBSD is the unavailability of computational tools to assess seismic risk to satisfy different performance objectives.

2.3 Challenges in PBSD

As previously mentioned, one of the essential building blocks of PBSD is the estimation of probability of failure (p_f) corresponding to a specific performance criterion. The engineering profession must have a reliability method to estimate seismic risk, the method must satisfy underlying physics commonly used in deterministic analysis, and information has to be available related to acceptable risk or target reliability levels to select different performance requirements. The basic intent is to propagate uncertainty from the variable or element level to the system level. There are three main challenges in PBSD: (1) limitations in current reliability evaluation methods for seismic loading applied in time domain, (2) reliability estimation satisfying underlying physics, and (3) target reliability levels to satisfy different performance requirements. These issues motivated this study.

2.3.1 Limitations in Current Reliability Methods for Seismic Loading Applied in Time Domain

As discussed earlier, reliability estimation of structures excited by seismic loading is an important step in implementing PBSD. In general, the state of the art in the reliability estimation procedures is advanced. However, they may not be appropriate to implement PBSD. The Pacific Earthquake Engineering Research (PEER) center developed a reliability approach known as Direct Differentiation Method (DDM) (Haukaas and Der Kiureghian, 2005; Der Kiureghian, Haukaas and Fujimura, 2006; Haukaas and Der Kiureghian, 2006). They assumed the structural parameters at their mean values and the loading could not be applied in time domain. They used an out-crossing approach (Koo, Der Kiureghian and Fujimura, 2005) with an importance sampling scheme (Au and Beck, 2001; Ching, Au and Beck, 2005). Au and Beck (1999) used an adaptive importance sampling methodology to compute the multidimensional integrals encountered in reliability analysis. However, multidimensional integrals are implicit for nonlinear steel structures. Other researchers (Hamburger, Foutch and Cornell, 2003; Cornell et al., 2002; Yun et al., 2002) studied the seismic performance of steel structures. They reported the need of reliability-based PBSD approaches. Wen (2001) proposed a reliability-based framework for PBSD. Unfortunately, a physics-based analytical approach for the structural analysis was not used. The above studies represent significant progress in the state of the art of PBSD, but they cannot be used to satisfy the objectives of this study.

Generally, the engineering profession uses FE formulations to study the seismic behavior of structures as realistically as possible. The most rigorous FE analysis requires the proper application of seismic loadings in time domain. The phrase "probability of failure" or "probability of not satisfying a performance requirement" implies that the risk needs to be evaluated just before failure in the presence of several sources of nonlinearities. Generally, three conditions must be taken into consideration for the proper calculation of p_f: (1) structures must be represented by FEs, (2) seismic loading must be applied in time domain, and (3) major sources of nonlinearity and uncertainty must be considered.

The seismic behavior of structures can be represented by LSFs, which are expressed in terms of Random Variables (RVs). The LSFs depend on prescribed performance requirements. As previously discussed, FORM can be used for seismic risk evaluation if LSFs are explicitly available. However, for nonlinear seismic loadings applied in time domain, LSFs are expected to be implicit and a function of time. For implicit LSFs, some of the reliability evaluation methods that can be used are: MCS, Response Surface Method (RSM), and sensitivity-based methods (Haldar and Mahadevan, 2000a). Using the sensitivity-based iterative perturbation method and FORM, the Stochastic Finite Element Method (SFEM) was developed by Haldar and Mahadevan (2000b).

For a simple structure excited by a typical earthquake time history, one deterministic analysis may take about 3 minutes. To estimate p_f of the order of 10^{-5}, one will require about 1 million simulations (Haldar and Mahadevan, 2000a). For the sake of discussion, if an individual without sophisticated knowledge of various advanced space reduction techniques or parallel computing decides to conduct only 10,000 simulations, it will require 30,000 minutes, or about 21 days of uninterrupted running of a computer. Obviously, the basic MCS is not practical. Thus, eliminating basic MCS, RSM can be attempted. However, basic RSM cannot be used because of several deficiencies that will be discussed later in this report. A novel reliability technique integrating FE analysis, FORM, improved RSM, and several advanced factorial schemes may be desirable. This technique will be introduced later in this study.

2.3.2 Reliability Estimation Satisfying Underlying Physics

Appropriate analytical modeling of structures satisfying underlying physics is a step in the right direction in implementing PBSD. Generally, mathematical models used to represent a structural system for reliability analysis may be too idealized and may not satisfy the underlying physics. For example, beam-to-column connections in steel structures are essentially PR with different rigidities (Razavi and Abolmaali, 2014; Brunesi, Nascimbene and Rassati, 2014, 2015; Pecce and Rossi, 2015; Nguyen and Kim, 2015; Tangaramvong et al., 2016; Pirmoz and Liu, 2017). The proper consideration of rigidities introduces another source of nonlinearity. If beam-to-column connections are realistically represented, structural dynamic properties of frequency, damping, stiffness, and mode shape are expected to be different. Inappropriate modeling may considerably overestimate the seismic response of structures (Reyes-Salazar, 2001). In addition, if one member of an indeterminate structure fails, it does not necessarily lead to system failure due to redundancy (Bertero and Bertero, 1999). Current smart designs, such as the capacity design method, intentionally introduce alternative load paths.

Improved modeling and energy dissipation features are also expected to add several sources of uncertainty. Stochastic information must be extracted by explicitly incorporating these desirable features. In deterministic formulation, the structures are generally represented by FEs to capture improved, sophisticated, and beneficial features. The corresponding FE-based reliability analysis procedure is also necessary for wider acceptance. The available literature about reliability methods considering the underlying physics of the problem in modeling connection conditions, is rare. This is a significant knowledge gap in understanding and implementing PBSD.

2.3.3 Target Reliability Levels to Satisfy Different Performance Requirements

Some other items related to PBSD are the target or acceptable reliability performance levels corresponding to specific LSFs. Such acceptable performance levels are required for reliability evaluations. As PBSD matures, adequate performance levels have been proposed in several research reports (FEMA-350, 2000; FEMA-351, 2000; FEMA-352, 2000; FEMA-353, 2000; FEMA-355C, 2000; FEMA-355F, 2000). However, the underlying reliability is still remained unknown. FEMA 350 (2000) proposed performance levels for

IO, LS, and CP in terms of probability of exceedance, earthquake return period, and allowable overall lateral and/or inter-story drifts. They are summarized in Table 2.2. The term *H* in Table 2.2 represents the total and story height of the building to consider the overall and inter-story drift LSFs, respectively.

Table 2.2 – Structural correlation of performance levels.

Performance Level	**Probability of Exceedance**	**Earthquake Return Period**	**Allowable Drift**
IO	50% in 50 years	72-year	0.007*H
LS	10% in 50 years	475-year	0.025*H
CP	2% in 50 years	2475-year	0.050*H

The main point is to relate performance levels with the corresponding reliabilities that the owner and/or engineer are willing to accept, and to evaluate the underlying risk of the structure associated with the performance level under consideration. The information summarized in Table 2.2 is applicable only for serviceability LSFs in terms of overall lateral and inter-story drift, respectively.

2.4 Ground Motion Simulations in PBSD

Commonly used building codes (ASCE/SEI 7-10, 2010; IBC, 2012) recommend the use of at least seven ground motions for structural seismic analysis. Such ground motions can be simulated (artificial) and/or recorded (real) time histories, depending on the availability of records in the zone. However, the question raised by the profession related to the above issue is: what is the associated risk of structures when they are subjected to artificial in comparison with real ground motions? This represents another knowledge gap in implementing PBSD. In order to solve this concern, the engineering profession needs to have two approaches: (1) a technique for the proper generation of artificial ground motions, and (2) a reliability-based framework to compute the seismic risk of structures. The novel reliability technique proposed later in this study represents a good option for the calculation of seismic risk of structures. On the other hand, several techniques have been proposed in the literature for the generation of simulated ground motions (Burks, Zimmerman and Baker, 2015; Cacciola and Deodatis, 2011; Cacciola and Zentner, 2012; Shinozuka and Deodatis, 1988; Suarez and Montejo, 2005; Yamamoto and Baker, 2013; Shields, 2014). Among the above and several other alternatives, the Broadband Platform (BBP) developed by the Southern California Earthquake Center (SCEC) (SCEC, 2016) will be used in this study for the simulation of ground motions, and its implementation in PBSD will be documented later in this dissertation.

2.5 Nonlinear Deterministic Seismic Analysis of Structures

In order to develop an ideal reliability technique to be applied in PBSD, several features related to theoretical as well as implementation issues of nonlinear deterministic seismic analysis of structures must be reviewed. Original research must be developed with an aim to have an efficient nonlinear deterministic seismic analysis method and to couple it with a reliability-based framework for the calculation of seismic risk. The technique must be very robust to fill the knowledge gap in developing PBSD. Due to the large amount of research in this area, only the previous works related to this research are reviewed in this section.

2.5.1 Seismic Analysis of Steel Structures

With the intention of introducing a novel reliability technique for PBSD of steel structures, the deterministic community must be satisfied with an efficient approach for the calculation of nonlinear seismic responses. It is very difficult to avoid nonlinearities in structures when excited by seismic loading because most of them develop nonlinear behavior just before failure. To evaluate the performance of steel structures in the presence of numerous sources of nonlinearity, a FE Method (FEM) is desirable since it is the first step in a conventional deterministic analysis. Several works related to nonlinear seismic analysis can be found in the literature documenting the dynamic response of steel structures (Roeder and Foutch, 1996; Neuenhofer and Filippou, 1997; Luco and Cornell, 2000; Foutch and Yun, 2002; Yun et al., 2002; Kim and Kim, 2009; Razavi and Abolmaali, 2014; Brunesi, Nascimbene and Rassati, 2014, 2015; Pecce and Rossi, 2015; Nguyen and Kim, 2015; Tangaramvong et al., 2016; Pirmoz and Liu, 2017).

As an alternative to the above publications, Haldar and Nee (1989) proposed the assumed stress-based FEM. As will be discussed later in this report, stress-based FEM would be the most appropriate nonlinear analysis technique for this study in terms of efficiency, accuracy, and robustness. The procedure can be used to study the seismic response of steel structures taking into consideration the presence of several sources of nonlinearities (geometric, material, and joint conditions). The stress-based FEM is an advanced methodology; it can properly consider the underlying physics of steel structures excited by earthquake loading. Reyes and Haldar (2001) used the stress-based FEM to study the seismic response of steel structures considering FR, PR, and composite beam-to-column connections. They demonstrated that the proper consideration of connections introduces a great amount of nonlinearity even when seismic loading is small. Mehrabian

(2002) used the stress-based FEM to model pre- and post-Northridge connections. As a result, the seismic behavior of several beam-to-column connections tested in the laboratory was analytically validated.

2.5.2 Implications of the Rigidity of Partially Restrained Connections in Steel Structures

The profession expects that the risk or reliability needs to be estimated considering structural behavior as realistically as practicable. As mentioned earlier, failure of numerous connections in steel frames during recent earthquakes attracted considerable attention from the research community. For the ease of discussion, a typical connection that failed during the 1994 Northridge earthquake is shown in Figure 2.2. It will be referred hereafter as the pre-Northridge connection.

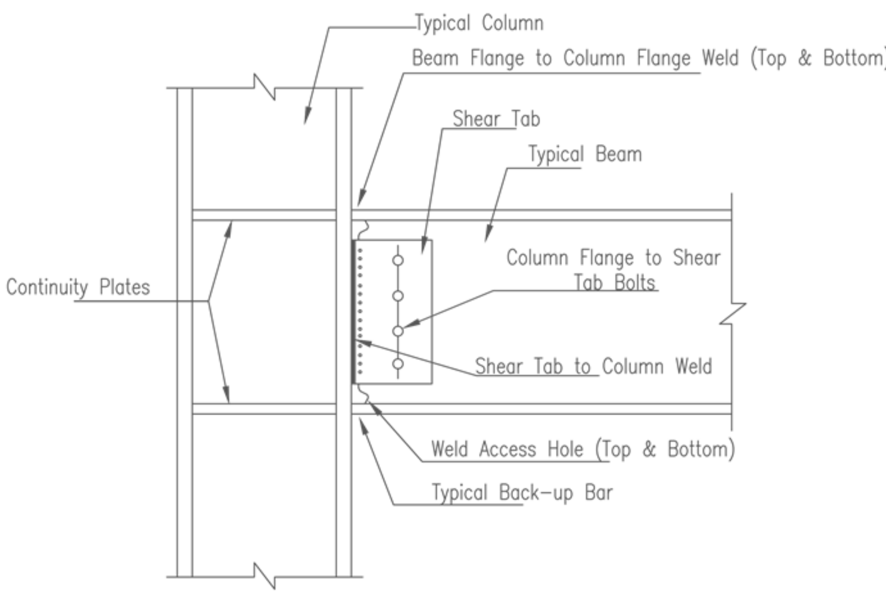

Figure 2.2 – Typical Pre-Northridge connection (Mehrabian, Haldar and Reyes-Salazar, 2005).

After an extensive study, SEAOC recommended not to use the above connection. Subsequently, several improved post-Northridge connections were proposed to provide more ductility and increase energy absorption capacity during seismic excitations. Some of the post-Northridge connections reported in the literature are: cover plated (Engelhardt and Sabol 1998), spliced beam (Popov, Yang and Chang, 1998), sided-plated, bottom haunch, connections with vertical ribs, connections with Reduced Beam Sections (RBS) or Dog-Boned (FEMA-350, 2000), and slotted-web beam-column connections (Richard, Allen and Partridge, 1997). Seismic Structural Design Associates, Inc. (SSDA) proposed a unique proprietary slotted-web (SlottedWeb^{TM}) moment connection by cutting slots in the web of the beam as shown in Figure 2.3. Richard, Allen and Partridge (1997) tested several full-scale beam-column connection models using ATC-24 test protocol and shared the test data with the research team at the University of Arizona led by Dr. Haldar. The test results clearly indicated that the slots in the web of the beam introduced desirable behavior without reducing the initial stiffness of the connection. However, the presence of two slots in the web raised concern to some scholars. To address the related issues in a more comprehensive way, the research team concluded that all connections used in steel frames are essentially PR-type with different rigidities.

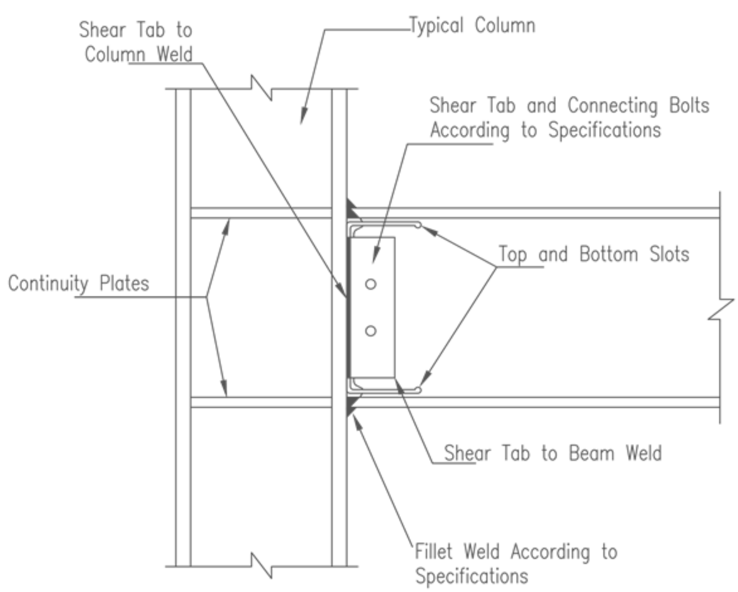

Figure 2.3 – Typical Post-Northridge connection (Mehrabian, Haldar and Reyes-Salazar, 2005).

The behavior of a PR connection is generally represented by moment-relative rotation (M-θ) curves. Several forms of M-θ curves are reported in the literature (Elsati and Richard, 1996). Because of its numerous advantages, Mehrabian, Haldar and Reyes-Salazar (2005) decided to use the four-parameter Richard model (Elsati and Richard, 1996). The Richard model was developed by considering test results and found to be representative of the behavior of PR connections. By using actual test data obtained by SSDA, Mehrabian, Haldar and Reyes-Salazar (2005) estimated the four parameters of the Richard curve. For the same connection without the slots (pre-Northridge connection), four Richard parameters were also estimated. Obviously, the parameters for the pre- and post-Northridge connections are very different. These will be discussed later in this dissertation.

2.6 Nonlinear Probabilistic Seismic Analysis of Structures

Another important topic to be reviewed before PBSD can be completely implemented is the nonlinear probabilistic seismic analysis of structures. Once the deterministic community is satisfied with a methodology for the calculation of seismic responses of steel structures, satisfying underlying physics, a reliability-based approach can be introduced. The research team at the University of Arizona made several efforts in order to propose an efficient, accurate, and robust reliability-based approach for the seismic risk evaluation of structures. Gao and Haldar (1995) evaluated the safety of steel structures considering PR connections; their methodology was based on FORM and SFEM. They developed a reliability-based framework for the safety evaluation of the steel frames. However, they applied the loads statically. Huh and Haldar (2001) proposed a novel reliability method for steel frames. They applied the seismic loading in time domain but they did not consider the contribution of PR connections. Lee and Haldar (2003) expanded the work by considering the interaction of shear wall with steel frames. However, they computed the reliability of the system using only FR connections. The above studies represent a very exceptional advancement in the seismic risk evaluation of steel structures. However, they should be expanded to consider the underlying physics of the problem as well as different PBSD requirements. Currently, there are several reliability methods available in the literature for the probabilistic seismic analysis of structures. However, they must be selected based on efficiency, accuracy, and compounding beneficial effects. A brief review of these methods in terms of reliability analysis concept is developed next.

2.7 Reliability Analysis Concept

The appropriate seismic risk evaluation of structural systems is a fundamental requirement for engineers and researchers. The reliability analysis concept is maturing, and several techniques have been reported in the literature (Haldar and Mahadevan, 2000a, b). Generally, the underlying structural safety is computed by a deterministic approach based on a safety factor concept. However, since the intended conservatism introduced depends largely on the uncertainty in the load and resistance of the structure, and experience of structural engineers, safety factor approaches may fail to convey the actual margin of safety in structural design. Consequently, a more rational approach must be used to explicitly compute the margin of safety considering uncertainties related to load and resistance variables.

Since uncertainties in load and resistance variables should be considered in reliability analysis, it may be difficult to satisfy the basic design requirements during the evaluation. A simple case of reliability analysis is illustrated in Figure 2.4. Two variables are considered, one related to the demand on the system (e.g., loads acting in a structure, S)

and the other related to the capacity of the system (e.g., resistance of the structure, R). Both S and R are random in nature. They are randomly characterized by mean (μ_S and μ_R), standard deviation (σ_S and σ_R), and corresponding probability density functions ($f_S(s)$ and $f_R(r)$). The nominal values of load and resistance are illustrated in Figure 2.4 as S_N and R_N, respectively. They are used in conventional safety factor approach. However, during the risk calculation, it is important to incorporate all the information related to S and R as shown in Figure 2.4.

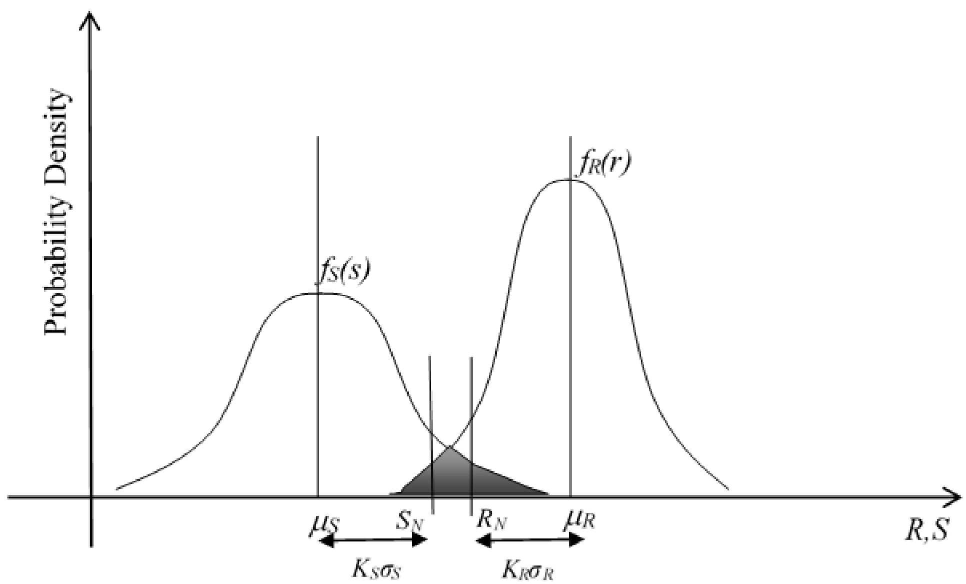

Figure 2.4 – Reliability analysis concept (Haldar and Mahadevan, 2000a).

Reliability or risk information can be extracted by using the relationship between variables, better known as performance function or LSF. The mathematical representation of the relationship or LSF can be expressed as:

$$g(R,S) = R - S \tag{2.1}$$

The expression $g(R, S) < 0$ represents the failure state. It is illustrated in Figure 2.4 as the shaded region or overlapped area (Ω) of the two curves. The failure event $P(R < S)$ or p_f can be calculated by computing the overlapped area between $f_S(s)$ and $f_R(r)$ as:

$$p_f = P(R < S) = P[g(R, S) < 0] = \iint_{\Omega}^{a} f_{R,S}(r, s) dr ds \tag{2.2}$$

where $f_{R,S}(r, s)$ is the joint probability density function of the resistance and load variables.

The integration of Equation (2.2) is performed over the failure region (Ω). Generally, the load (S) and resistance (R) variables are function of other Random Variables (RVs) as gravity, lateral, and accidental loads, and/or sectional and material properties. Hence, Equation (2.1) can be expressed in terms of multiple RVs as:

$$g(\mathbf{X}) = g(x_1, x_2, \dots, x_n) \tag{2.3}$$

where **X** is the vector representing the load and resistance RVs $(x_1, x_2, \dots, x_n)$.

The failure surface or limit state can be defined as $g(\mathbf{X}) = 0$. It represents the boundary between the safe and unsafe region in the design parameter space, i.e., the state of a structure representing the limit between the appropriate and inappropriate performance. The failure surface and the safe and unsafe regions are illustrated in Figure 2.5, corresponding to S and R. The limit state representation or LSF plays an important role in the calculation of reliability or risk. LSFs can be explicit or implicit functions of basic RVs. They can be represented in simple or complicated form.

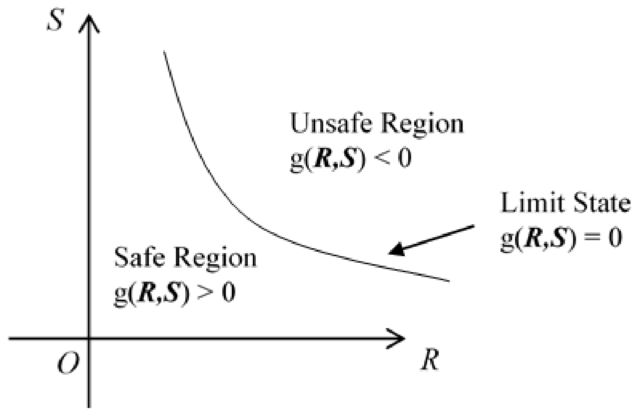

Figure 2.5 – Limit state concept (Haldar and Mahadevan, 2000a).

Combining Equations (2.2) and (2.3), and considering that the failure occurs when $g(\mathbf{X}) < 0$, the p_f can be calculated as:

$$p_f = \int \dots \int_{g(\mathbf{X})<0}^{a} f_X(x_1, x_2, \dots, x_n) dx_1 dx_2 \dots dx_n \tag{2.4}$$

where $f_X(x_1, x_2, \dots, x_n)$ is the joint probability density function for the basic RVs represented by the vector **X**.

The integration indicated in Equation (2.4) is performed over the failure region represented as $g(\mathbf{X}) < 0$. If the RVs are statistically independent, the joint probability density function can be replaced in Equation (2.4) by the product of individual Probability Density Functions (PDFs). In general, the joint probability density function of RVs is almost impossible to obtain. Even if it is available, solving multiple integrals is extremely complicated. Hence, an alternative is to use analytical approximations to solve the integral represented by Equation (2.4).

Analytical approximations are often restricted to use only mean (μ) and coefficient of variation (*COV*) values because the information about RVs may only be sufficient to evaluate μ and *COV* (Cornell, 1969; Ang and Cornell 1974). This prompted to the development of the Mean Value First-Order Second-Moment (MVFOSM) method. However, MVFOSM fails to consider the distributional information of RVs, even when it is available. The above issue was addressed in the literature by introducing the First and Second Order Reliability Methods (FORM/SORM) (Haldar and Mahadevan, 2000a, b). SORM performs the reliability analysis by approximating the nonlinear performance function, including a linear performance function with uncorrelated non-normal variables, to a second-order representation. SORM requires a tremendous computational effort since it requires second-order partial derivatives of the performance function that are extremely difficult to evaluate for structures. SORM is beyond the scope of this work. On the other hand, there is no obvious evidence demonstrating that SORM results are more accurate in comparison with FORM. Hence, FORM may be more practical than SORM for the implementation of PBSD considering conceptual simplicity and efficiency. FORM is used in this research, and is explained next.

2.7.1 First Order Reliability Method

FORM has been widely used for structural reliability problems. It is extensively available in the literature (Rackwitz and Fissler, 1978; Chen and Lind 1982; Mahadevan and Haldar, 2000a, b). A brief review about FORM is presented in this section. FORM represents an important part of the novel reliability technique discussed later in this research.

Before FORM can be reviewed, the MVFOSM method should be introduced. MVFOSM is based on the first order Taylor series approximation of the performance function, considering mean values of RVs (Cornell, 1969). In the previous section, the reliability analysis concept was introduced in terms of resistance (R) and load (S), as illustrated in Figure 2.4. It can be demonstrated that the mean and variance of the performance function or LSF can be expressed as:

$$\mu_g = \mu_R - \mu_S \tag{2.5}$$

and

$$\sigma_g^2 = \sigma_R^2 + \sigma_S^2 \tag{2.6}$$

If R and S are normally distributed and statistically independent RVs, p_f can be calculated as:

$$p_f = p(g < 0) = \Phi\left[-\frac{\mu_R - \mu_S}{\sqrt{\sigma_R^2 + \sigma_S^2}}\right] = \Phi\left[-\frac{\mu_g}{\sigma_g}\right] \tag{2.7}$$

where Φ is the Cumulative Density Function (CDF) of standard normal RVs.

The ratio of mean and variance in Equation (2.7) can be expressed as:

$$\beta = \frac{\mu_g}{\sigma_g} \tag{2.8}$$

where β is the safety or reliability index. As β increases, p_f decreases, and vice versa.

As previously discussed, the problem may be generalized for multiple RVs using Taylor series expansion of the performance function as follows.

$$\begin{aligned} g(\mathbf{X}) = g(\bar{\mathbf{X}}) &+ \sum_{i=1}^{n} \frac{\partial g}{\partial X_i}(X_i - \bar{X}_i) \\ &+ \frac{1}{2}\sum_{i=1}^{n}\sum_{j=1}^{n} \frac{\partial g^2}{\partial X_i \partial X_j}\left(X_i - \bar{\bar{X}}_i\right)\left(X_j - \bar{\bar{X}}_j\right) + \cdots \end{aligned} \tag{2.9}$$

where partial derivatives are evaluated using the mean values of RVs.

Truncating the high order terms up to the linear terms, the first order approximate mean and variance of $g(\mathbf{X})$ are obtained as:

$$\mu_g \approx g(\mu_{X_1}, \mu_{X_2}, \ldots, \mu_{X_n}) \tag{2.10}$$

and

$$\sigma_g^2 \approx \sum_{i=1}^{n} \sum_{j=1}^{n} \frac{\partial g}{\partial X_i} \frac{\partial g}{\partial X_j} Cov(X_i, X_j) \tag{2.11}$$

where $Cov(X_i, X_j)$ is the covariance of X_i and X_j.

If the RVs are statistically independent, the variance can be expressed as:

$$\sigma_g^2 \approx \sum_{i=1}^{n} \left(\frac{\partial g}{\partial X_i}\right)^2 Var(X_i) \tag{2.12}$$

Hence, the safety index β expressed in Equation (2.8), can be calculated using Equations (2.10), (2.11), and (2.12).

The above expressions represent the main intent of MVFOSM. However, this technique may not be accepted as an all-encompassing reliability method due to its failure to incorporate distributional information of RVs, even when it is available. Thus, the value of the safety index computed in Equation (2.8) fails to be constant under different but mechanically formulations of the performance or LSF. The above issue was addressed by Hasofer and Lind (1974). They implemented the Advanced First-Order Second Moment (AFOSM) method using the reduced coordinate system of RVs.

The AFOSM introduced by Hasofer and Lind (1974) is only applicable for normal distributed RVs. AFOSM defines β as the minimum distance from origin to the failure surface in the reduced coordinate system as illustrated in Figure 2.6.

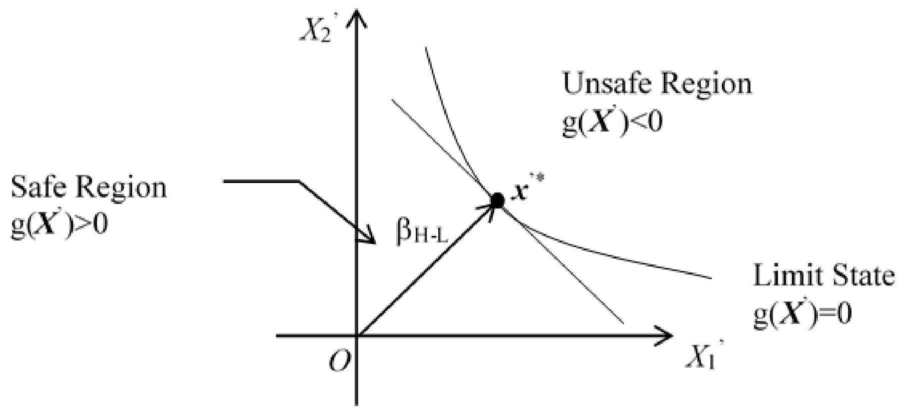

Figure 2.6 – Reliability using reduced coordinate system (Haldar and Mahadevan, 2000a).

In order to implement AFOSM, for a nonlinear performance function or LSF, every RV in the real coordinate system should be transformed to the reduced coordinate system as:

$$X_i' = \frac{X_i - \mu_{X_i}}{\sigma_i}, \quad (i = 1,2,\dots,n) \tag{2.13}$$

where X_i' is a RV with zero mean and unit standard deviation.

Using Equation (2.13), the performance function in the original coordinate system can be transformed to the corresponding reduced coordinate system as:

$$g(\mathbf{X}') = g(X_1', X_2', \dots, X_n') \tag{2.14}$$

Figure 2.6 illustrates the RVs in the reduced coordinate system, the point $\boldsymbol{x}'^*$ represents the worst combination of the stochastic RVs. It is commonly known as the Most Probable Failure Point (MPFP). For nonlinear performance function or LSFs, the calculation of β (minimum distance from the origin to $\boldsymbol{x}'^*$) becomes an optimization problem which is described as follows.

The limit performance function $g(\boldsymbol{X}') = 0$ must be satisfied, while the distance D must be minimized as:

$$D = \sqrt{\boldsymbol{x}'^{t}\boldsymbol{x}'} \tag{2.15}$$

Using the Lagrange Multipliers (Shinozuka, 1983), the minimum distance can be calculated as:

$$\beta = -\frac{\sum_{i=1}^{n} x_i'^{*} \left(\frac{\partial g}{\partial X_i'}\right)^{*}}{\sqrt{\sum_{i=1}^{n} \left(\frac{\partial g}{\partial X_i'}\right)^{2*}}} \tag{2.16}$$

where the derivatives $\left(\frac{\partial g}{\partial X_i'}\right)^{*}$ are evaluated at the design point, $(x_1'^{*}, x_2'^{*}, \ldots, x_n'^{*})$.

The updated design point in reduced coordinate system can be expressed as:

$$x_i'^{*} = -\propto_i \cdot \beta; \;\; (i = 1,2,..,n) \tag{2.17}$$

where

$$\propto_i = \frac{\left(\frac{\partial g}{\partial X_i'}\right)^{*}}{\sqrt{\sum_{i=1}^{n} \left(\frac{\partial g}{\partial X_i'}\right)^{2*}}} \tag{2.18}$$

where $\propto_i$ are the direction cosines along the coordinate axis $\mathbf{X}_\mathrm{i}'$.

In the original space of RVs, the design point (x_i^{*}) can be expressed as:

$$x_i^{*} = \mu_{X_i} - \propto_i \sigma_{x_i} \beta \tag{2.19}$$

The reliability index β calculated using AFOSM can be exactly related to the probability of failure when all RVs are normally distributed. However, this is not common in structural problems. Rackwitz and Fiessler (1978) suggested transformation of non-normal RVs to equivalent normally distributed RVs. The transformation can be done by equating CDF and PDF of the non-normal variables to the equivalent normal variables at the corresponding checking points. Considering statistically independent non-normal random variables, the equivalent mean and standard deviation can be obtained as:

$$\sigma_{X_i}^N = \frac{\emptyset\left\{\Phi^{-1}\left[F_{X_i}(x_i^*)\right]\right\}}{f_{X_i}(x_i^*)} \tag{2.20}$$

and

$$\mu_{X_i}^N = x_i^* - \Phi^{-1}[F_{X_i}(x_i^*)]\, \sigma_{Xi}^N \tag{2.21}$$

where F_{X_i} and f_{X_i} are the non-normal distribution and density functions of X_i, respectively; Φ and $\emptyset$ are the CDF and PDF of standard RVs.

Once the values of $\mu_{X_i}^N$ and $\sigma_{X_i}^N$ have been determined, the reliability index can be calculated for the non-normal random variable cases using Equation (2.16). The Rackwitz-Fissler approach, also commonly known as FORM reliability method, has been extensively used in the literature. This is considered an effective reliability analysis tool because of its simplicity. However, FORM can be difficult to implement when performance functions or LSFs are implicit. This is the case for structures subjected to seismic loading. In order to calculate p_f and β, LSFs must be properly generated. Several methodologies are reported in the literature to approximately generate implicit LSFs. The Response Surface Method (RSM) can be used, as will be discussed next.

2.7.2 Response Surface Method

RSM is an important element of the proposed reliability technique for the implementation of PBSD. It can be defined as a set of statistical techniques to find the best value of the response. The main objective of RSM in this study is to generate the original complex and implicit LSFs using simple and explicit polynomials (Bucher and Bourgund, 1990; Rajashekhar and Ellingwood, 1993; Kim and Na, 1997). The accuracy of RSM depends on the appropriateness of the Response Surface (RS) generated. The essential components of RSM are: the degree of polynomial to be used to represent LSFs, the experimental region and codified values, the selection of sampling or design points, and the determination of the center point. However, as previously discussed, basic RSM may not be efficient for the generation of LSFs required in this study. It has three major deficiencies: (1) it cannot incorporate the distributional information of RVs even when it is widely available, (2) if the responses are not evaluated in the failure region, which is expected to be unknown, the estimated risk may not be acceptable, and (3) the number of experimental sampling points necessary to generate a Response Surface (RS) is an open question; the optimum number must be decided in an objective way. The integration of several procedures to improve the efficiency and accuracy of RSM in generating LSFs is discussed later.

2.7.3 Monte Carlo Simulation

Among many reliability methods, MCS is an easy, robust, and consistent alternative for extracting risk or reliability information (Haldar and Mahadevan, 2000a, b). MCS can be used for both explicit and implicit LSFs. In order to simulate realistic combinations for the values of the input variables, MCS generates a set of pseudo-random numbers with appropriate probability distribution. For every set, the load effect and the failure status corresponding to a LSF are evaluated using a deterministic analysis, for example FEM. Then, the p_f is calculated, performing a large number of simulations, using the following equation:

$$p_f = \frac{N_f}{N} \tag{2.22}$$

where N is the total number of simulation or deterministic FE analysis, and N_f is the number of cases failing to satisfy the performance criteria.

MCS is generally characterized by several essential elements, such as: defining the problem in terms of all RVs, quantifying the probabilistic characteristics of all RVs in terms of their PDFs, generating values of RVs, performing deterministic analysis, evaluating p_f using Equation (2.22), and determining the efficiency and accuracy of the simulation. The main deficiency of MCS is defined in terms of efficiency. If the p_f is very small, say for example 10^{-6}, and the number of RVs is considerable large, the proper calculation of p_f could be extremely complicated and time consuming. Thus, MCS is generally used to evaluate the accuracy of reliability methods as FORM and SORM or to verify new reliability techniques (Lee and Moon, 2014). In this study, MCS is used to verify the accuracy of the novel reliability technique in implementing PBSD.

2.8 The Necessity of a Unified Time-Domain Reliability Technique for Implementing PBSD

As reviewed earlier, several studies have been introduced in the literature about PBSD. Unfortunately, they failed to recommend an acceptable risk evaluation procedure. The knowledge gap in the profession is the risk evaluation of structures considering all major sources of nonlinearity and uncertainty, applying the seismic loading in time domain. In order to study stochastic behavior of dynamic systems, the classical random vibration approach can be used (Lin and Cai, 2004). The basic random vibration concept, its derivatives, and perturbation methods to address uncertainty-related issues including the

First or Second Order Taylor Series, Neumann Expansion, Karhunen-Loeve Orthogonal Expansion, Polynomial Chaos, etc., have numerous deficiencies that limit their application potential. Most of them do not satisfy the physics-based representation of large nonlinear systems, are developed for relatively small numbers of dynamic degrees of freedom, ignore the distribution information of the system parameters, and are valid only for small amounts of randomness even when it can be significantly amplified at the system level. Some of the recently proposed novel features to improve dynamic behavior, reviewed earlier, also cannot be incorporated. The uncertainty in the dynamic loading is usually represented in the form of power spectral density functions; these are essentially applicable for linear systems, and the dynamic loading cannot be applied in time domain. The development of the random vibration concept was an important research topic during the latter half of the twentieth century and presented some deficiencies in explicitly considering major sources of nonlinearity and uncertainty for large systems (Kanegaonkar, Haldar and Ramesh, 1986). To address the above issue, several uncertainty quantification methods for large-scale computational models were proposed, including Reduced Order Models (ROMs), Surrogate Models, Bayesian Methods, Stochastic Dimension Reduction Techniques, Efficient Monte Carlo Methods (e.g. importance sampling), etc. Some of them are problem-specific and will not satisfy the objectives of the proposed study. In order to fill the knowledge gap, a very robust reliability-based technique is proposed in this study by implementing PBSD (Gaxiola-Camacho, Haldar and Reyes-Salazar, 2015; Gaxiola-Camacho et al., 2017a, b, c; Villegas-Mercado et al., 2017). One of the main features of the approach is that seismic loading will be applied in time domain incorporating major sources of nonlinearity and uncertainty. This technique will compute seismic risk in terms of β and p_f based on reliability theory.

2.9 Summary and Concluding Remarks

An extensive literature review related to PBSD was presented in this chapter. Currently available reliability approaches to implement PBSD were reviewed. Previous studies about PBSD document the necessity of reliability techniques for the proper calculation of structural risk. Based on the review, the main knowledge gap in the profession is the calculation of risk considering major sources of uncertainty and nonlinearity applying seismic loading in time domain. At the end of this chapter it was properly justified the necessity of a unified time-domain reliability technique for implementing PBSD. This represents the main objective of this study.

CHAPTER 3
DETERMINISTIC FINITE ELEMENT METHOD FOR STEEL STRUCTURES

3.1 Introduction

Before the introduction of a reliability-based framework, the deterministic community must be satisfied with an efficient, accurate, and robust FEM. Among structural engineers, the use of displacement-based FEM is common. However, in this procedure, numerous elements are required to properly model the structure, and the calculation of the tangent stiffness matrix must be done many times during the analysis, using numerical integrations. Displacement-based FEM represents a considerable advancement in FE representation of structures. However, it cannot be used to achieve the objective of this research. As an alternative, the assumed stress-based FEM is used in this study. A comprehensive explanation of the theoretical foundation of the algorithm is beyond the scope of this dissertation, and only the essential features that directly pertain to this research are briefly discussed in this chapter. A complete formulation of the assumed stress-based FEM can be found in the literature (Haldar and Nee, 1989; Zhou, 1992; Gao, 1994; Reyes-Salazar, 1997; Huh, 1999; Lee, 2000; Mehrabian, 2002).

3.2 Assumed Stress-Based Finite Element Method

Because of its numerous attractive features to study nonlinear behavior of steel frames, the assumed stress-based FEM is used in this study. The research team led by Dr. Haldar at the University of Arizona has developed a comprehensive computer program using stress-based FEM (Haldar and Nee, 1989; Zhou, 1992; Gao, 1994; Reyes-Salazar, 1997; Huh, 1999; Lee, 2000; Mehrabian, 2002). It requires few elements to describe a large deformation configuration without compromising accuracy, and the tangent stiffness matrix can be obtained directly without any integration. In addition, information on PR connections can be incorporated in the FEM algorithm without losing its basic simplicity. Stress-based FEM has been extensively verified (Haldar and Nee, 1989; Zhou, 1992; Gao, 1994; Gao and Haldar, 1995; Reyes-Salazar, 1997; Huh, 1999; Reyes-Salazar and Haldar, 2000; Lee, 2000; Reyes-Salazar and Haldar, 2001; Huh and Haldar, 2001; Mehrabian, 2002; Lee and Haldar, 2003; Mehrabian, Haldar and Reyes-Salazar, 2005; Mehrabian, Ali and Haldar, 2009). Basically, the assumed stress-based FEM is used in this study to calculate deterministic nonlinear responses of steel frames in the presence of FR and PR connections, when excited by the seismic loading applied in time domain. Major sources of nonlinearity considered in the formulation are large deformations, material properties, and connection conditions. Both *P-δ* and *P-Δ* effects are considered for large deformation. Material nonlinearity arises as a result of the constitutive relationship of the material. Considering the usual practice in the profession, the numerical complexity of the problem under consideration, and structures made with steel emphasized in this research, the material nonlinearity is considered to be elastic-perfectly plastic (Hinton and Owen, 1986). Nonlinearity caused by the PR connection condition is also incorporated. In order to clarify the concept, the dynamic governing equations required for the structural analysis of frames and the solution strategy are briefly presented next.

3.3 Dynamic Governing Equations and Solution Strategy

For large structural systems, the nonlinear dynamic governing equation is expressed as:

$$\mathbf{M}\ddot{\mathbf{D}}_{t+\Delta t}^{(n)} + \mathbf{C}_t\dot{\mathbf{D}}_{t+\Delta t}^{(n)} + \mathbf{K}_t^{(n)}\Delta\mathbf{D}_{t+\Delta t}^{(n)} = \mathbf{F}_{t+\Delta t}^{(n)} - \mathbf{R}_{t+\Delta t}^{(n-1)} - \mathbf{M}\ddot{\mathbf{D}}_{g,(t+\Delta t)}^{(n)} \tag{3.1}$$

where $\mathbf{M}$, $\mathbf{C}_t$, and $\mathbf{K}_t^{(n)}$represent the mass, damping, and global stiffness matrix of the n^{th} iteration at time t, respectively; the vectors $\ddot{\mathbf{D}}_{t+\Delta t}^{(n)}$, $\dot{\mathbf{D}}_{t+\Delta t}^{(n)}$, $\Delta\mathbf{D}_{t+\Delta t}^{(n)}$, and $\ddot{\mathbf{D}}_{g,(t+\Delta t)}^{(n)}$ are the acceleration, velocity, incremental displacement, and ground acceleration of the n^{th} iteration at time $t+\Delta t$, respectively; $\mathbf{F}_{t+\Delta t}^{(n)}$ is the external load vector of the n^{th} iteration at time $t+\Delta t$; and $\mathbf{R}_{t+\Delta t}^{(n-1)}$ is the internal force vector of the $(n\text{-}1)^{th}$ iteration at time $t+\Delta t$.

In order to calculate every matrix and vector contained in Equation (3.1), the following procedure is introduced. First, the mass matrix can be represented as lumped or consistent. Second, for every beam-column element, the tangent stiffness matrix and the internal force vector can be expressed explicitly at a given time t and n^{th} iteration, depending on the consideration of material nonlinearity. These calculations are not provided in this study; they are extensively reported in the literature (Kondoh and Atluri, 1987; Shi and Atluri, 1988; Haldar and Nee, 1989). Finally, the damping matrix is considered to be viscous in Equation (3.1).

Since the mass and stiffness matrixes are readily available from the FE formulation, the Rayleigh-type damping is used in this study. Thus, damping matrix can be expressed as (Leger and Dussault, 1992):

$$\mathbf{C}_t = \alpha\mathbf{M} + \gamma\mathbf{K}^t \tag{3.2}$$

where α and γ are proportional constants that can be estimated from the first two natural frequencies of the structure under consideration (Clough and Penzien, 1993).

The step-by-step direct integration numerical analysis procedure, using the Newmark method, is utilized to solve Equation (3.1). The solution strategy is introduced as follows. At every time step Δt, the displacement and velocity vectors can be expressed as (Bathe, 1982):

$$\mathbf{D}_{t+\Delta t}^{(n)} = \mathbf{D}_t + \dot{\mathbf{D}}_t \Delta t + \left[\left(\frac{1}{2} - \beta_N\right)\ddot{\mathbf{D}}_t + \beta_N \ddot{\mathbf{D}}_{t+\Delta t}^{(n)}\right]\Delta t^2 \tag{3.3}$$

and

$$\dot{\mathbf{D}}_{t+\Delta t}^{(n)} = \dot{\mathbf{D}}_t + \left[(1-\eta)\ddot{\mathbf{D}}_t + \eta \ddot{\mathbf{D}}_{t+\Delta t}^{(n)}\right]\Delta t \tag{3.4}$$

where β_N and η are parameters required in the Newmark method to obtain integration stability and accuracy. In this research, $\beta_N = 1/4$ and $\eta = 1/2$ are assumed. For these values at every Δt interval, the acceleration vector is constant and the procedure is expected to be stable.

Hence, the acceleration at time $t+\Delta t$ and n^{th} iteration can be expressed as:

$$\ddot{\mathbf{D}}_{t+\Delta t}^{(n)} = \frac{1}{\beta_N}\left[\frac{1}{\Delta t^2}\left(\mathbf{D}_{t+\Delta t}^{(n)} - \mathbf{D}_t - \dot{\mathbf{D}}_t \Delta t\right) - \left(\frac{1}{2} - \beta_N\right)\ddot{\mathbf{D}}_t\right] \tag{3.5}$$

And the velocity at time $t+\Delta t$ and n^{th} iteration can be derived as:

$$\dot{\mathbf{D}}_{t+\Delta t}^{(n)} = \dot{\mathbf{D}}_t + \left[\left(1 - \frac{\eta}{2\beta_N}\right)\ddot{\mathbf{D}}_t + \frac{\eta}{\beta_N \Delta t^2}\left(\mathbf{D}_{t+\Delta t}^{(n)} - \mathbf{D}_t - \dot{\mathbf{D}}_t \Delta t\right)\right]\Delta t \tag{3.6}$$

It is supposed that the displacement and dynamic force vectors at time $t+\Delta t$ and n^{th} iteration can be expressed in incremental form as:

$$\mathbf{D}_{t+\Delta t}^{(n)} = \mathbf{D}_{t+\Delta t}^{(n-1)} + \Delta \mathbf{D}_{t+\Delta t}^{(n)} \tag{3.7}$$

and

$$\mathbf{F}_{t+\Delta t}^{(n)} = \mathbf{F}_{t+\Delta t}^{(n-1)} + \Delta \mathbf{F}_{t+\Delta t}^{(n)} \tag{3.8}$$

Substituting Equations (3.2), (3.5), and (3.6) into Equation (3.1), manipulating it, assembling similar terms together, and using Equations (3.7) and (3.8), the nonlinear dynamic governing equation can be expressed as:

$$\mathbf{K}_D^t \Delta\mathbf{D}_{t+\Delta t}^{(n)} = \mathbf{F}_{D(t+\Delta t)}^{(n)} - \mathbf{R}_{t+\Delta t}^{(n-1)} \tag{3.9}$$

where $\mathbf{K}_D^t$ is the dynamic tangent stiffness matrix of the system at time *t*; $\Delta\mathbf{D}_{t+\Delta t}^{(n)}$ and $\mathbf{F}_{D(t+\Delta t)}^{(n)}$ are the incremental displacement vector and modified external load vector of the n^{th} iteration at time $t+\Delta t$, respectively; and $\mathbf{R}_{t+\Delta t}^{(n-1)}$ was defined earlier.

It can be demonstrated that the dynamic tangent stiffness matrix can be expressed as:

$$\mathbf{K}_D^t = f_1\mathbf{M} + f_2\mathbf{K}^t \tag{3.10}$$

And the modified external load vector $\mathbf{F}_{D(t+\Delta t)}^{(n)}$ can be expressed as (Lee and Haldar, 2003):

$$\mathbf{F}_{D(t+\Delta t)}^{(n)} = \mathbf{F}_{D(t+\Delta t)}^{(n-1)} + \Delta\mathbf{F}_{D(t+\Delta t)}^{(n)} \tag{3.11}$$

where $\mathbf{F}_{D(t+\Delta t)}^{(n-1)}$ is the modified external force vector of the $(n\text{-}1)^{th}$ iteration at time $t+\Delta t$; and $\Delta\mathbf{F}_{D(t+\Delta t)}^{(n)}$ is the incremental modified external force vector of the n^{th} iteration at time $t+\Delta t$.

The incremental modified external force vector $\Delta\mathbf{F}_{D(t+\Delta t)}^{(n)}$ of the n^{th} iteration at time $t+\Delta t$ can be represented as:

$$\Delta\mathbf{F}_{D(t+\Delta t)}^{(n)} = \Delta\mathbf{F}_{t+\Delta t}^{(n)} - \mathbf{M}\Delta\ddot{\mathbf{D}}_{g,(t+\Delta t)}^{(n)} \tag{3.12}$$

And the modified external vector $\mathbf{F}_{D(t+\Delta t)}^{(n-1)}$ of the $(n\text{-}1)^{\text{th}}$ iteration at time $t+\Delta t$ can be expressed as:

$$\mathbf{F}_{D(t+\Delta t)}^{(n-1)} = \mathbf{F}_{t+\Delta t}^{(n-1)} + \mathbf{P}_{t+\Delta t}^{(n-1)} - \mathbf{M}\ddot{\mathbf{D}}_{g,(t+\Delta t)}^{(n-1)} \tag{3.13}$$

where $\mathbf{P}_{t+\Delta t}^{(n-1)}$ is the modified force vector contributed by the displacement, velocity, and acceleration at time *t* and the displacement vector at time $t+\Delta t$. it can be represented as:

$$\mathbf{P}_{t+\Delta t}^{(n-1)} = \mathbf{M}\left[f_1\mathbf{D}_t + f_3\dot{\mathbf{D}}_t + f_4\ddot{\mathbf{D}}_t - f_1\mathbf{D}_{t+\Delta t}^{(n-1)}\right] + \mathbf{K}^t\left[f_5\mathbf{D}_t + f_6\dot{\mathbf{D}}_t + f_7\ddot{\mathbf{D}}_t - f_5\mathbf{D}_{t+\Delta t}^{(n-1)}\right] \tag{3.14}$$

where the coefficients f_i's are constants evaluated in terms of α, γ, η, β_N, and Δt as (Lee and Haldar, 2003):

$$f_1 = \frac{1}{\beta_N \Delta t^2} + \frac{\eta\alpha}{\beta_N \Delta t} \tag{3.15}$$

$$f_2 = \frac{\eta\gamma}{\beta_N \Delta t} + 1 \tag{3.16}$$

$$f_3 = \frac{1}{\beta_N \Delta t} + \frac{\eta\alpha}{\beta_N} - \alpha \tag{3.17}$$

$$f_4 = \left(\frac{1}{2\beta_N} - 1\right) + \eta\alpha\left(\frac{1}{2\beta_N} - \frac{1}{\eta}\right)\Delta t \tag{3.18}$$

$$f_5 = \frac{\eta\alpha}{\beta_N \Delta t} \tag{3.19}$$

$$f_6 = \frac{\eta\gamma}{\beta_N} - \gamma \tag{3.20}$$

$$f_7 = \left(\frac{\eta\gamma}{2\beta_N} - \gamma\right)\Delta t \tag{3.21}$$

Now Equation (3.9) can be solved using the modified Newton-Raphson method with arc-length control (Lee and Haldar, 2003). Using the above FE algorithm, the deterministic responses of structures excited by the seismic loading applied in time domain can be estimated. As mentioned earlier, the research team developed and verified a sophisticated computer program to implement it. The above formulation is essentially for all beam to column connections to be FR type. The algorithm needs to be modified to consider the presence of PR connections, as discussed next.

3.4 Partially Restrained Beam-to-Column Connection Models

As mentioned earlier, the comprehensive properties of a PR connection are commonly described in terms of the relationship between the moment transmitted by the connection, M, and the relative rotation angle, θ, of connecting members. This relationship is commonly represented by M-θ curves. There are many analytical models to represent PR connections. Some of the most important are briefly reviewed next.

3.4.1 Linear, Bilinear, and Piecewise Models

In the past, models representing M-θ relationships of connections were assumed to be linear. Generally, linear models depend on the initial stiffness, which represents the connection behavior for the entire range of loading. However, since the stiffness of the connection decreases as the moment increases, linear models represent a crude approximation of real M-θ relationships of connections. In order to address this issue, bilinear models were introduced in the literature (Lionberger and Weaver, 1969). Bilinear models are generally implemented using matrix analysis. They combine initial stiffness with a lower stiffness at a specific transition moment. Unfortunately, linear and bilinear models provide a rudimentary representation of M-θ relationships of connections. As an alternative, the piecewise model can be introduced. This model is very similar to bilinear model; the only difference is that the piecewise model uses several straight lines to represent the M-θ relationship. Linear, bilinear, and piecewise models are easy to use. However, discontinuity in connection stiffness may cause considerable numerical problems, particularly at the transition points.

3.4.2 Polynomial Model

Other analytical model to represent M-θ relationships of connections was introduced by Frye and Morris (1975). They proposed a M-θ curve using an odd power polynomial. Generally, this polynomial gives a better approximation in comparison with linear, bilinear, and piecewise models. However, the polynomial model represents an inherent oscillatory approximation. In some cases, the first derivative of this function (connection stiffness) may be discontinuous or possibly negative, which is generally physically impossible. Hence, it may provide erroneous estimates of the connection stiffness at several transition points.

3.4.3 Cubic-B-Spline Model

As an alternative to the above analytical models, Jones, Kirby and Nethercot (1980) proposed the Cubic B-Spline Model. This model uses a cubic polynomial to fit segments of the M-θ curve. The first and second derivatives are maintained between adjacent segments, using a cubic function. Using this model, good representations of M-θ curves are expected. However, several parameters need to be evaluated, making the Cubic-B-Spline Model inefficient.

3.4.4 Exponential Models

Some other options for analytical modelling of M-θ curves are exponential models. Chen and Lui (1987) proposed a M-θ representation of connections from an experimentally obtained monotonic loading. However, at least six parameters must be evaluated to use this model. This fact makes this option very time consuming. As an alternative, modified exponential models were proposed by Chen and Kishi (1989). Unfortunately, similar to the model proposed by Chen and Liu (1987), a great number of parameters were required to define *M-θ* curves.

3.4.5 Richard 4-Parameter Model

The Richard 4-Parameter Model represents the *M-θ* curve of beam-to-column connections by simply evaluating four parameters: initial stiffness (k), plastic stiffness (k_P), reference moment (M_0), and curve shape parameter (N). Several studies demonstrated the valuable advantages related to use this model (El-Salti, 1992; Elsati and Richard, 1996; Richard, Allen and Partridge, 1997; Reyes-Salazar, 1997; Reyes-Salazar and Haldar, 2000; Reyes-Salazar and Haldar, 2001; Mehrabian, 2002; Mehrabian, Haldar and Reyes-Salazar, 2005; Mehrabian, Ali and Haldar, 2009).

Among all the previously introduced analytical models to represent *M-θ* curves of connections, the research team at the University of Arizona found the Richard 4-Parameter model to be the best option. It is used in this study to incorporate rigidities of beam-to-column connections. The Richard 4-Parameter model is relatively easy to differentiate for the calculation of stiffness and other parameters involved in the process. It is practical, beneficial, and suitable to include this model in the computer algorithm presented earlier. The incorporation of this model in the FE algorithm is presented next.

3.5 Incorporation of Connection Rigidities Using Richard 4-Parameter Model

The Richard 4-parameter *M-θ* model is selected in this study to represent the flexible behavior of connections in steel frames. Using this model, a typical *M-θ* curve can be expressed as:

$$M(\theta) = \frac{(k - k_P)\theta}{\left(1 + \left|\frac{(k - k_P)\theta}{M_0}\right|^N\right)^{\frac{1}{N}}} + k_P\theta \tag{3.22}$$

where M is the connection moment and other terms were defined earlier in Section 3.4.5.

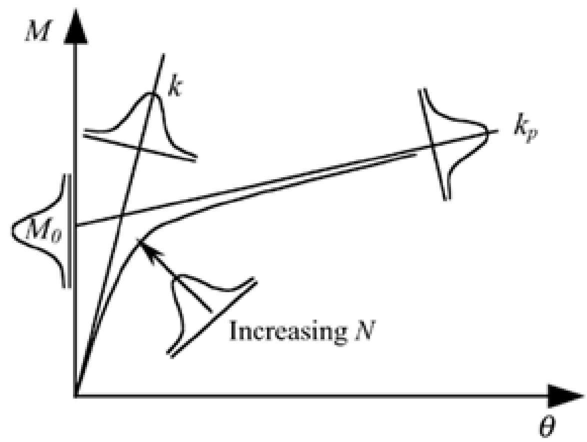

Figure 3.1 – *M*-*θ* curve using the Richard four-parameter model.

Four Richard parameters are illustrated in Figure 3.1. An ordinary beam-column element is used to represent a PR connection in the FE algorithm. However, since the stiffness representing the partial rigidity depends on θ, the stiffness of connection elements needs to be updated at each iteration. It is accomplished by updating the Young's modulus (E_c) as:

$$E_c(\theta) = \frac{l_c}{I_c} K_c(\theta) = \frac{l_c}{I_c} \frac{\partial M(\theta)}{\partial \theta} \tag{3.23}$$

where l_c, I_c, and $K_c(\theta)$ are the length, the moment of inertia, and the tangent stiffness of the connection element, respectively.

The term $K_c(\theta)$ in Equation (3.23) is calculated by taking the first derivative of Equation (3.22) with respect to θ. It can be represented as:

$$K_c(\theta) = \frac{\partial M(\theta)}{\partial \theta} = \frac{(k - k_P)}{\left(1 + \left|\frac{(k - k_P)\theta}{M_0}\right|^N\right)^{\frac{N+1}{N}}} + k_P \tag{3.24}$$

The Richard four-parameter model represents only the monotonically increasing loading portion of the M-θ curve. However, the unloading and reloading behavior of PR connections need to be considered for the nonlinear seismic analysis. The behavior is developed using the Masing rule as suggested by Colson (1991). A general type of Masing model can be defined with a virgin loading curve as:

$$f(M, \theta) = 0 \tag{3.25}$$

and its unloading and reloading curve can be described as:

$$f\left(\frac{M - M_a}{2}, \frac{\theta - \theta_a}{2}\right) = 0 \tag{3.26}$$

where (M_a, θ_a) is the load reversal point as shown in Figure 3.2.

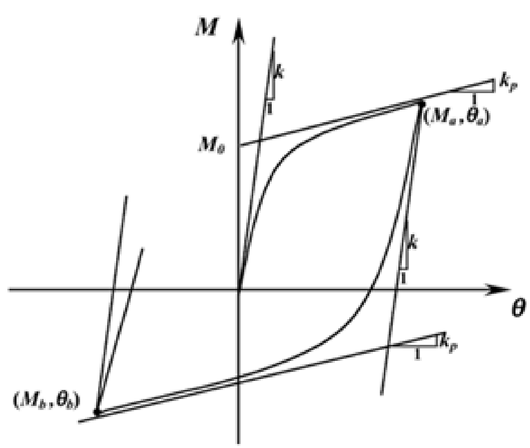

Figure 3.2 – Loading, unloading, and reverse loading model for PR connections.

Using the Masing rule and the Richard four-parameter model represented by Equations (3.22) and (3.24), the unloading and reloading behavior of a PR connection can be generated as:

$$M(\theta) = M_a - \frac{(k - k_P)(\theta_a - \theta)}{\left(1 + \left|\frac{(k - k_P)(\theta_a - \theta)}{2M_0}\right|^N\right)^{\frac{1}{N}}} - k_P(\theta_a - \theta) \tag{3.27}$$

and

$$K_c(\theta) = \frac{\partial M(\theta)}{\partial \theta} = \frac{(k - k_P)}{\left(1 + \left|\frac{(k - k_P)(\theta_a - \theta)}{2M_0}\right|^N\right)^{\frac{N+1}{N}}} + k_P \tag{3.28}$$

If (M_b, θ_b) is the next load reversal point, as shown in Figure 3.2, the reloading relation between M and θ can be obtained by simply replacing (M_a, θ_a) with (M_b, θ_b) in Equations (3.27) and (3.28). Hence, Equations (3.22) and (3.24) are used when the connection is loading, and Equations (3.27) and (3.28) are used when the connection is unloading and reloading. It represents the hysteretic behavior of a PR connection. The required four parameters (k, k_P, M_0, and N) of the Richard model are estimated using available experimental results (Elsati and Richard, 1996). The above algorithm has been extensively verified and applied for deterministic response of steel structures excited by seismic loading applied in time domain considering FR and PR connections (Reyes-Salazar, 1997; Reyes-Salazar and Haldar, 2000; Reyes-Salazar and Haldar, 2001; Mehrabian, 2002; Mehrabian, Haldar and Reyes-Salazar, 2005; Mehrabian, Ali and Haldar, 2009). The above formulations are incorporated in the novel reliability technique to implement PBSD. These formulations will be discussed later in this study.

3.6 Summary and Concluding Remarks

An efficient and accurate deterministic FEM for steel structures was discussed in this chapter. Among many FEM alternatives, the assumed stress-based FEM was selected to be used in the implementation of PBSD. It represents a fundamental part of the novel reliability technique presented later in this research. In order to consider the real behavior of structures excited by seismic loading, several PR connection models were discussed for the proper consideration of rigidities of beam-to-column connections. At the end of this chapter, the Richard 4-parameter model was selected for the incorporation of connection rigidities. During the structural risk evaluation, the FEM method discussed in this chapter will be used for the deterministic calculation of seismic responses. It represents a fundamental part of the novel reliability technique for PBSD implementation.

CHAPTER 4
RESPONSE SURFACE METHOD

4.1 Introduction

Once the deterministic community is satisfied with an appropriate FEM approach for the calculation of structural responses, a methodology is necessary to generate as accurate as possible the implicit LSFs. It represents one more step in proposing a novel reliability technique to be implemented in PBSD. Among many alternatives, the RSM is used in this research for the proper construction of polynomials representing LSFs. First, the polynomial representation of response surfaces is introduced. Then, the selection of the experimental region to construct the response surface is discussed in terms of both saturated and central composite designs. In addition, three experimental designs are discussed. At the end, advantages of proposed experimental designs and some recommendations addressing limitations of RSM are discussed.

4.2 Polynomial Representation of a Response Surface

The polynomial representation of a response surface is the first step in RSM. It may be decided in terms of efficiency and accuracy. Obviously, in the context of PBSD, it is not expected to be linear. It is reported in the literature that the selection of more than second-order polynomials for a response surface can be very problematic (Khuri and Cornell, 1996). In addition, the calculation effort increases proportionally to the number of RVs involved in the risk evaluation. Considering several characteristics of polynomials and the dynamic response of steel structures excited by seismic loading, the response surface is represented by a second-order polynomial without or with cross terms as:

$$\hat{g}(\mathbf{X}) = b_0 + \sum_{i=1}^{k} b_i X_i + \sum_{i=1}^{k} b_{ii} X_i^2 \tag{4.1}$$

and

$$\hat{g}(\mathbf{X}) = b_0 + \sum_{i=1}^{k} b_i X_i + \sum_{i=1}^{k} b_{ii} X_i^2 + \sum_{i=1}^{k-1} \sum_{j>1}^{k} b_{ij} X_i X_j \tag{4.2}$$

where X_i (i=*1,2,…*,k) is the i^{th} RV; k is the total number of RVs involved in the problem; b_0, b_i, b_{ii} and b_{ij} are the unknown coefficients to be determined; and $\hat{g}(\mathbf{X})$ is the approximate representation of the original unknown LSF $g(\mathbf{X})$.

The number of coefficients required to define Equations (4.1) and (4.2) are $2k + 1$, and $(k + 1)(k + 2)/2$, respectively. For example, if $k = 6$, the number of unknown coefficients required to define Equations (4.1) and (4.2) will be 13 and 28, respectively. However, if k is large, say 60, as expected for a realistic structure, the corresponding numbers will be 121 and 1891, respectively, indicating a significant increase in computational time if Equation (4.2) is used. Additionally, the selection of experimental region to generate response information plays an important role in the efficiency of the procedure. This is discussed next.

4.3 Experimental Region and Coded Variables

In order to generate an efficient and accurate representation of a performance function or LSF, the experimental region should be kept to a minimum (Khuri and Cornell, 1996). Therefore, it is important to determine the adequate range of the region for an experimental design. The corresponding uncertainty in every RV is incorporated in the model depending on the experimental region. It is done by increasing or decreasing the experimental region using an arbitrary amount. Hence, in the physical variable space, the coordinate of every i^{th} RV for the j^{th} experimental sampling point can be defined as:

$$X_{ij} = X_i^C \pm h_i x_{ij} \sigma_{X_i} \quad where\ i = 1,2,\dots,k \quad and \quad j = 1,2,\dots,N \qquad (4.3)$$

where k is the number of RVs; N is the number of experimental sampling points; X_i^C and σ_{X_i} are the coordinate of the center point and the standard deviation of a RV X_i, respectively; h_i is an arbitrary factor that defines the experimental region; and x_{ij} is the coded variable.

The coded variable (x_{ij}) is introduced in order to facilitate the determination of coefficients in Equations (4.1) and (4.2). From Equation (4.3), it can be defined as:

$$x_{ij} = \frac{X_{ij} - X_i^c}{h_i \sigma_i} \quad where\ i = 1,2,\dots,k \quad and \quad j = 1,2,\dots,N \qquad (4.4)$$

all the terms of Equation (4.4) were defined earlier. It is easy observed from Equation (4.4) that the coded values at the center points of the random variables are zero.

Equation (4.4) represents the required transformation from the system of the input variables to a coded variable space. Since coding eliminates the units of measurements of the input variable, it is easier to form $\mathbf{X}$ or $\mathbf{X}^t\mathbf{X}$ matrix required in the coefficient estimation of a polynomial. Once the experimental region and coded values have been introduced, the accuracy in coefficient estimation of Equations (4.1) and (4.2) can be considerably improved. At the same time, the computational time is decreased. However, experimental designs should be introduced for the proper selection of observed values. They are introduced in the next section.

4.4 Experimental Designs

To generate response information, several deterministic FE analyses need to be conducted at specific points commonly known as sampling points, following an experimental design. The experimental design is also expected to influence the accuracy and efficiency of the algorithm. Even though the number of sampling points should be kept as minimum as possible, they must be at least equal to the number of unknown coefficients of the required polynomial. Two commonly used experimental designs reported in the literature are Saturated Design (SD) and Central Composite Design (CCD) (Khuri and Cornell, 1996). SD is less accurate, but more efficient since it requires only as many deterministic FE analysis (sampling points) as the total number of unknown coefficients necessary to define the polynomial by solving a set of linear equations. In addition, a second-order polynomial without and with cross terms can be used to generate a polynomial representation using SD, requiring $2k + 1$ and $(k + 1)(k + 2)/2$ number of deterministic FE analysis, respectively. On the other hand, CCD is more accurate but less efficient since it can generate only a second-order polynomial with cross terms and a regression analysis is needed to obtain the unknown coefficients. CCD consists of one center point, two axial points located on the axis of each RV at a distance "α" equal to $\sqrt[4]{2^k}$ measured from the center point, and 2^k factorial points. Hence, the total number of deterministic FE analysis (sampling points) in CCD is equal to $2^k + 2k + 1$. More comprehensive discussions on SD and CCD can be found in the literature (Box, Hunter and Hunter, 1978; Faravelli, 1989; Khuri and Cornell, 1996). Based on accuracy and efficiency providing compounding beneficial effects, three experimental designs are introduced in this section. They are discussed next.

4.4.1 Experimental Design 1: SD and Second Order Polynomial without Cross Terms

This experimental design alternative uses SD and a second order polynomial without cross terms as expressed in Equation (4.1). The sampling points in Experimental Design 1 are one center point and $2k$ axial points (located at +1 and -1, respectively for every RV in coded values). Therefore, a total number of sampling points equal to $2k + 1$ is required in this design. Figure 4.1 illustrates the sampling points required for Experimental Design 1 using three RVs ($k = 3$): X_1, X_2, and X_3 (Khuri and Cornell, 1996).

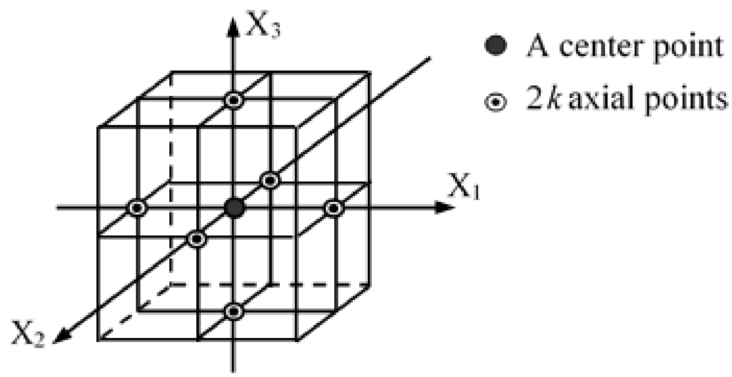

Figure 4.1 – Sampling points required in Experimental Design 1 ($k = 3$).

For this experimental design, the original performance function or LSF represented as $g(\mathbf{X})$ or **Y**, can be expressed as:

$$\mathbf{Y} = \mathbf{Xb} + \boldsymbol{\varepsilon} \tag{4.5}$$

where **Y** is the actual response vector; **b** is the vector of unknown coefficients; **ε** is the vector of random errors; and **X** represents the matrix of sampling points in coded values, as presented in Table 4.1.

The unknown coefficients denoted as b_0, b_i, and b_{ii} in Equation (4.1) can be obtained by solving a set of simultaneous equations represented as:

$$\mathbf{b} = \mathbf{X}^{-1}\mathbf{Y} \tag{4.6}$$

Experimental Design 1 is considerable efficient because few number of sampling point will be required to generate a polynomial representation. However, it cannot cover the sample space between axes.

Table 4.1 – Representation of X using Experimental Design 1 (Huh, 1999).

	x_0	x_1	x_2	·····	x_{k-1}	x_k	x_1^2	x_2^2	·····	x_{k-1}^2	x_k
1	+1	-1	0	·····	0	0	+1	0	·····	0	0
2	+1	+1	0	·····	0	0	+1	0	·····	0	0
3	+1	0	-1	·····	0	0	0	+1	·····	0	0
4	+1	0	+1	·····	0	0	0	+1	·····	0	0
⋮	⋮	⋮	⋮	·····	⋮	⋮	⋮	⋮	·····	⋮	⋮
2*k*-3	+1	0	0	·····	-1	0	0	0	·····	+1	0
2*k*-2	+1	0	0	·····	+1	0	0	0	·····	+1	0
2*k*-1	+1	0	0	·····	0	-1	0	0	·····	0	+1
2*k*	+1	0	0	·····	0	+1	0	0	·····	0	+1
2*k*+1	+1	0	0	·····	0	0	0	0	·····	0	0

4.4.2 Experimental Design 2: SD and Second Order Polynomial with Cross Terms

Other experimental design that must be discussed is SD using a second order polynomial with cross terms. It is referred hereafter as Experimental Design 2. For this design, the inclusion of cross terms in the polynomial representation may increase the accuracy as presented in Equation (4.2). The sampling points used in this design are one center point, $2k$ axial points (located at +1 and -1, respectively for every RV in coded values), and $k(k-1)/2$ edge points. An edge point can be defined as a k-vector having ones in the i^{th} and j^{th} location and zeros elsewhere. Hence, the total number of sampling points required in Experimental Design 2 are $2k+1+k(k-1)/2$ or $(k+1)(k+2)/2$. Figure 4.2 illustrates this experimental design in terms of three RVs ($k=3$): X_1, X_2, and X_3 (Khuri and Cornell, 1996).

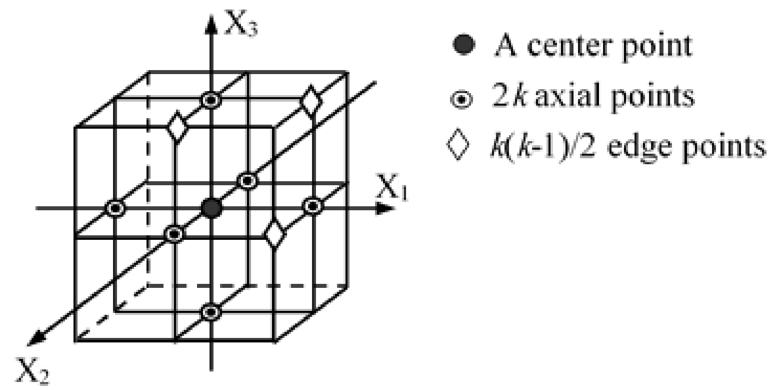

Figure 4.2 – Sampling points required in Experimental Design 2 ($k=3$).

In the context of SD, the real performance function or LSF represented as $g(\mathbf{X})$ or $\mathbf{Y}$, can be calculated as:

$$\mathbf{Y} = \mathbf{X}\mathbf{b} + \boldsymbol{\varepsilon} \tag{4.7}$$

where $\mathbf{Y}$ is the original response vector; $\mathbf{b}$ is the unknown coefficients vector; $\boldsymbol{\varepsilon}$ is the vector of random errors; and $\mathbf{X}$ is the experimental sampling point matrix in coded values, as presented in Table 4.2.

The unknown coefficients vector $\mathbf{b}$ represented in terms of b_0, b_i, b_{ii} and b_{ij} in Equation (4.2), can be calculated by solving a set of linear equations represented as:

$$\mathbf{b} = \mathbf{X}^{-1}\mathbf{Y} \tag{4.8}$$

It is clearly demonstrated that using SD with a polynomial with cross terms increases accuracy of the response representation. However, when a polynomial with cross terms is used to generate a response surface, as shown in this section, the required sampling points are increased. Hence, for Experimental Design 2, efficiency is compromised but accuracy is increased with respect to Experimental Design 1.

Table 4.2 – Representation of X using Experimental Design 2 (Huh, 1999).

	x_0	x_1	x_2	⋯⋯	x_{k-1}	x_k	x_1^2	x_2^2	⋯⋯	x_{k-1}^2	x_k^2	$x_{1,2}$	$x_{1,3}$	⋯	$x_{1,k}$	$x_{2,3}$	⋯	$x_{k-1,k}$
1	+1	-1	0	⋯⋯	0	0	+1	0	⋯⋯	0	0	0	0	⋯	0	0	⋯	0
2	+1	+1	0	⋯⋯	0	0	+1	0	⋯⋯	0	0	0	0	⋯	0	0	⋯	0
3	+1	0	-1	⋯⋯	0	0	0	+1	⋯⋯	0	0	0	0	⋯	0	0	⋯	0
4	+1	0	+1	⋯⋯	0	0	0	+1	⋯⋯	0	0	0	0	⋯	0	0	⋯	0
:	:	:	:	⋯⋯	:	:	:	:	⋯⋯	:	:	:	:	⋯	:	:	⋯	:
2*k*-3	+1	0	0	⋯⋯	-1	0	0	0	⋯⋯	+1	0	0	0	⋯	0	0	⋯	0
2*k*-2	+1	0	0	⋯⋯	+1	0	0	0	⋯⋯	+1	0	0	0	⋯	0	0	⋯	0
2*k*-1	+1	0	0	⋯⋯	0	-1	0	0	⋯⋯	0	+1	0	0	⋯	0	0	⋯	0
2*k*	+1	0	0	⋯⋯	0	+1	0	0	⋯⋯	0	+1	0	0	⋯	0	0	⋯	0
2*k*+1	+1	-1	+1	⋯⋯	0	0	+1	+1	⋯⋯	0	0	+1	0	⋯	0	0	⋯	0
2*k*+2	+1	+1	0	⋯⋯	0	0	+1	0	⋯⋯	0	0	0	+1	⋯	0	0	⋯	0
:	:	:	:	⋯⋯	:	:	:	:	⋯⋯	:	:	:	:	⋯	:	:	⋯	:
:	+1	+1	0	⋯⋯	+1	0	+1	0	⋯⋯	+1	0	0	0	⋯	0	0	⋯	0
:	+1	+1	0	⋯⋯	0	+1	+1	0	⋯⋯	0	+1	0	0	⋯	+1	0	⋯	0
:	+1	0	+1	⋯⋯	0	0	0	+1	⋯⋯	0	0	0	0	⋯	0	+1	⋯	0
:	:	:	:	⋯⋯	:	:	:	:	⋯⋯	:	:	:	:	⋯	:	:	⋯	:
:	+1	0	+1	⋯⋯	+1	0	0	+1	⋯⋯	+1	0	0	0	⋯	0	0	⋯	0
:	+1	0	+1	⋯⋯	0	+1	0	+1	⋯⋯	0	+1	0	0	⋯	0	0	⋯	0
:	:	:	:	⋯⋯	:	:	:	:	⋯⋯	:	:	:	:	⋯	:	:	⋯	:
:	+1	0	0	⋯⋯	+1	+1	0	0	⋯⋯	+1	+1	0	0	⋯	0	0	⋯	+1
(*k*+1)(*k*+2)/2	+1	0	0	⋯⋯	0	0	0	0	⋯⋯	0	0	0	0	⋯	0	0	⋯	0

4.4.3 Experimental Design 3: CCD and Second Order Polynomial with Cross Terms

CCD represents the most accurate experimental design used in this research. It is restricted to the use of a polynomial with cross terms as indicated in Equation (4.2). It is known in this research as Experimental Design 3. It is represented by three items: (1) a complete 2^k factorial design with factor levels coded to the usual +1, -1 values, (2) one center point, and (3) two axial points for every RV at a distance "α" equal to $\sqrt[4]{2^k}$ with respect to the center point. Therefore, the total number of sampling points for Experimental Design 3 will be $2^k + 2k + 1$. It requires way much more sampling points than previous experimental designs. Figure 4.3 illustrates Experimental Design 3 based on three RVs ($k = 3$): X_1, X_2, and X_3 (Khuri and Cornell, 1996).

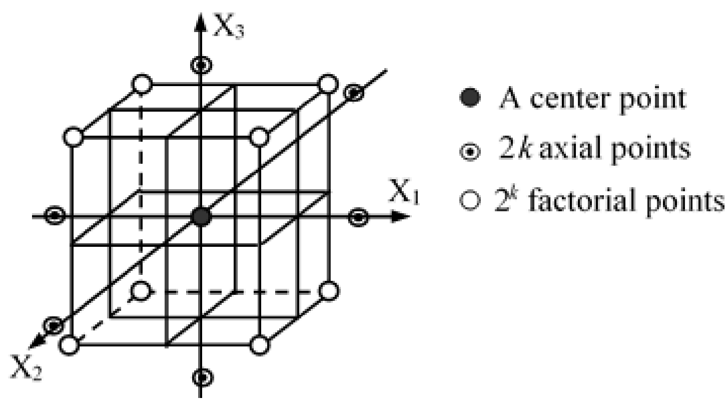

Figure 4.3 – Sampling points required in Experimental Design 3 ($k = 3$).

The actual performance function or LSF expressed as $g(\mathbf{X})$ or **Y**, can be represented in matrix form as:

$$\mathbf{Y} = \mathbf{Xb} + \boldsymbol{\varepsilon} \tag{4.9}$$

where **Y** is the vector of actual responses; **b** is the vector of unknown coefficients; **ε** is the vector of random errors; and **X** is the sampling point matrix expressed in coded values, as presented in Table 4.3.

Table 4.3 – Representation of X using Experimental Design 3 (Huh, 1999).

	x_0	x_1	x_2	⋯⋯	$x_{k\text{-}1}$	x_k	x_1^2	x_2^2	⋯⋯	$x_{k\text{-}1}^2$	x_k^2	$x_{1,2}$	$x_{1,3}$	⋯	$x_{1,k}$	$x_{2,3}$	⋯	$x_{k\text{-}1,k}$
1	+1	-1	-1	⋯⋯	-1	-1	+1	+1	⋯⋯	+1	+1	+1	+1	⋯	+1	+1	⋯	+1
2	+1	+1	-1	⋯⋯	-1	-1	+1	+1	⋯⋯	+1	+1	-1	-1	⋯	-1	+1	⋯	+1
3	+1	-1	+1	⋯⋯	-1	-1	+1	+1	⋯⋯	+1	+1	-1	+1	⋯	+1	-1	⋯	+1
4	+1	+1	+1	⋯⋯	-1	-1	+1	+1	⋯⋯	+1	+1	+1	-1	⋯	-1	-1	⋯	+1
:	:	:	:	⋯⋯	:	:	:	:	⋯⋯	:	:	:	:	⋯	:	:	⋯	:
:	:	:	:	⋯⋯	:	:	:	:	⋯⋯	:	:	:	:	⋯	:	:	⋯	:
2*k*-3	+1	-1	-1	⋯⋯	+1	+1	+1	+1	⋯⋯	+1	+1	+1	-1	⋯	-1	-1	⋯	+1
2*k*-2	+1	+1	-1	⋯⋯	+1	+1	+1	+1	⋯⋯	+1	+1	-1	+1	⋯	+1	-1	⋯	+1
2*k*-1	+1	-1	+1	⋯⋯	+1	+1	+1	+1	⋯⋯	+1	+1	-1	-1	⋯	-1	+1	⋯	+1
2*k*	+1	+1	+1	⋯⋯	+1	+1	+1	+1	⋯⋯	+1	+1	+1	+1	⋯	+1	+1	⋯	+1
2*k*+1	+1	-α	0	⋯⋯	0	0	α^2	0	⋯⋯	0	0	0	0	⋯	0	0	⋯	0
2*k*+2	+1	+α	0	⋯⋯	0	0	α^2	0	⋯⋯	0	0	0	0	⋯	0	0	⋯	0
2*k*+3	+1	0	-α	⋯⋯	0	0	0	α^2	⋯⋯	0	0	0	0	⋯	0	0	⋯	0
2*k*+4	+1	0	+α	⋯⋯	0	0	0	α^2	⋯⋯	0	0	0	0	⋯	0	0	⋯	0
:	:	:	:	⋯⋯	:	:	:	:	⋯⋯	:	:	:	:	⋯	:	:	⋯	:
2^k+2*k*-3	+1	0	0	⋯⋯	-α	0	0	0	⋯⋯	α^2	0	0	0	⋯	0	0	⋯	0
2^k+2*k*-2	+1	0	0	⋯⋯	+α	0	0	0	⋯⋯	α^2	0	0	0	⋯	0	0	⋯	0
2^k+2*k*-1	+1	0	0	⋯⋯	0	-α	0	0	⋯⋯	0	α^2	0	0	⋯	0	0	⋯	0
2^k+2*k*	+1	0	0	⋯⋯	0	+α	0	0	⋯⋯	0	α^2	0	0	⋯	0	0	⋯	0
2^k+2*k*+1	+1	0	0	⋯⋯	0	0	0	0	⋯⋯	0	0	0	0	⋯	0	0	⋯	0

The least squares estimates $\hat{\mathbf{b}}$, represented in the terms b_0, b_i, b_{ii} and b_{ij} in Equation (4.2), can be obtained by conducting least squares (regression) analysis as:

$$\hat{\mathbf{b}} = (\mathbf{X}^{\mathrm{t}}\mathbf{X})^{-1}\mathbf{X}^{\mathrm{t}}\mathbf{Y} \tag{4.10}$$

This experimental design is more accurate but less efficient than the previously discussed. Hence, at this point, a comparison in terms of accuracy and efficiency must be introduced between the three experimental designs.

4.4.4 Comparison Among Experimental Designs

Since every sampling point represents a deterministic nonlinear FE analysis, the number of sampling points is directly related to the efficiency of the experimental design. Table 4.4 summarizes the efficiency among the above experimental designs.

Table 4.4 – Comparison among the three experimental designs.

Experimental Design	**Polynomial Representation**	**Number of Unknown Coefficients (*p*)**	**Number of Sampling Points (*N*)**	***k***	***p***	***N***
1 (SD)	Equation (4.1)	$2k+1$	$2k+1$	4 12 20	9 25 41	9 25 41
2 (SD)	Equation (4.2)	$\frac{(k+1)(k+2)}{2}$	$\frac{(k+1)(k+2)}{2}$	4 12 20	15 91 231	15 91 231
3 (CCD)	Equation (4.2)	$\frac{(k+1)(k+2)}{2}$	2^k+2k+1	4 12 20	15 91 231	25 4121 1048617

Experimental Design 1 represents the most efficient alternative. However, it has some deficiencies related to accuracy. In order to address this issue, Experimental Design 2 can be introduced. Unfortunately, efficiency is compromised since more sampling points are required to define the polynomial representation. Another option may be Experimental Design 3. However, more sample points than Experimental Design 1 and 2 are required. Hence, a combination of experimental designs must be proposed in order to produce compounding beneficial effects in terms of accuracy and efficiency. Such integration is explained in Chapter 5.

4.5 Limitations Using RSM

As discussed earlier, RSM represents an attractive alternative to generate the implicit LSF required during the risk evaluation. However, RSM should be modified because of some limitations. Using basic RSM, uncertainty of every RV is incorporated using Equation (4.3). However, distributional information is not considered during the response generation. In addition, experimental region is arbitrarily selected. As a consequence, the generation of the polynomial is not performed in the failure region (MPFP). Furthermore, the number of sampling points is an open question. Since reliability evaluation represents an iterative approach, the best combination of experimental designs must be selected during the location of the MPFP. Hence, RSM must be improved by integrating it with several others approaches. This improvement is explained in Chapter 5 where the novel reliability technique for implementing PBSD is introduced.

4.6 Summary and Concluding Remarks

A technical description of RSM was presented in this chapter. In order to generate a response surface, both polynomials without and with cross terms were recommended, depending on the desired accuracy and efficiency. In addition, three experimental designs were proposed for the construction of the polynomial representation. A comparison among them was addressed as well. At the end of this chapter, several limitations related to RSM were documented. In order to address RSM limitations, an integration of several methodologies must be proposed. It is discussed in Chapter 5 of this dissertation in terms of a novel reliability technique.

CHAPTER 5
A NOVEL RELIABILITY TECHNIQUE FOR IMPLEMENTATION OF PBSD

5.1 Introduction

Until this point, several concerns and issues related to PBSD have been discussed. The main knowledge gap in implementing PBSD is the seismic risk calculation considering nonlinearities and uncertainties, applying seismic loading in time domain. In order to consider several nonlinearities in steel structures excited by seismic loading, a FEM was introduced in this research. However, in the context of reliability evaluation, in addition to a sophisticated FEM, a methodology is required for generating the implicit LSFs. To address this issue, it was documented that RSM can be used. Unfortunately, several issues make RSM inadequate. Basically, RSM must be modified in order to overcome its deficiencies. This chapter presents an integration of several methodologies to address the issues related to RSM. Such integration is explained in terms of a novel reliability technique for implementation of PBSD. First, an advanced experimental design is proposed by integrating SD and CCD. Then, finite element evaluation is introduced by using the previously discussed FEM. Next, an explicit polynomial representation is proposed for every global iteration during the reliability evaluation. Subsequently, the algorithm will start locating the Most Probable Failure Point (MPFP) and β, it is discussed by introducing FORM. Basically, the novel reliability technique represents an integration of RSM, FEM, and FORM to calculate the MPFP, β, and p_f. In addition, the evaluation of performance levels is introduced in this chapter, as well as the estimation of LSFs in terms of overall lateral and inter-story drift, respectively. Furthermore, the incorporation of uncertainties in loads and resistance-related parameters is discussed in this chapter. Finally, in order to validate and demonstrate the robustness of the novel reliability technique, several steel buildings are studied.

5.2 Integration of RSM, FEM, and FORM to Calculate MPFP, $\boldsymbol{\beta}$, and $\boldsymbol{p_f}$

In order to calculate seismic risk, a novel reliability technique is proposed in this dissertation. Such technique works based on the integration of RSM, FEM, and FORM. In the context of risk analysis, the reliability technique works iteratively until the MPFP, β, and p_f are calculated. It is explained in this section in terms of eight items: (1) advanced experimental design integrating SD and CCD, (2) finite element evaluation, (3) polynomial representation, (4) FORM evaluation, (5) reduction of RVs, (6) evaluation of performance levels, (7) incorporation of uncertainties in loads and resistance-related parameters, and (8) structural reliability calculation.

5.2.1 Advanced Experimental Design Integrating SD and CCD

The first step in the iterative process of the novel reliability technique is to define the experimental design. For every iteration, an experimental design should be defined depending on the desired accuracy and efficiency. In this research, an advanced experimental design is proposed integrating SD and CCD. During the first and intermediate iterations, in order to add efficiency, sampling points will be selected by using SD and a second order polynomial without cross terms. This was defined in Chapter 4 as Experimental Design 1. Accuracy will be incorporated during the last iteration using CCD and a second order polynomial with cross terms. In Chapter 4, this was defined as Experimental Design 3. Figure 5.1 illustrates the process in terms of experimental designs.

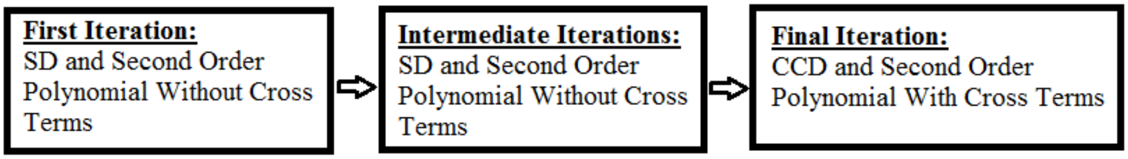

Figure 5.1 – Novel reliability technique process in terms of experimental designs.

For every iteration, depending on the experimental design used, sampling points (X_{ij}) will be selected around a center point (X_i^C) as:

$$X_{ij} = X_i^C \pm h_i x_{ij} \sigma_{X_i} \quad where\ i = 1,2, \dots, k \quad and \quad j = 1,2, \dots, N \tag{5.1}$$

where all terms were defined earlier in Chapter 4, Section 4.3. Equation (5.1) is similar to Equation (4.3). It is introduced here one more time for clarification purposes.

At the beginning of every iteration, the selection of the center point (X_i^C) is critical for calculating the MPFP, β, and p_f. During the first iteration, the center point (X_i^C) will be considered as the mean value (μ_{X_i}) of the corresponding RV. For intermediate and final iterations, the center point (X_i^C) will be considered as the coordinates of the MPFP (x_i^*) of the previous iteration. For every iteration, the center point selection is illustrated in Figure 5.2. It is important to note that the MPFP and β are calculated during every single iteration using FORM, and the process of the novel reliability technique stops when a tolerance criterion is satisfied in terms of β values. This will be discussed later in this research.

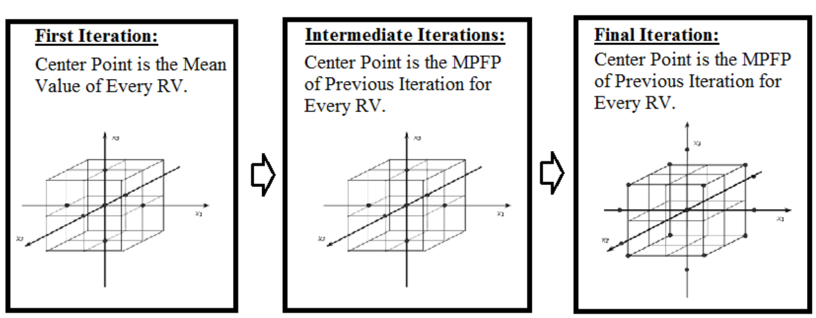

Figure 5.2 – Center point selection for every iteration.

From the above discussion, it is obvious that the proposed reliability technique represents an iterative process. For every iteration, experimental designs and center point selection were described. At this point of the process, sampling points will be available. The following step is to perform nonlinear finite element evaluations using every sampling point.

5.2.2 Finite Element Evaluation

Once sampling points are selected, they are used for finite element evaluations during every iteration of the process. This represents an essential part of the novel reliability technique for the implementation of PBSD. Considering its numerous advantages, the stress-based FEM discussed in Chapter 3 is used for the calculation of deterministic seismic responses. Finite element evaluation is shown in Figure 5.3.

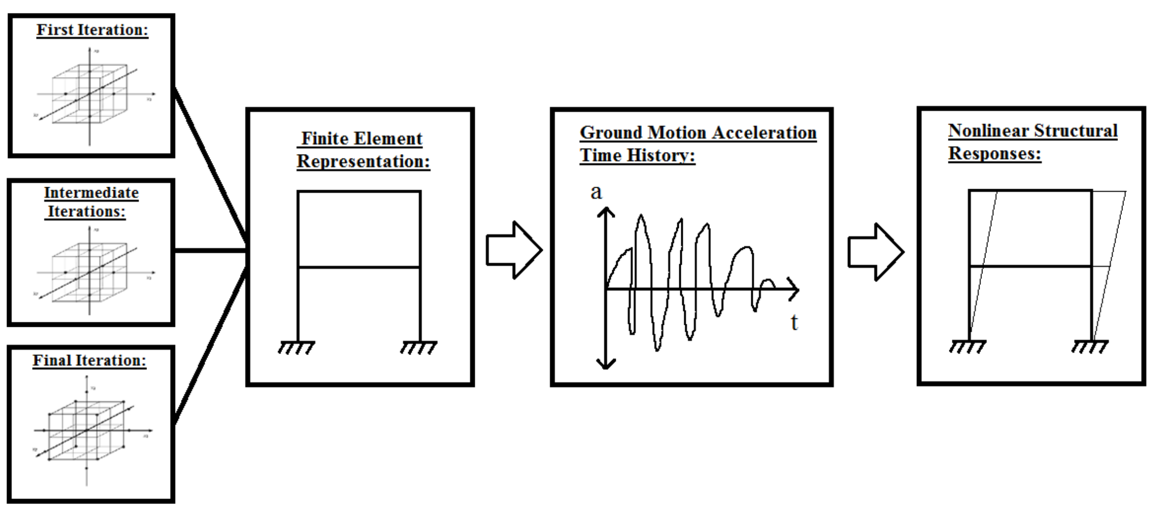

Figure 5.3 – Finite element evaluation.

After every single deterministic nonlinear finite element analysis is completed, a tremendous amount of data will be available in terms of nonlinear structural responses.

Using such data, a polynomial will be generated depending on the experimental design corresponding to the iteration. This is discussed in the next section.

5.2.3 Polynomial Representation

As previously discussed, the polynomial representation will be generated depending on the experimental design assigned to the iteration. For the novel reliability technique proposed in this research, two types of polynomials will be used for the representation: (1) for the first and intermediate iterations, a second order polynomial without cross terms [Equation (4.1)], and (2) for the last iteration, a second order polynomial with cross terms [Equation (4.2)]. In addition, in order to obtain the unknown coefficients of the corresponding polynomial, for the first and intermediate iterations, a set of linear equations will be solved, and for the final iteration, a regression analysis will be performed. The process corresponding to the polynomial representation is illustrated in Figure 5.4. In order to incorporate distributional information of every RV and to generate the polynomials representation in the failure region, FORM is integrated in the process as discussed next.

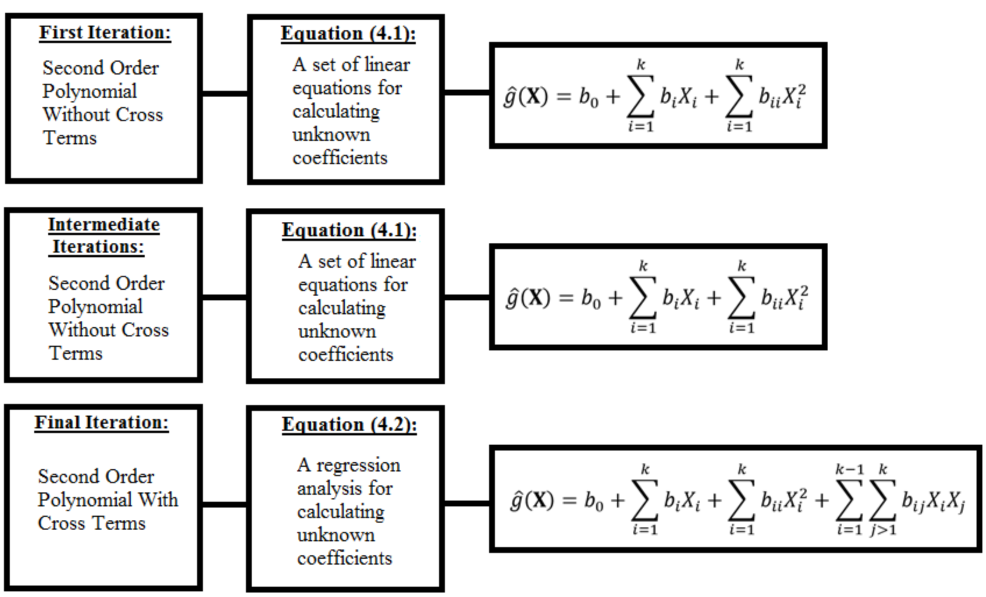

Figure 5.4 – Polynomial representation process.

5.2.4 FORM Evaluation

FORM evaluation is an essential part of the novel reliability technique. It incorporates distributional information of every single RV in the algorithm and helps to generate the polynomial in the failure region. As previously discussed, for the first iteration, the center point (X_i^C) is considered to be the mean value of every RV. Then, sampling points are selected around the first center point (μ_{X_i}) and finite element evaluations are performed. Subsequently, a polynomial representation is generated using Equation (4.1). Once the explicit polynomial representation is available, the first FORM evaluation is performed and the corresponding MPFP and β are calculated. However, these MPFP and β values cannot be considered as the final ones. Then, an iterative process will start repeating the previously described stages. However, for intermediate and final iterations, the central point will be taken as the MPFP of the previous iteration. The iterative process continues until a convergence criterion is reached. This will be discussed later. During every iteration, the FORM evaluation is performed following the next 8 steps.

- Step 1: Define the proper LSF.
- Step 2: Assume the initial values of the design point (x_i^*). Generally, the initial values are taken as the mean values (μ_{X_i}) of every RV.
- Step 3: If there are non-normal distributed RVs, their equivalent normal standard deviation ($\sigma_{X_i}^N$) and mean ($\mu_{X_i}^N$) must be computed as:

$$\sigma_{X_i}^N = \frac{\emptyset\left\{\Phi^{-1}\left[F_{X_i}(x_i^*)\right]\right\}}{f_{X_i}(x_i^*)} \tag{5.2}$$

and

$$\mu_{X_i}^N = x_i^* - \Phi^{-1}[F_{X_i}(x_i^*)]\, \sigma_{Xi}^N \tag{5.3}$$

where all the terms were introduced in Chapter 2.

- Step 4: Evaluate $\left(\frac{\partial g}{\partial X_i}\right)^{\prime *}$ and α_i at $x_i'^*$ as:

$$\alpha_i = \frac{\left(\frac{\partial g}{\partial X_i'}\right)^*}{\sqrt{\sum_{i=1}^{k}\left(\frac{\partial g}{\partial X_i'}\right)^{2*}}} \tag{5.4}$$

- Step 5: Obtain the new design point $x_i'^*$in terms of β as:

$$x_i^* = \mu_{X_i}^N - \alpha_i \beta \sigma_{X_i}^N \qquad (i = 1,2, \dots, k) \tag{5.5}$$

- Step 6: Substitute the new $x_i'^*$ in the LSF as $g(\boldsymbol{x}'^*) = 0$ and solve again for β.
- Step 7: Using the β value obtained in Step 6, reevaluate $x_i'^*$.
- Step 8: Repeat Step 4 to 7 until β converges to a tolerance criterion.

Generally, FORM process locates the MPFP as shown in Figure 5.5.

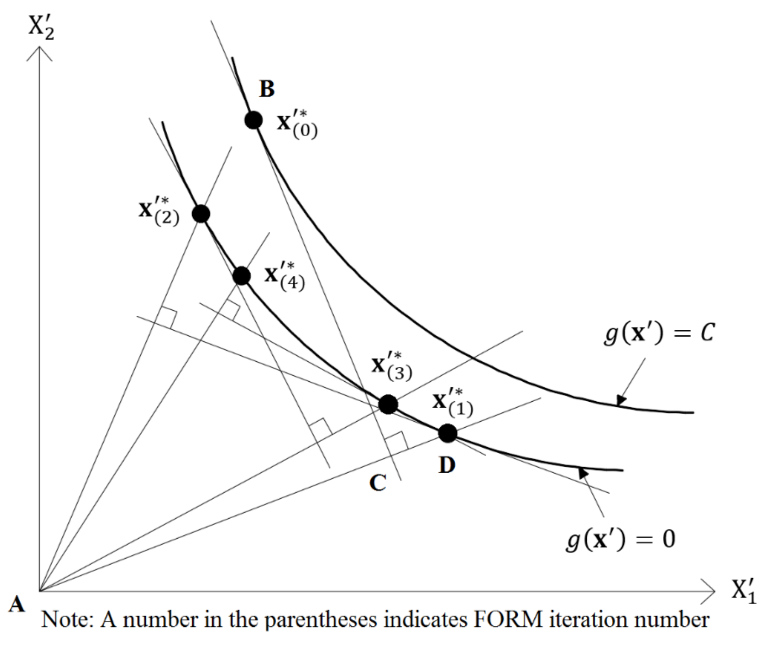

Figure 5.5 – FORM iteration process.

In the novel reliability technique proposed in this study, FORM calculates MPFP and β. However, the calculation can be very time consuming if a great number of RVs is involved in the process. This is common in large structures. In order to increase efficiency, the number of RVs can be reduced considering only the most significant of them. This is discussed in the next section.

5.2.5 Reduction of RVs

The novel reliability technique proposed in this research integrates SD and CCD in an advanced experimental design. Generally, the number of RVs considered during the risk evaluation determines the efficiency of the process. This was discussed in Table 4.4, Chapter 4, Section 4.4.4. It is obvious that when the number of RVs (k) is large, CCD cannot be implemented. It is known to the profession that the propagation of uncertainties from the parameter to system level is very non-uniform. A measure called the sensitivity index can be used to quantify the influence of each RV (Haldar and Mahadevan, 2000a). In the context of FORM, the sensitivity index of a variable X_i is the directional cosine $\alpha_i(X_i)$ of the unit normal variable at the checking or design point. The gradient vector of the LSF in the standard normal variable space can be used for this purpose and will be available from the FORM evaluation. RVs with low sensitivity index at the end of the first iteration can be treated as deterministic at their mean values in the subsequent iterations. The reduction of the total number of RVs significantly improves efficiency without compromising accuracy. The reduced number of RVs will be denoted hereafter in this research as k_r. In order to clarify the importance of reduction of RVs, suppose that during the last iteration, CCD and $k = 30$ are used. Then, the required number of experimental sampling points or deterministic FE evaluations will be $2^k + 2 * k + 1 = 2^{30} + 2 * 30 +$

1 =1,073,741,885. On the other hand, if a reduction in the number of RVs is performed and $k_r = 7$ is used, the required number of experimental sampling points will be $2^{k_r} + 2 * k_r + 1 = 2^7 + 2 * 7 + 1 = 143$. It can be observed that if a reduction of RVs is performed, the number of deterministic FE evaluations can be substantially reduced.

In terms of the novel reliability technique, SD and Equation (4.1) are used in the first and intermediate iterations to increase efficiency, and CCD and Equation (4.2) are used during the final iteration to increase accuracy. For clarification purposes, suppose that it will take three iterations to calculate the seismic risk of a steel structure. Then, if $k = 40$ and $k_r = 7$, the required number of experimental sampling points or deterministic FE evaluations will be $(2 * k + 1) + (2 * k_r + 1) + (2^{k_r} + 2 * k_r + 1) = (2 * 40 + 1) + (2 * 7 + 1) + (2^7 + 2 * 7 + 1) = 239$. Hence, the novel reliability technique captures the efficiency of SD and the accuracy of CCD. It requires only hundreds as compared with thousands or millions of MCS.

5.2.6 Evaluation of Performance Levels

Until this point, the discussion about the novel reliability technique has properly documented its efficiency and accuracy for risk calculation. However, concerning its implementation in PBSD, the calculation of risk must be obtained in terms of performance levels. Then, information about polynomial representations discussed above should be related to specific performance levels. If performance levels are properly defined, LSFs implementing PBSD can be generated. As previously discussed, FEMA-350 (2000) defined three performance levels: IO, LS, CP. They were described earlier in Chapter 2, Table 2.1. Since PBSD is implemented in terms of multiple target performance levels, FEMA-350 (2000) suggested allowable drift values (δ_{allow}) for CP, LS, and IO performance levels in terms of earthquake return period and probability of exceedance. They were summarized in Chapter 2, Table 2.2. The information provided in Table 2.2 is essentially for LSFs in terms of overall lateral and inter-story drift. Considering that a steel structure may fail due to excessive lateral deflection because of a major seismic excitation, overall lateral and inter-story drift LSFs need to be considered in implementing PBSD.

5.2.6.1 Overall Lateral and Inter-Story Drift LSFs

A typical LSF represents a functional relationship of the performance criterion to be used and load and resistance-related design variables present in a formulation. Conceptually, it can be represented as:

$$g(\mathbf{X}) = \delta_{allow} - y_{max}(\mathbf{X}) = \delta_{allow} - \hat{g}(\mathbf{X}) \tag{5.6}$$

where δ_{allow} is the permissible or allowable value to satisfy a specific performance requirement, $\hat{g}(\mathbf{X})$ is the polynomial representation of the behavior of the load and resistance-related design variables, and **X** is a vector representing all the design variables. At present, two LSFs related to the overall lateral and inter-story drifts are being discussed in the profession to implement PBSD. Their allowable or recommended values are suggested in FEMA-350 (2000). They were summarized earlier in Chapter 2, Table 2.2.

5.2.7 Incorporation of Uncertainties in Loads and Resistance-Related Parameters

For the risk evaluation of real structures excited by the seismic loading in time domain, uncertainty associated with all major load and resistance-related parameters must be considered. The novel reliability technique proposed in this research incorporates uncertainties as discussed below.

5.2.7.1 Uncertainties in Resistance-related Parameters

The uncertainties associated with resistance-related parameters are widely reported in the literature (Ellingwood, 1980; Haldar and Mahadevan, 2000a, b; Nowak and Collins, 2012). The appropriate information is used in this research. Later in this dissertation, the novel reliability technique will be demonstrated by considering the performances of several steel structures. All structural elements will be represented by W-sections reported in the steel construction manual (AISC, 2011). Young's modulus (E), yield stress of columns (Fy_c) and girders (Fy_g), cross sectional area (A), and moment of inertia (I_x) of W-sections used for structural elements will be considered as RVs with a lognormal distribution with Coefficient of Variation (COV) of 0.06, 0.10, 0.10, 0.05, and 0.05.

5.2.7.2 Uncertainties in Gravity Loads

In most design guidelines (ASCE/SEI 7-10, 2010; IBC, 2012), gravity loads are classified as Dead Load (DL) and Live Load (LL). The uncertainties associated with both are available in the literature (Ellingwood, 1980; Haldar and Mahadevan, 2000a, b; Nowak and Collins, 2012); similar information is used in this study. DL and LL are represented by a normal and Type 1 distributions with COV of 0.10 and 0.25, respectively. They will be discussed later in this report.

5.2.7.3 Uncertainties in PR Beam-to-Column Connections

During the finite element evaluation part of the novel reliability technique presented in this research, rigidities of PR beam-to-column connections will be considered. The Richard 4-Parameter Model is used for the proper incorporation of connection rigidities in the algorithm. It has been reported in the literature (Haldar and Mahadevan, 2000b) that the four parameters defining the 4-Richard model are randomly distributed. Such parameters were introduced earlier in Chapter 3 as k, k_P, M_0, and N. The four parameters will be considered as RVs with a normal distribution and COV of 0.15, 0.15, 0.15, and 0.05 for k, k_P, M_0, and N, respectively.

5.2.7.4 Uncertainties in Seismic Loading

As proposed in this study, in implementing PBSD, the seismic loading needs to be applied in time domain. Consideration of uncertainties in seismic loading is very challenging and still evolving. Uncertainty associated with the intensity and the frequency contents needs to be considered. In order to incorporate the uncertainty in the intensity, a factor (g_e) is considered in this study. It is considered to be a RV with a Type 1 distribution and with a COV of 0.2. To incorporate uncertainty in the frequency contents, several recent design guidelines (ASCE/SEI 7-10, 2010; IBC, 2012) suggest consideration of at least seven time histories expected for the location. For PBSD, multiple performance levels must be considered and the corresponding risk or the Probability of Exceedance (PE) or reliabilities need to be estimated, as suggested by FEMA-350 (2000) and SAC project (FEMA-351, 2000; FEMA-352, 2000; FEMA-353, 2000; FEMA-355C, 2000; FEMA-355F, 2000). Somerville (1997) developed three sets of ground motion time histories related to 2%, 10%, and 50% PE in 50 years for the Los Angeles (LA) area. They are correlated in this research with the performance levels of CP, LS, and IO, respectively. For every performance level, ten ground motions with two horizontal orthogonal components were proposed, providing twenty time histories per set. Somerville (1997) applied Scale Factors (SFs) to match specific target response spectral values, on average, for periods at 0.3, 1.0, 2.0, and 4.0 seconds for site category S_D (firm soil), as suggested by the United States Geological Survey (USGS). Specific information on these earthquake (EQ) sets is summarized later in this research. The three sets of ground motions will be used for the reliability evaluation of several steel frames.

5.2.8 Structural Reliability Calculation

In summary, the proposed novel reliability technique appears to be complicated in implementing PBSD. For proper comprehension, it is elaborated further. In the proposed algorithm, the necessary response information will be generated at the sampling points by calculating the maximum responses caused by an earthquake time history using FEM. In the first iteration, an approximation of the Limit State Function (LSF) will be generated by using SD and Equation (4.1). The mean values of all RVs in the normal variable space will be considered as center points. At the end of the first iteration, in the context of FORM, the first β, MPFP, and sensitivity indexes (α_i) of all RVs will be available. RVs with low sensitivity indexes will be considered as deterministic at their mean values and k will be reduced to k_r. The next iteration will start by using k_r number of RVs and the previously obtained MPFP as center point. A new LSF will be reconstructed using SD and Equation (4.1). Using the updated LSF, FORM will calculate β and MPFP. It will be used as center point for the next iteration of the novel reliability technique. The overall updating in center points will continue until β values for two consecutive iterations converge to a pre-established tolerance level. In the context of the proposed reliability technique, in the final iteration, CCD and Equation (4.2) will be used to generate a polynomial. Using the information on the required performance level, the corresponding LSF will be generated using the regression analysis. In general, it usually takes three to four iterations to reach convergence in terms of β values. Once the final β is found, the coordinates of the last checking point ($\boldsymbol{x}^*$) or MPFP will be calculated as:

$$\beta = \sqrt{(\boldsymbol{x}^*)^t(\boldsymbol{x}^*)} \tag{5.7}$$

Finally, based on the converged value of β, the corresponding p_f can be estimated as:

$$p_f = \Phi(-\beta) = 1.0 - \Phi(\beta) \tag{5.8}$$

A flowchart of the novel reliability approach in implementing PBSD is illustrated in Figure 5.6.

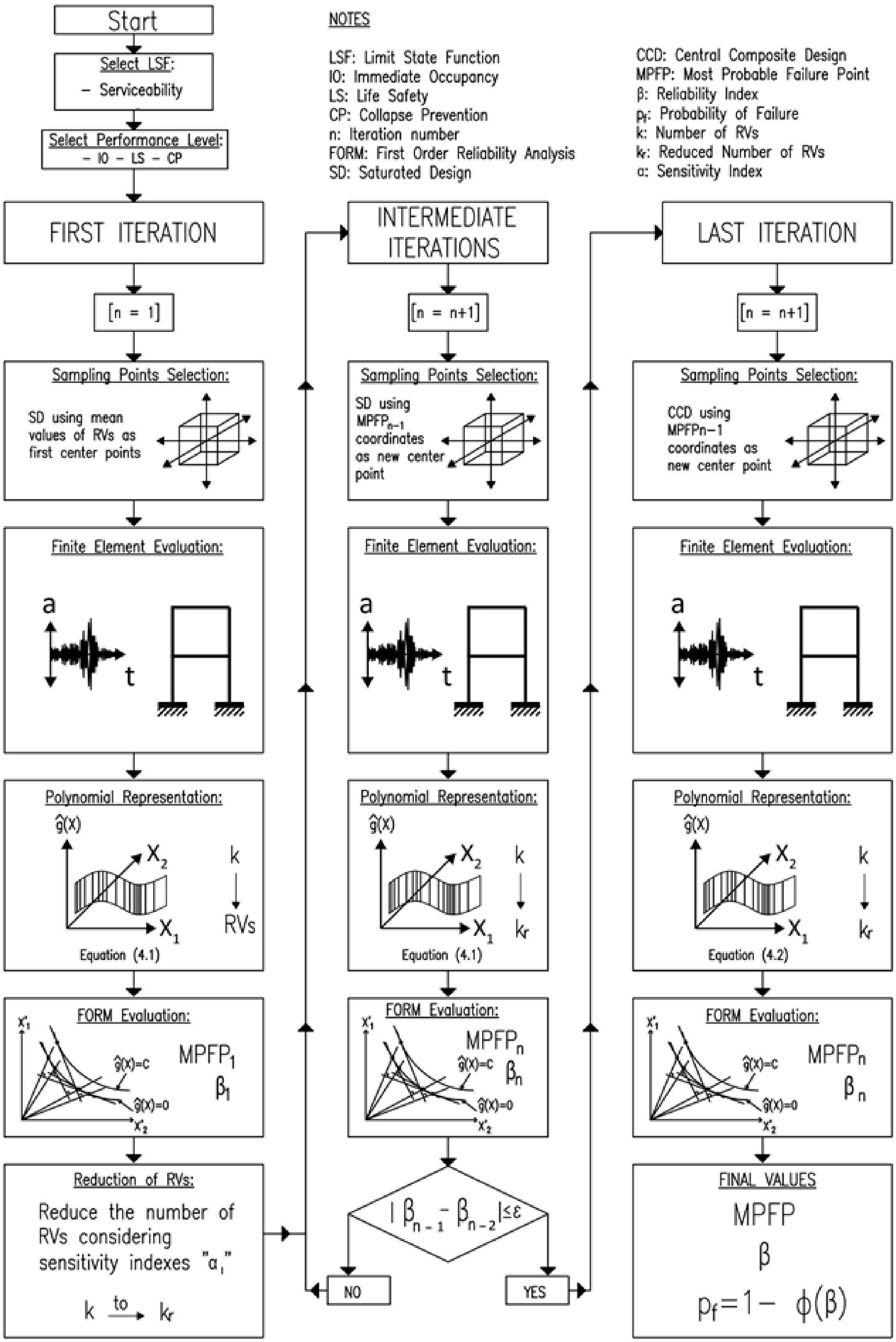

Figure 5.6 – Novel reliability technique flowchart.

5.3 Numerical Validation and Implementation of the Novel Reliability Technique in PBSD

Before accepting a new procedure, it is essential to verify its accuracy and efficiency. In addition, for this study, it is important to document the implementation potential in PBSD. To meet these objectives, four numerical examples are considered. Verification is demonstrated by studying a 2-story steel frame, excited using three acceleration time histories recorded during the 1994 Northridge earthquake. Reliability is calculated using the novel reliability technique and the well-established MCS. For implementation potential of the novel reliability technique in PBSD, three steel structures are considered: 3-, 9-, and 20-story. Their associated seismic risk is calculated considering FR and PR connections, and several ground motions in terms of IO, LS, and CP performance levels. Verification and implementation of the novel reliability technique are discussed next.

5.3.1 Verification - Accuracy: 2-Story Steel Frame

To verify accuracy of the proposed reliability technique, a 2-story steel frame shown in Figure 5.7-(a) is considered first. A relatively small structure is studied to facilitate the comparison of reliability estimations using the novel reliability technique and standard MCS. As previously discussed in this study, beam-to-column connections are considered to be either FR or PR type. Two types of PR connections are considered for the risk evaluation. The first type is denoted as pre-Northridge connections without any slots in the web (see Figure 2.2, Chapter 2) and the second type is denoted as post-Northridge connections (see Figure 2.3, Chapter 2) with two slot in the web of the beam. The four parameters (k, k_P, M_0, and N) of the Richard model to define every type of connection are summarized Table 5.1.

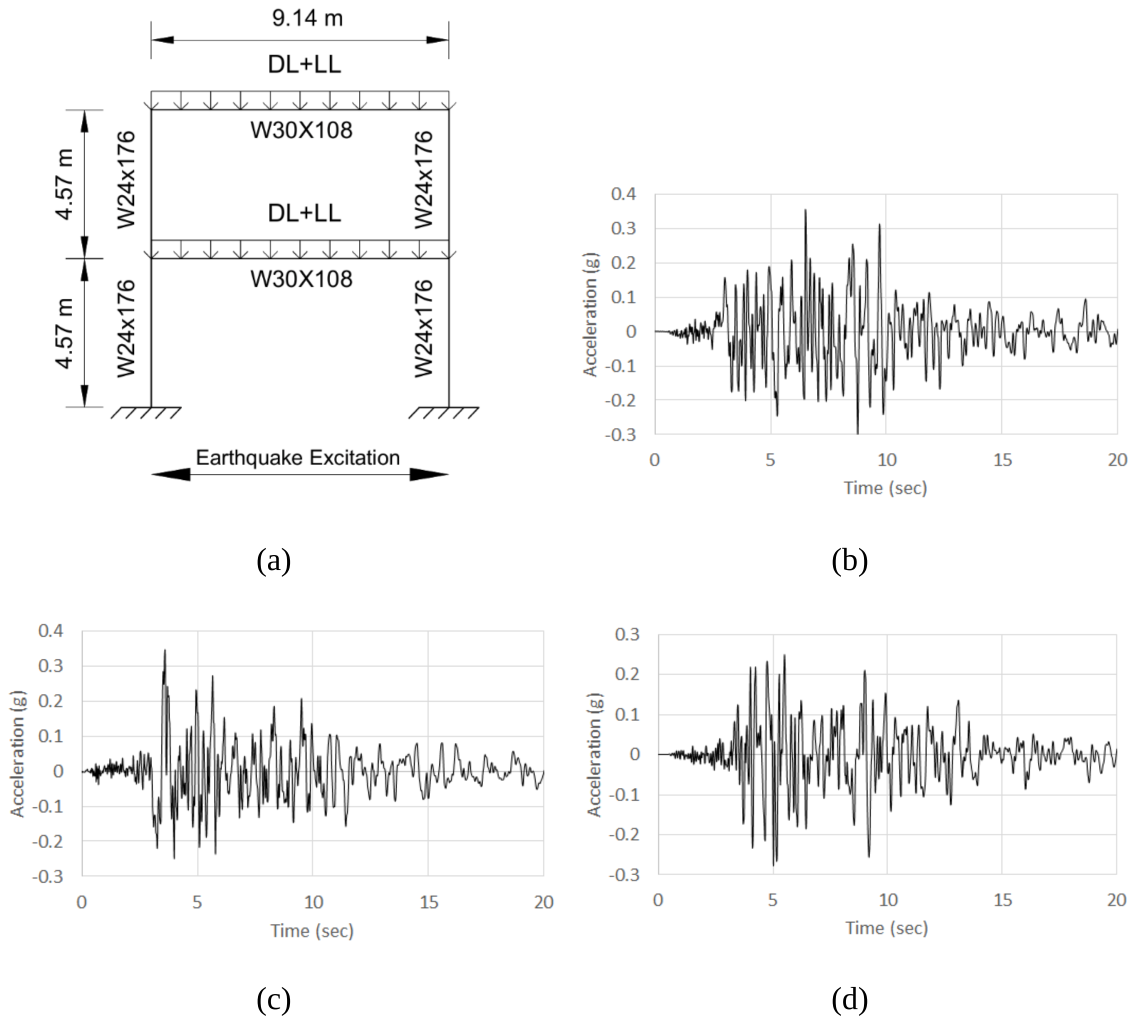

Figure 5.7 – (a) 2-story frame used for validations; (b) Canoga park station time history; (c) Nordhoff fire station; (d) Roscoe Blvd. station.

The frame is excited by three time histories recorded during the 1994 Northridge earthquake, as shown in Figure 5.7-(b), -(c), and -(d).

Table 5.1 – Pre- and Post-Northridge 4-Richard parameters of 2-Story steel frame.

Parameter	**PR Connection**	
	pre-Northridge	**post-Northridge**
k (kN-m/rad)	6.6663E+05	1.9546E+07
k_P (kN-m/rad)	1.1113E+04	4.5194E+03
M_0 (kN-m)	7.7835E+02	2.0145E+03
N	1.10	1.00

All RVs required to analyze the frame are summarized in Table 5.2. The information on uncertainty associated with them is also presented in Table 5.2. The uncertainty is expressed in terms of distribution, mean to nominal ratio ($\bar{X}/X_N$), nominal value, mean value, and coefficient of variation (COV). For this numerical example, $k = 14$ and $k_r = 5$. Reliability index, β, and p_f are estimated using the novel reliability technique for both LSFs of overall lateral and inter-story drift at the second-floor level, respectively. Beam-to-column connections are assumed to be FR, PR (pre-Northridge), and PR (post-Northridge) types. The allowable overall lateral and inter-story drift are considered to be 2.86 and 1.43 cm, respectively.

Table 5.2 – Uncertainty of RVs used for 2-story steel frame.

Random Variable	**Distribution**	$\bar{X}/X_N$	**Nominal** (X_N)	**Mean** ($\bar{X}$)	**COV**
E (kN/m^2)	Lognormal	1.00	1.9995E+08	1.9995E+08	0.06
Fy (kN/m^2)	Lognormal	1.05	3.4474E+05	3.6197E+05	0.10
A (m^2)	Lognormal	1.00	*	**	0.05
I_x (m^2)	Lognormal	1.00	*	**	0.05
DL (kN/m^2)	Normal	1.05	3.8304	4.0219	0.10
LL (kN/m^2)	Type 1	0.50	2.3940	1.1970	0.25
k (kN-m/rad)	Normal	1.00	*	***	0.15
kp (kN-m/rad)	Normal	1.00	*	***	0.15
Mo (kN-m)	Normal	1.00	*	***	0.15
N	Normal	1.00	*	***	0.05
g_e	Type 1	1.00	1.00	1.00	0.20

*Nominal value ($\boldsymbol{X_N}$) is calculated using mean value ($\bar{\boldsymbol{X}}$) and $\bar{\boldsymbol{X}}/\boldsymbol{X_N}$.
** Mean values of *A* and I_x can be found in steel construction manual (AISC, 2011). They are considered RVs for every girder and column.
***Mean values of four Richard parameters are reported in Table 5.1.

The β and p_f values for the two LSFs are shown in Table 5.3. They are estimated using 50,000 cycles of MCS. The Total Number of Deterministic Analyses (TNDA) required to implement the Novel Reliability Technique (NRT) is 94. Higher probabilities of failure of the frame for both LSFs in the presence of pre-Northridge PR connections, indicates their weaknesses compared with the FR and post-Northridge connections. The study confirms the recommendation made by SEAOC that pre-Northridge steel beam to column connections should not be used any more. However, in all cases, p_f values obtained by the

NRT and MCS methods are very similar indicating that the proposed method is accurate. Results also indicate that when NRT is used, similar reliability information can be extracted using only 94 TNDA instead of 50,000 corresponding to MCS.

Table 5.3 – Reliability results for 2-Story steel frame.

Ground Motion	LSF	Method	FR		PR (pre-Northridge)		PR (post-Northridge)	
			***β* (TNDA)**	***p_f***	***β* (TNDA)**	***p_f***	***β* (TNDA)**	***p_f***
Canoga Park Station	**Overall Drift**	**NRT**	3.5232 (94)	0.000213	3.4063 (94)	0.000329	3.6208 (94)	0.000147
		MCS	3.5149 (50,000)	0.000220	3.4141 (50,000)	0.000320	3.6331 (50,000)	0.000140
	Inter-story Drift	**NRT**	3.2429 (94)	0.000592	2.9825 (94)	0.001400	3.3357 (94)	0.000425
		MCS	3.2389 (50,000)	0.000600	2.9845 (50,000)	0.001420	3.3139 (50,000)	0.000460
Nordhoff Fire Station	**Overall Drift**	**NRT**	3.6949 (94)	0.000110	3.1690 (94)	0.000765	3.8853 (94)	0.000051
		MCS	3.7190 (50,000)	0.000100	3.1708 (50,000)	0.000760	3.8461 (50,000)	0.000060
	Inter-story Drift	**NRT**	3.2954 (94)	0.000491	2.8544 (94)	0.002200	3.5170 (94)	0.000218
		MCS	3.3139 (50,000)	0.000460	2.8627 (50,000)	0.002100	3.5149 (50,000)	0.000220
Roscoe Blvd Station	**Overall Drift**	**NRT**	3.6508 (94)	0.000131	3.0009 (94)	0.001300	3.9039 (94)	0.000040
		MCS	3.6331 (50,000)	0.000140	3.0068 (50,000)	0.001320	4.1075 (50,000)	0.000020
	Inter-story Drift	**NRT**	3.2528 (94)	0.000571	2.8192 (94)	0.002400	3.5969 (94)	0.000161
		MCS	3.2585 (50,000)	0.000560	2.8149 (50,000)	0.002440	3.5985 (50,000)	0.000160

5.3.2 Implementation Potential in PBSD – 3-, 9-, and 20-Story Steel Buildings

After verifying the accuracy of the NRT, it is now necessary to document or showcase its implementation potential in PBSD. To meet this objective, 3-, 9-, and 20-story steel buildings designed by experts in the Los Angeles area are considered. They are shown in Figures 5.8, 5.9, and 5.10. The sizes of the structural members are illustrated in the same Figures; as reported in FEMA-355C (2000).

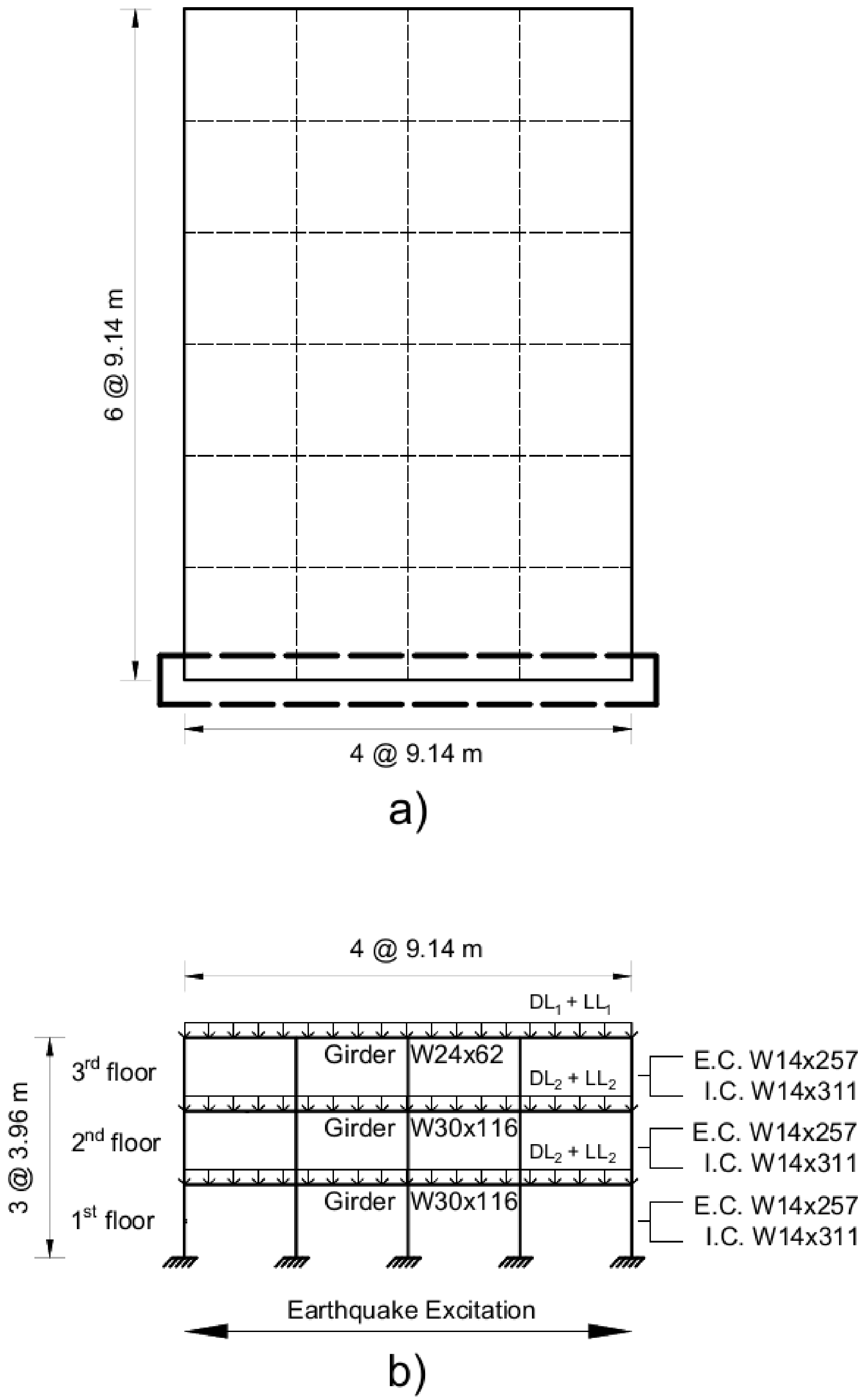

Figure 5.8 – 3-Story Building: (a) Plan view; (b) Elevation (E.C.=Exterior Columns; I.C.=Interior Columns).

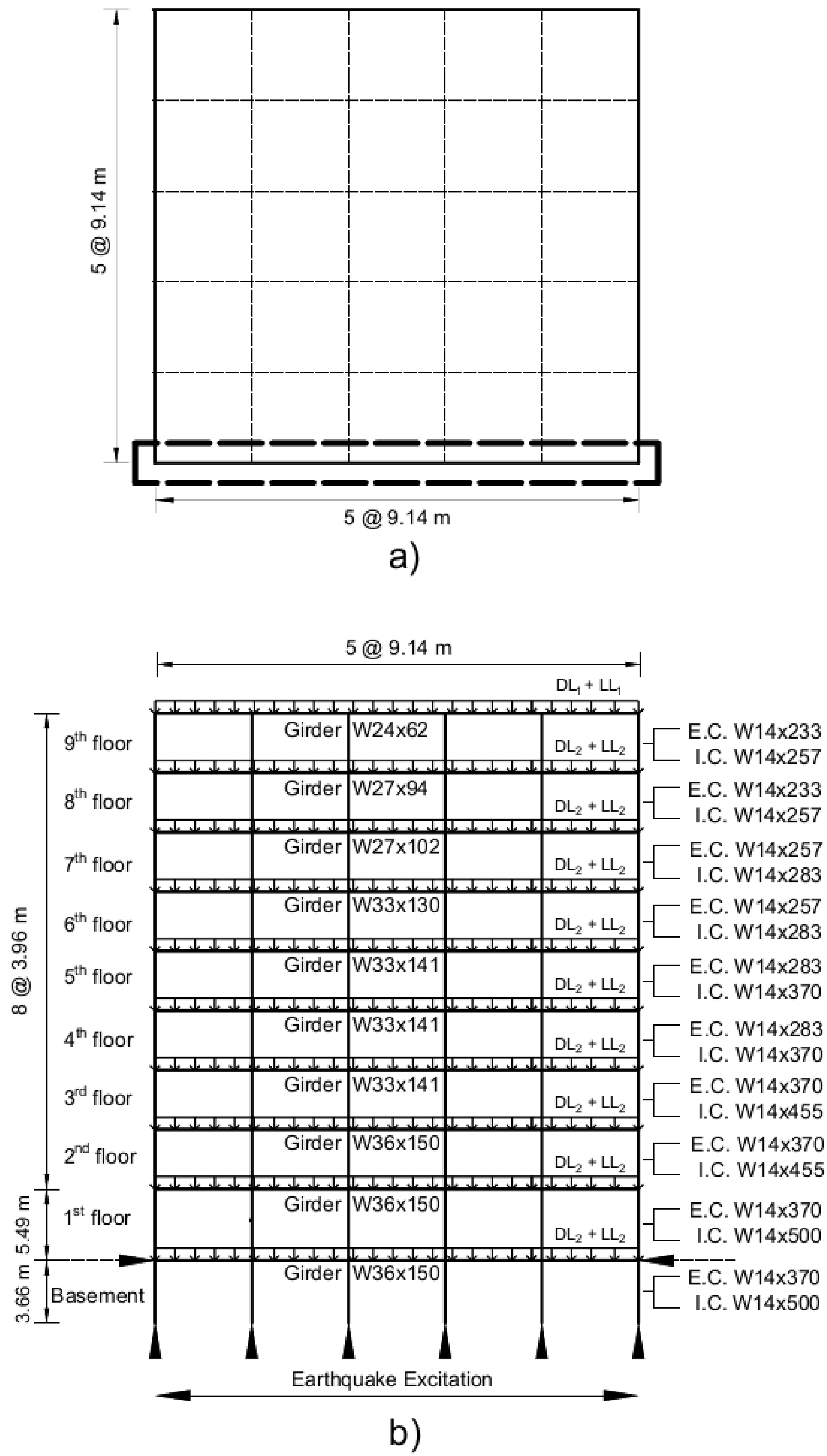

Figure 5.9 – 9-Story Building: (a) Plan view; (b) Elevation (E.C.=Exterior Columns; I.C.=Interior Columns).

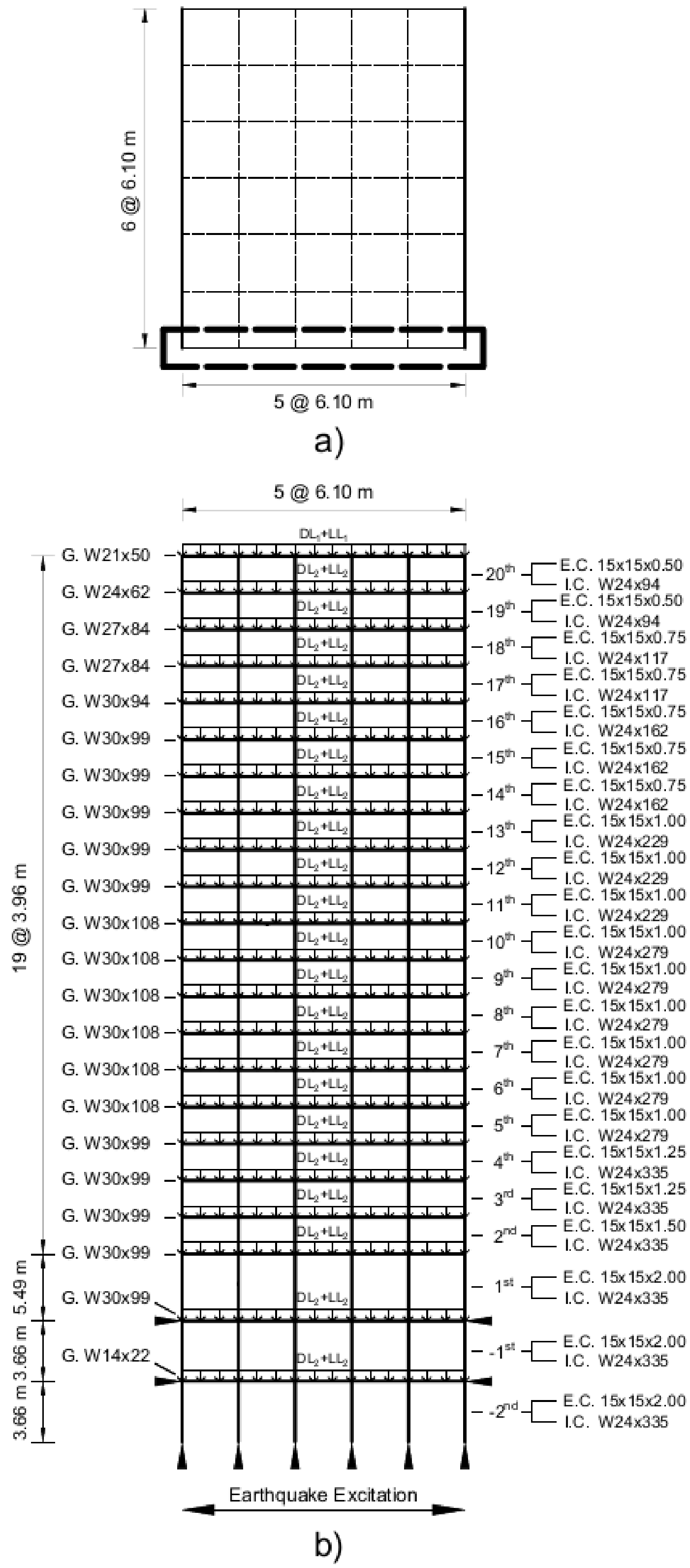

Figure 5.10 –20-Story Building: (a) Plan view; (b) Elevation (E.C.=Exterior Columns; I.C.=Interior Columns; G=Girder).

Information on RVs and uncertainty associated with the above steel buildings, required for the reliability analysis, is summarized in Table 5.4. The corresponding k values for the 3-, 9-, and 20-story buildings are 25, 91, and 110, respectively. In addition, for the three buildings, k_r is found to be 7.

Table 5.4 – Uncertainty of RVs used for 3-, 9-, and 20-story steel frames.

Random Variable	**Distribution**	$\bar{X}/X_N$	**Nominal (X_N)**	**Mean ($\bar{X}$)**	**COV**
E (kN/m^2)	Lognormal	1.00	1.9995E+08	1.9995E+08	0.06
Fy_G (kN/m^2)*	Lognormal	1.35	2.4821E+05	3.3509E+05	0.10
Fy_C (kN/m^2)*	Lognormal	1.15	3.4474E+05	3.9645E+05	0.10
A (m^2)	Lognormal	1.00	**	***	0.05
I_x (m^2)	Lognormal	1.00	**	***	0.05
DL_1 (kN/m^2)	Normal	1.05	3.9740	4.1727	0.10
DL_2 (kN/m^2)	Normal	1.05	4.5965	4.8263	0.10
LL_1 (kN/m^2)	Type 1	0.40	2.3940	0.9576	0.25
LL_2 (kN/m^2)	Type 1	0.40	2.3940	0.9576	0.25
k (kN-m/rad)	Normal	1.00	**	****	0.15
kp (kN-m/rad)	Normal	1.00	**	****	0.15
Mo (kN-m)	Normal	1.00	**	****	0.15
N	Normal	1.00	**	****	0.05
g_e	Type 1	1.00	1.00	1.00	0.20

*Yield stress of girder or column cross section reported in FEMA-355C.
**Nominal value ($\boldsymbol{X_N}$) is calculated using mean value ($\bar{\boldsymbol{X}}$) and $\bar{\boldsymbol{X}}/\boldsymbol{X_N}$.
***Mean values of A and I_x can be found in steel construction manual (AISC, 2011). They are considered RVs for every girder and column.
****Mean values of four Richard parameters are reported in Table 5.5.

Since SEAOC recommended not to use pre-Northridge connections anymore, they are not considered in following discussions. In the previous numerical example, the superiority of post-Northridge connections was demonstrated. Hence, only post-Northridge connections (see Figure 2.3, Chapter 2) are considered for the seismic risk evaluation of the 3-, 9-, and 20-story frames, respectively. The four parameters (k, k_P, M_0, and N) of the Richard model corresponding to every building are summarized in Table 5.5. They are required to define the corresponding M-θ relationship curves. In order to study the beneficial effect of using post-Northridge connections, the three steel structures are analyzed considering FR and PR (post-Northridge) beam-to-column connections.

Table 5.5 – 4-Richard parameters for the 3-, 9-, and 20-story buildings considering post-Northridge beam-to-column connections.

Model	**Level***	**Girder**	**Four Richard Parameters**			
			***k* (kN-m/rad)**	***kp* (kN-m/rad)**	***Mo* (kN-m)**	***N***
3-Story	Roof	W24X62	8.6433E+06	4.5194E+03	8.1519E+02	1.00
	3	W30X116	2.1354E+07	4.5194E+03	2.2134E+03	1.00
	2	W30X116	2.1354E+07	4.5194E+03	2.2134E+03	1.00
9-Story	Roof	W24X62	8.6433E+06	4.5194E+03	8.1519E+02	1.00
	9	W27X94	1.5705E+07	4.5194E+03	1.5920E+03	1.00
	8	W27X102	1.7230E+07	4.5194E+03	1.7597E+03	1.00
	7	W33X130	2.6382E+07	4.5194E+03	2.7664E+03	1.00
	6	W33X141	2.9037E+07	4.5194E+03	3.0585E+03	1.00
	5	W33X141	2.9037E+07	4.5194E+03	3.0585E+03	1.00
	4	W33X141	2.9037E+07	4.5194E+03	3.0585E+03	1.00
	3	W36X150	3.2822E+07	4.5194E+03	3.4748E+03	1.00
	2	W36X150	3.2822E+07	4.5194E+03	3.4748E+03	1.00
	1	W36X150	3.2822E+07	4.5194E+03	3.4748E+03	1.00
20-Story	Roof	W21X50	6.2142E+06	4.5194E+03	5.4798E+02	1.00
	20	W24X62	8.6433E+06	4.5194E+03	8.1519E+02	1.00
	19	W27X84	1.3784E+07	4.5194E+03	1.3807E+03	1.00
	18	W27X84	1.3784E+07	4.5194E+03	1.3807E+03	1.00
	17	W30X99	1.7626E+07	4.5194E+03	1.8032E+03	1.00
	16	W30X99	1.7626E+07	4.5194E+03	1.8032E+03	1.00
	15	W30X99	1.7626E+07	4.5194E+03	1.8032E+03	1.00
	14	W30X99	1.7626E+07	4.5194E+03	1.8032E+03	1.00
	13	W30X99	1.7626E+07	4.5194E+03	1.8032E+03	1.00
	12	W30X99	1.7626E+07	4.5194E+03	1.8032E+03	1.00
	11	W30X108	1.9546E+07	4.5194E+03	2.0145E+03	1.00
	10	W30X108	1.9546E+07	4.5194E+03	2.0145E+03	1.00
	9	W30X108	1.9546E+07	4.5194E+03	2.0145E+03	1.00
	8	W30X108	1.9546E+07	4.5194E+03	2.0145E+03	1.00
	7	W30X108	1.9546E+07	4.5194E+03	2.0145E+03	1.00
	6	W30X108	1.9546E+07	4.5194E+03	2.0145E+03	1.00
	5	W30X99	1.7626E+07	4.5194E+03	1.8032E+03	1.00
	4	W30X99	1.7626E+07	4.5194E+03	1.8032E+03	1.00
	3	W30X99	1.7626E+07	4.5194E+03	1.8032E+03	1.00
	2	W30X99	1.7626E+07	4.5194E+03	1.8032E+03	1.00
	1	W30X99	1.7626E+07	4.5194E+03	1.8032E+03	1.00
	-1	W14X22	1.8755E+06	4.5194E+03	7.0729E+01	1.00

*See Figures 5.8, 5.9, and 5.10 for more details.

As mentioned earlier, one of the major design variables is the future design earthquake time history. Since the profession is not capable of predicting it with confidence at present, the procedure suggested by Somerville (1997) is followed in this study. To consider a large amount of uncertainty, both in the amplitude and frequency contents, three sets of ground motions recommended by Somerville (1997) are used to excite the previously introduced steel buildings. Every set consists of ten (each with two orthogonal components) recorded and simulated ground motions representing return periods of 2475-year (2% probability of exceedance in 50 years), 475-year (10% probability of exceedance in 50 years), and 72-year (50% probability of exceedance in 50 years), respectively. The individual components of all the records were rotated to 45° with respect to the fault in order to study the directivity effects. The ground motions were scaled (the same scaling factor was used for the two components of a ground motion) such that, on average, their spectral values match with a least square error the USGS mapped values at 0.3, 1.0, and 2.0 seconds, and an additional predicted value at 4.0 seconds (Somerville, 1997). The target response spectra provided by USGS was based on the S_B/S_C soil type boundaries. Then, it was properly modified to represent soil type S_D (stiff soil associated with a measured shear wave velocity between 183 to 366 m/sec). Tables 5.6, 5.7 and 5.8 summarize the three sets of ground motions proposed by Somerville (1997) in terms of earthquake number (EQ), name, magnitude (Mw), scale factor (SF), peak ground acceleration (PGA), and excitation time (Time), respectively. More details about these sets of ground motions can be found in the literature (FEMA 355-C, 2000; Somerville, 1997).

Table 5.6 summarizes the set of ground motions corresponding to 2% probability of exceedance in 50 years (2475-year return period). These earthquakes are from near-fault recordings or simulations. The corresponding SFs are relatively close to unity. Recorded time histories are from the 1974 Tabas, 1989 Loma Prieta, 1994 Northridge, and 1995 Kobe earthquakes. Simulated time histories have a magnitude 7.1. They correspond to both Palos Verdes (a strike-slip fault) and Elysian Park (a blind thrust fault). In this study, ground motions corresponding to 2% Probability of Exceedance (PE) in 50 years are related to CP performance level as recommended in FEMA-350 (2000).

Table 5.6 – Ground motions corresponding to 2% PE in 50 years and CP performance level.

EQ	**Name**	**Mw**	**SF**	**PGA (g)**	**Time (sec)**
1	1995 Kobe	6.9	1.15	1.282	25.0
2	1995 Kobe	6.9	1.15	0.920	25.0
3	1989 Loma Prieta	7.0	0.82	0.418	20.0
4	1989 Loma Prieta	7.0	0.82	0.473	20.0
5	1994 Northridge	6.7	1.29	0.868	14.0
6	1994 Northridge	6.7	1.29	0.943	14.0
7	1994 Northridge	6.7	1.61	0.926	15.0
8	1994 Northridge	6.7	1.61	1.329	15.0
9	1974 Tabas	7.4	1.08	0.808	25.0
10	1974 Tabas	7.4	1.08	0.991	25.0
11	Elysian Park (simulated)	7.1	1.43	1.295	18.0
12	Elysian Park (simulated)	7.1	1.43	1.186	18.0
13	Elysian Park (simulated)	7.1	0.97	0.782	18.0
14	Elysian Park (simulated)	7.1	0.97	0.680	18.0
15	Elysian Park (simulated)	7.1	1.10	0.991	18.0
16	Elysian Park (simulated)	7.1	1.10	1.100	18.0
17	Palos Verdes (simulated)	7.1	0.90	0.711	25.0
18	Palos Verdes (simulated)	7.1	0.90	0.776	25.0
19	Palos Verdes (simulated)	7.1	0.88	0.500	25.0
20	Palos Verdes (simulated)	7.1	0.88	0.625	25.0

Ground motions related to 10% probability of exceedance in 50 years are summarized in Table 5.7. These ground motions were obtained from records of crustal earthquakes on soil category S_D. In order to match target values, these time histories were scaled by factors around 0.8 and 3.0. Two ground motions of the magnitude 7.3, corresponding to 1992 Landers earthquake, are included to represent large earthquakes on the San Andreas Fault at a comparable distance from Los Angeles. The remaining eight time histories are near-fault recordings of strike slip, oblique, and thrust earthquakes, ranging in magnitude from 6.0 to 7.0. In this research, as suggested in FEMA-350 (2000), ground motions corresponding to 10% probability of exceedance in 50 years are related to LS performance level.

Table 5.7 – Ground motions corresponding to 10% PE in 50 years and LS performance level.

EQ	Name	Mw	SF	PGA (g)	Time (sec)
21	Imperial Valley, 1940	6.9	2.01	0.461	25.0
22	Imperial Valley, 1940	6.9	2.01	0.675	25.0
23	Imperial Valley, 1979	6.5	1.01	0.393	15.0
24	Imperial Valley, 1979	6.5	1.01	0.488	15.0
25	Imperial Valley, 1979	6.5	0.84	0.301	15.0
26	Imperial Valley, 1979	6.5	0.84	0.234	15.0
27	Landers, 1992	7.3	3.20	0.421	30.0
28	Landers, 1992	7.3	3.20	0.425	30.0
29	Landers, 1992	7.3	2.17	0.519	30.0
30	Landers, 1992	7.3	2.17	0.360	30.0
31	Loma Prieta, 1989	7.0	1.79	0.665	16.0
32	Loma Prieta, 1989	7.0	1.79	0.969	16.0
33	Northridge, 1994, Newhall	6.7	1.03	0.678	15.0
34	Northridge, 1994, Newhall	6.7	1.03	0.657	15.0
35	Northridge, 1994, Rinaldi	6.7	0.79	0.533	14.0
36	Northridge, 1994, Rinaldi	6.7	0.79	0.579	14.0
37	Northridge, 1994, Sylmar	6.7	0.99	0.569	15.0
38	Northridge, 1994, Sylmar	6.7	0.99	0.817	15.0
39	North Palm Springs, 1986	6.0	2.97	1.018	16.0
40	North Palm Springs, 1986	6.0	2.97	0.986	16.0

Table 5.8 presents the set of ground motions related to 50% probability of exceedance in 50 years. These ground motions were obtained from records of crustal earthquakes on soil category S_D. Magnitude ranges from 5.7 to 7.7. In order to match the corresponding target response spectrum, SFs applied to this set of ground motions varies around 0.4 and 3.6. This set of ground motions is related to the IO performance level (FEMA-350, 2000). In summary, ground motions presented in Tables 5.6, 5.7, and 5.8 will be used to excite the three structures presented earlier (Figures 5.8, 5.9, and 5.10). Then, reliability information will be extracted in terms of both LSFs overall lateral drift and inter-story drift, respectively, as recommended by FEMA-350 (2000).

Table 5.8 – Ground motions corresponding to 50% PE in 50 years and IO performance level.

EQ	Name	Mw	SF	PGA (g)	Time (sec)
41	Coyote Lake, 1979	5.7	2.28	0.589	12.0
42	Coyote Lake, 1979	5.7	2.28	0.333	12.0
43	Imperial Valley, 1979	6.5	0.40	0.143	15.0
44	Imperial Valley, 1979	6.5	0.40	0.112	15.0
45	Kern, 1952	7.7	2.92	0.144	30.0
46	Kern, 1952	7.7	2.92	0.159	30.0
47	Landers, 1992	7.3	2.63	0.337	25.0
48	Landers, 1992	7.3	2.63	0.307	25.0
49	Morgan Hill, 1984	6.2	2.35	0.318	20.0
50	Morgan Hill, 1984	6.2	2.35	0.546	20.0
51	Parkfield, 1966, Cholame	6.1	1.81	0.780	15.0
52	Parkfield, 1966, Cholame	6.1	1.81	0.631	15.0
53	Parkfield, 1966, Cholame	6.1	2.92	0.693	15.0
54	Parkfield, 1966, Cholame	6.1	2.92	0.790	15.0
55	North Palm Springs, 1986	6.0	2.75	0.517	20.0
56	North Palm Springs, 1986	6.0	2.75	0.379	20.0
57	San Fernando, 1971	6.5	1.30	0.253	20.0
58	San Fernando, 1971	6.5	1.30	0.231	20.0
59	Whittier, 1987	6.0	3.62	0.768	15.0
60	Whittier, 1987	6.0	3.62	0.478	15.0

Structural reliability results corresponding to CP performance level (EQ-1 to EQ-20) and both LSFs overall lateral and inter-story drift are presented in Tables 5.9 and 5.10, respectively. Results are documented in terms of the three structures discussed earlier, using the allowable values (δ_{allow}) recommended by FEMA-350 (2000) (see Table 2.2, Chapter 2). For the 3-, 9-, and 20-story structures, the corresponding overall lateral drift allowable values are 59.44, 185.85, and 403.65 cm, respectively. Risk related to inter-story drift of the 3-, 9-, and 20-story buildings is calculated considering the 2nd, 4th, and 11th floors, respectively, using an allowable value equal to 19.81 cm. The above values correspond to CP performance level associated with earthquakes having a return period of 2475-year (see Table 5.6).

Table 5.9 –Reliability corresponding to overall drift LSF and CP performance level.

CP (2475-Year Return Period) - Overall Drift						
EQ	3-Story		9-Story		20-Story	
	FR	PR	FR	PR	FR	PR
	***β* (*TNDA*)**	***β* (*TNDA*)**	***β* (*TNDA*)**	***β* (*TNDA*)**	***β* (*TNDA*)**	***β* (*TNDA*)**
1	7.720 (209)	8.005 (239)	4.304 (341)	4.439 (341)	2.927 (379)	2.809 (394)
2	9.388 (209)	10.972 (209)	6.318 (341)	5.960 (341)	5.398 (379)	6.802 (379)
3	5.745 (209)	4.125 (209)	7.456 (356)	8.835 (341)	5.595 (394)	4.753 (379)
4	8.380 (209)	8.180 (209)	4.090 (356)	4.807 (341)	4.680 (379)	4.739 (379)
5	6.415 (209)	6.523 (209)	5.227 (356)	5.322 (341)	8.024 (394)	8.449 (379)
6	9.563 (209)	8.486 (209)	4.553 (356)	4.615 (341)	7.274 (379)	8.428 (379)
7	11.204 (209)	11.634 (209)	6.330 (341)	6.828 (341)	4.365 (379)	4.584 (409)
8	3.880 (209)	3.922 (209)	4.668 (356)	4.798 (356)	5.257 (379)	5.254 (379)
9	5.826 (209)	6.638 (209)	9.000 (341)	9.635 (356)	8.490 (394)	9.231 (379)
10	6.282 (209)	6.399 (239)	8.038 (341)	8.970 (341)	4.808 (409)	3.760 (409)
11	5.346 (209)	5.537 (209)	4.631 (341)	5.725 (341)	4.436 (379)	4.533 (379)
12	8.622 (209)	9.530 (209)	4.289 (341)	4.308 (341)	6.624 (379)	6.550 (409)
13	9.584 (209)	10.463 (209)	6.990 (341)	6.712 (341)	4.573 (379)	4.611 (379)
14	8.467 (209)	9.451 (209)	6.462 (341)	6.749 (341)	4.546 (409)	4.525 (409)
15	6.741 (209)	6.732 (209)	3.820 (341)	4.029 (341)	3.020 (394)	3.032 (409)
16	8.362 (209)	6.282 (209)	3.733 (341)	3.890 (356)	2.693 (379)	2.737 (409)
17	9.535 (209)	9.963 (209)	5.540 (356)	5.657 (341)	5.987 (379)	5.877 (379)
18	9.373 (224)	11.034 (209)	4.051 (356)	4.181 (341)	4.365 (409)	4.417 (379)
19	7.004 (209)	8.824 (209)	7.125 (341)	7.419 (356)	9.021 (379)	9.313 (409)
20	5.878 (224)	4.753 (224)	4.550 (356)	4.748 (341)	4.147 (379)	4.217 (379)

Several observations can be made related to Tables 5.9 and 5.10, respectively. The reliability index, β, values are very different for the three buildings when each of them is excited by 20 earthquake time histories. The results are expected since the frequency contents of each record are different. This observation justifies the use of multiple time histories to design a structure as suggested in more recent design guidelines (ASCE/SEI 7-

10, 2010). Furthermore, β values for FR connections are very similar to PR using post-Northridge connections. In addition, it can be observed in Tables 5.9 and 5.10 that only hundreds of *TNDA* are required for extracting the corresponding reliability information.

Table 5.10 –Reliability corresponding to inter-story drift LSF and CP performance level.

CP (2475-Year Return Period) - Inter-Story Drift						
EQ	**3-Story**		**9-Story**		**20-Story**	
	FR	**PR**	**FR**	**PR**	**FR**	**PR**
	***β* (*TNDA*)**	***β* (*TNDA*)**	***β* (*TNDA*)**	***β* (*TNDA*)**	***β* (*TNDA*)**	***β* (*TNDA*)**
1	8.393 (239)	8.761 (209)	3.830 (341)	3.952 (341)	3.849 (379)	3.887 (409)
2	9.512 (209)	9.790 (209)	5.999 (341)	5.553 (356)	5.500 (409)	5.242 (379)
3	5.925 (209)	5.374 (239)	6.206 (341)	7.062 (341)	5.075 (379)	5.186 (379)
4	8.571 (209)	8.524 (209)	4.690 (356)	4.421 (371)	4.292 (379)	4.388 (379)
5	5.836 (209)	5.896 (209)	4.723 (341)	4.796 (341)	5.701 (394)	5.720 (394)
6	7.681 (209)	8.169 (239)	4.175 (356)	4.219 (356)	3.835 (409)	4.015 (379)
7	8.709 (209)	9.021 (209)	5.969 (341)	6.342 (341)	4.581 (379)	4.584 (409)
8	5.520 (209)	5.475 (209)	4.055 (341)	4.169 (356)	4.412 (394)	4.436 (379)
9	4.962 (209)	5.480 (239)	8.296 (356)	8.564 (341)	7.474 (379)	7.469 (379)
10	5.814 (209)	5.972 (209)	7.587 (341)	8.157 (356)	3.230 (379)	3.620 (409)
11	4.742 (209)	5.010 (209)	4.135 (341)	4.255 (341)	4.549 (379)	5.984 (409)
12	7.060 (239)	7.721 (239)	3.938 (356)	3.920 (371)	3.504 (409)	3.795 (379)
13	9.209 (209)	8.598 (209)	6.939 (341)	7.332 (341)	4.116 (379)	4.170 (379)
14	7.805 (209)	8.643 (209)	4.419 (341)	4.589 (341)	4.287 (379)	4.260 (409)
15	5.478 (209)	5.818 (209)	3.468 (356)	3.672 (356)	2.337 (379)	2.429 (379)
16	8.748 (239)	8.778 (209)	3.334 (341)	3.498 (341)	2.321 (379)	2.435 (409)
17	7.385 (209)	7.279 (209)	5.300 (341)	5.385 (356)	6.773 (394)	5.993 (409)
18	8.782 (239)	9.842 (209)	3.643 (356)	3.775 (341)	4.048 (379)	4.127 (409)
19	7.266 (209)	7.714 (209)	6.643 (341)	7.013 (341)	8.119 (409)	7.968 (379)
20	6.611 (239)	6.093 (209)	4.143 (356)	4.345 (341)	3.922 (394)	3.997 (409)

Tables 5.11 and 5.12 summarize the reliability results of the three steel structures, corresponding to LS performance level and ground motions related to a 475-year return period (EQ-21 to EQ-40, see Table 5.7). In Tables 5.11 and 5.12, both LSFs are considered overall lateral and inter-story drift, respectively (FEMA-350, 2000).

Table 5.11 –Reliability corresponding to overall drift LSF and LS performance level.

LS (475-Year Return Period) - Overall Drift						
EQ	**3-Story**		**9-Story**		**20-Story**	
	FR	**PR**	**FR**	**PR**	**FR**	**PR**
	***β* (*TNDA*)**	***β* (*TNDA*)**	***β* (*TNDA*)**	***β* (*TNDA*)**	***β* (*TNDA*)**	***β* (*TNDA*)**
21	4.929 (209)	5.605 (209)	6.690 (341)	6.969 (341)	4.549 (379)	4.910 (409)
22	6.804 (209)	7.172 (209)	6.701 (341)	6.754 (341)	6.302 (409)	6.417 (379)
23	4.180 (224)	4.332 (209)	6.795 (341)	7.017 (356)	4.199 (379)	5.708 (379)
24	7.636 (209)	7.321 (209)	2.737 (356)	3.916 (341)	8.169 (409)	8.381 (409)
25	7.594 (209)	7.117 (209)	7.369 (341)	7.487 (341)	6.549 (409)	6.585 (379)
26	6.115 (209)	6.020 (209)	6.854 (356)	6.777 (341)	6.806 (379)	6.258 (394)
27	6.725 (224)	6.720 (209)	7.168 (341)	7.177 (371)	3.183 (394)	3.175 (409)
28	9.284 (209)	11.395 (209)	6.778 (356)	6.832 (341)	4.753 (409)	4.016 (394)
29	7.774 (224)	7.443 (209)	3.473 (356)	3.634 (341)	6.580 (379)	6.083 (379)
30	10.246 (209)	9.776 (209)	5.416 (341)	5.468 (356)	4.949 (379)	4.021 (379)
31	5.638 (209)	5.729 (209)	4.309 (341)	4.429 (341)	4.309 (379)	4.320 (379)
32	4.061 (209)	4.189 (224)	8.302 (356)	8.551 (371)	3.378 (379)	3.832 (379)
33	4.583 (209)	4.900 (209)	5.102 (341)	4.967 (356)	5.578 (379)	5.851 (379)
34	4.736 (209)	5.820 (209)	3.933 (356)	4.005 (341)	5.651 (409)	5.479 (409)
35	5.520 (209)	5.613 (209)	4.310 (356)	4.368 (341)	6.837 (409)	6.750 (379)
36	8.521 (209)	8.865 (209)	3.766 (341)	3.828 (356)	4.271 (379)	4.402 (409)
37	3.720 (209)	4.771 (209)	5.446 (356)	5.767 (356)	4.235 (379)	4.299 (379)
38	3.103 (209)	3.144 (209)	3.904 (356)	4.032 (356)	4.396 (409)	4.393 (379)
39	4.164 (224)	3.915 (209)	6.854 (341)	6.932 (356)	4.133 (409)	4.753 (409)
40	2.727 (209)	4.660 (209)	4.048 (341)	4.120 (356)	4.862 (379)	4.860 (379)

For overall lateral drift, the allowable values are 29.72, 92.93, and 201.83 cm, corresponding to the 3-, 9-, and 20-story frames, respectively. For inter-story drift, the allowable drift used is equal to 9.91 cm. It is related to the story height of the 2nd, 4th, and 11th floor levels, corresponding to the 3-, 9-, and 20-story structures, respectively.

Table 5.12 –Reliability corresponding to inter-story drift LSF and LS performance level.

LS (475-Year Return Period) - Inter-Story Drift						
EQ	**3-Story**		**9-Story**		**20-Story**	
	FR	**PR**	**FR**	**PR**	**FR**	**PR**
	***β* (*TNDA*)**	***β* (*TNDA*)**	***β* (*TNDA*)**	***β* (*TNDA*)**	***β* (*TNDA*)**	***β* (*TNDA*)**
21	9.156 (224)	9.431 (209)	4.295 (356)	4.658 (341)	4.450 (409)	4.854 (409)
22	4.777 (209)	4.643 (209)	6.426 (341)	6.430 (356)	4.600 (379)	4.728 (379)
23	8.105 (209)	8.295 (209)	6.333 (341)	6.575 (356)	5.708 (409)	5.850 (409)
24	6.789 (209)	6.732 (209)	10.079 (341)	9.086 (356)	6.304 (379)	7.274 (409)
25	10.083 (224)	10.668 (209)	6.871 (356)	7.036 (341)	4.632 (409)	4.961 (379)
26	7.976 (224)	8.156 (209)	6.988 (341)	7.116 (356)	7.578 (379)	8.245 (409)
27	8.505 (224)	8.540 (209)	6.645 (371)	6.663 (356)	6.481 (409)	6.164 (394)
28	9.884 (224)	10.199 (209)	6.367 (341)	6.432 (356)	7.003 (379)	7.012 (409)
29	9.072 (209)	9.608 (209)	3.153 (356)	3.315 (356)	3.977 (409)	3.028 (409)
30	9.811 (209)	8.912 (209)	5.098 (341)	5.036 (356)	3.556 (379)	3.111 (379)
31	8.491 (209)	8.455 (224)	3.935 (356)	4.078 (356)	3.603 (379)	3.671 (394)
32	6.047 (209)	6.128 (224)	7.973 (371)	8.858 (356)	3.010 (409)	2.847 (379)
33	4.126 (209)	4.457 (209)	4.378 (341)	4.443 (356)	3.257 (379)	3.479 (409)
34	8.141 (209)	8.706 (224)	3.466 (356)	3.536 (341)	4.058 (409)	4.033 (409)
35	4.960 (224)	5.023 (209)	3.933 (371)	4.008 (356)	4.764 (379)	4.769 (409)
36	8.898 (209)	9.374 (209)	3.392 (356)	3.439 (356)	3.190 (379)	3.337 (379)
37	9.661 (209)	10.774 (209)	5.111 (356)	5.353 (341)	3.790 (394)	3.780 (409)
38	4.559 (209)	4.612 (209)	3.292 (356)	3.410 (356)	3.604 (379)	3.627 (379)
39	5.738 (224)	5.724 (209)	6.640 (341)	6.846 (341)	2.860 (379)	3.793 (409)
40	5.592 (209)	6.511 (209)	3.595 (341)	3.628 (341)	3.732 (409)	3.786 (379)

Numerous interesting observations can be made by analyzing Tables 5.11 and 5.12. In terms of β values, results clearly indicate that designing a structure for one earthquake time history is inadequate. Designing a structure using multiple time histories, as suggested in ASCE/SEI 7-10 (2010), is a step in the right direction. From the results presented in Tables 5.11 and 5.12, it can be justified that the allowable values suggested in FEMA-350 (2000) are reasonable. The β values fall within a range, satisfying the intent of the code (ASCE/SEI 7-10, 2010). It is important to mention as well that β values for PR using a post-Northridge connection are very similar to the corresponding ones using FR connection. In addition, it can be observed in Tables 5.11 and 5.12 that *TNDAs* required for extracting the corresponding reliability information range from 209 to 409.

Reliability results of IO performance level associated with ground motions with a return period of 72-year (EQ-41 to EQ-60, see Table 5.8) are reported in Tables 5.13 and 5.14, corresponding to overall lateral and inter-story drift, respectively. Considering IO performance level, allowable drift values for overall lateral LSF related to the 3-, 9-, and 20-story structures are 8.32, 26.02, and 56.51 cm, respectively (FEMA-350, 2000). For inter-story drift LSF, the allowable drift value is equal to 2.77 cm, corresponding to the 2nd, 4th, and 11th floor levels of the 3-, 9-, and 20-story steel frames, respectively. Quite a lot of interesting comments can be documented with respect to Tables 5.13 and 5.14. Similar to the other performance levels analyzed, it can be observed in Tables 5.13 and 5.14 that β values vary between different ground motions. It demonstrates that several ground motions should be used when the seismic performance of structures is evaluated. On the other hand, similar values of β are observed for FR and PR (post-Northridge) connections, reflecting the beneficial effect of using PR (post-Northridge) connections.

Table 5.13 –Reliability corresponding to overall drift LSF and IO performance level.

IO (72-Year Return Period) - Overall Drift						
EQ	**3-Story**		**9-Story**		**20-Story**	
	FR	**PR**	**FR**	**PR**	**FR**	**PR**
	***β* (*TNDA*)**	***β* (*TNDA*)**	***β* (*TNDA*)**	***β* (*TNDA*)**	***β* (*TNDA*)**	***β* (*TNDA*)**
41	2.145 (224)	2.230 (209)	2.682 (356)	2.722 (356)	2.771 (379)	2.770 (409)
42	6.510 (209)	6.483 (224)	3.623 (356)	3.773 (341)	4.215 (394)	4.214 (379)
43	8.993 (209)	9.184 (209)	4.560 (356)	4.676 (356)	3.344 (379)	3.508 (394)
44	10.014 (224)	10.537 (209)	7.412 (341)	7.414 (341)	2.020 (379)	2.452 (409)
45	8.020 (209)	8.304 (209)	4.880 (356)	4.954 (341)	4.323 (409)	4.411 (379)
46	8.685 (209)	8.895 (224)	5.111 (341)	5.120 (341)	4.484 (379)	4.299 (409)
47	4.217 (209)	4.393 (209)	3.595 (341)	3.814 (356)	2.493 (394)	2.164 (394)
48	6.404 (209)	6.981 (209)	7.125 (356)	7.390 (341)	2.372 (379)	2.010 (409)
49	6.905 (209)	6.207 (224)	3.638 (341)	3.850 (356)	2.599 (409)	2.580 (379)
50	5.105 (224)	5.088 (224)	4.502 (341)	5.205 (341)	4.475 (409)	4.676 (379)
51	2.162 (209)	2.174 (224)	4.325 (356)	4.416 (371)	3.138 (379)	3.070 (409)
52	2.140 (209)	2.219 (224)	7.049 (341)	7.016 (356)	7.675 (379)	7.969 (379)
53	4.853 (209)	4.922 (209)	4.238 (356)	4.274 (356)	6.686 (394)	7.121 (409)
54	3.297 (224)	3.368 (209)	3.980 (356)	4.465 (356)	4.083 (409)	4.038 (379)
55	5.681 (209)	5.994 (209)	3.124 (341)	3.191 (356)	4.405 (379)	4.346 (409)
56	7.650 (209)	7.864 (224)	3.145 (356)	3.121 (341)	3.325 (409)	3.001 (379)
57	7.076 (224)	7.845 (224)	5.852 (341)	5.879 (341)	4.505 (379)	4.187 (394)
58	7.989 (209)	7.930 (209)	3.345 (341)	3.496 (356)	3.287 (409)	3.362 (379)
59	2.284 (209)	2.603 (224)	1.447 (341)	1.495 (356)	2.998 (379)	3.096 (379)
60	2.404 (224)	2.601 (209)	1.449 (341)	1.362 (341)	4.385 (409)	4.379 (379)

In summary, it is observed in Tables 5.13 and 5.14 that only hundreds of *TNDA* are required to compute the corresponding β values. This verifies the efficiency of the novel reliability technique proposed in this dissertation.

Table 5.14 –Reliability corresponding to inter-story drift LSF and IO performance level.

IO (72-Year Return Period) - Inter-Story Drift						
	3-Story		9-Story		20-Story	
EQ	FR	PR	FR	PR	FR	PR
	***β* (*TNDA*)**	***β* (*TNDA*)**	***β* (*TNDA*)**	***β* (*TNDA*)**	***β* (*TNDA*)**	***β* (*TNDA*)**
41	1.548 (209)	1.644 (209)	2.277 (341)	2.194 (341)	2.575 (394)	2.751 (409)
42	5.873 (209)	5.851 (224)	3.119 (371)	3.302 (371)	3.598 (379)	3.670 (379)
43	9.621 (224)	9.964 (224)	4.287 (356)	4.368 (341)	3.026 (379)	3.214 (379)
44	9.142 (209)	9.762 (224)	6.890 (356)	6.919 (356)	4.500 (379)	4.811 (409)
45	7.423 (209)	7.555 (224)	4.352 (341)	4.503 (356)	3.525 (409)	3.854 (379)
46	7.863 (224)	8.025 (224)	4.610 (356)	4.632 (341)	4.071 (394)	4.140 (409)
47	3.704 (209)	3.885 (209)	3.202 (371)	3.416 (341)	2.419 (409)	2.171 (379)
48	5.559 (224)	6.000 (209)	6.671 (341)	7.554 (356)	2.070 (379)	2.000 (409)
49	4.584 (209)	4.686 (209)	3.192 (341)	3.414 (356)	2.120 (409)	2.064 (379)
50	4.529 (209)	4.504 (224)	4.504 (356)	4.390 (341)	3.142 (379)	4.483 (394)
51	1.568 (224)	1.584 (209)	4.101 (356)	4.146 (371)	2.195 (409)	2.416 (409)
52	1.561 (209)	1.652 (209)	6.201 (341)	7.502 (356)	3.907 (379)	2.736 (394)
53	4.266 (209)	4.290 (224)	3.666 (356)	3.791 (356)	6.125 (394)	6.405 (409)
54	2.766 (224)	2.843 (209)	3.860 (341)	4.396 (356)	2.436 (409)	2.614 (379)
55	5.086 (209)	5.331 (209)	2.730 (356)	2.775 (341)	2.964 (379)	3.085 (409)
56	5.611 (209)	5.918 (224)	2.695 (341)	2.691 (356)	4.913 (409)	4.020 (394)
57	6.362 (224)	6.947 (209)	5.756 (356)	5.653 (341)	2.676 (409)	2.621 (379)
58	7.598 (209)	7.276 (224)	2.996 (341)	3.139 (356)	3.809 (379)	2.743 (409)
59	2.347 (224)	2.433 (224)	1.406 (356)	1.439 (341)	3.500 (409)	3.450 (379)
60	1.892 (224)	2.104 (209)	2.017 (341)	1.946 (356)	2.362 (379)	2.226 (394)

For the ease of discussions, the mean, $\beta\mu$, values are given in Table 5.15 and the information is used in the subsequent discussions. Higher β values indicate lower probability of failure (p_f). Generally, $\beta\mu$ values are observed to be the highest for the CP performance level and lowest for the IO performance level, confirming the intent of the PBSD guidelines (FEMA-350, 2000). For most of the cases, $\beta\mu$ values for the overall lateral drift are found to be higher than the inter-story drift, indicating the latter is more critical. It is also interesting to note the distinct separations of performance levels of CP, LS, and IO in Table 5.15. This indicates that the SFs to match target spectral values at certain frequencies are rational (Somerville, 1997). The results also demonstrate that the performance of buildings when connections are considered to be FR and post-Northridge PR types, are very similar. The presence of two slots in the web of the beam in beam-column connections does not reduce their stiffness; in fact, they improve their behavior. The study also indicate that post-Northridge connections significantly improve the behavior and are expected to provide adequate structural reliability. For seismically active regions, designing beam-to-column connections as post-Northridge PR type instead of FR type, is expected to be economical.

Table 5.15 – Mean Structural reliability (βμ) of 3-, 9-, and 20-story buildings.

Performance Level	**Structure**	**Overall Lateral Drift**		**Inter-Story Drift**	
		FR	**PR**	**FR**	**PR**
		βμ ***(p_f)***	***βμ*** ***(p_f)***	***βμ*** ***(p_f)***	***βμ*** ***(p_f)***
CP (2475-Year Return Period)	**3-Story**	7.666 (8.8818E-15)	7.873 (1.7764E-15)	7.200 (3.0109E-13)	7.398 (6.9167E-14)
	9-Story	5.559 (1.3566E-08)	5.881 (2.0390E-09)	5.075 (1.9375E-07)	5.251 (7.5638E-08)
	20-Story	5.311 (5.4513E-08)	5.431 (2.8020E-08)	4.596 (2.1534E-06)	4.685 (1.3998E-06)
LS (475-Year Return Period)	**3-Story**	5.903 (1.7848E-09)	6.225 (2.4078E-10)	7.518 (2.7756E-14)	7.747 (4.6629E-15)
	9-Story	5.498 (1.9206E-08)	5.652 (7.9296E-09)	5.399 (3.3507E-08)	5.497 (1.9315E-08)
	20-Story	5.184 (1.0859E-07)	5.225 (8.7078E-08)	4.508 (3.2721E-06)	4.617 (1.9466E-06)
IO (72-Year Return Period)	**3-Story**	5.627 (9.1685E-09)	5.791 (3.4984E-09)	4.945 (3.8072E-07)	5.113 (1.5854E-07)
	9-Story	4.254 (1.0499E-05)	4.382 (5.8797E-06)	3.927 (4.3006E-05)	4.109 (1.9869E-05)
	20-Story	3.879 (5.2443E-05)	3.883 (5.1588E-05)	3.297 (4.8862E-04)	3.274 (5.3018E-04)

Figures 5.11, 5.12, and 5.13 are introduced in order to document similarities among FR and PR (post-Northridge) connections in terms of structural reliability (β values).

Figure 5.11 illustrates reliability indexes (β) corresponding to the 3-story building using FR and PR (post-Northridge) connections, respectively. A proper affinity can easily be detected in terms of structural risk when FR and PR (post-Northridge) connections are used. However, a higher variability is observed for overall lateral drift in comparison with inter-story drift.

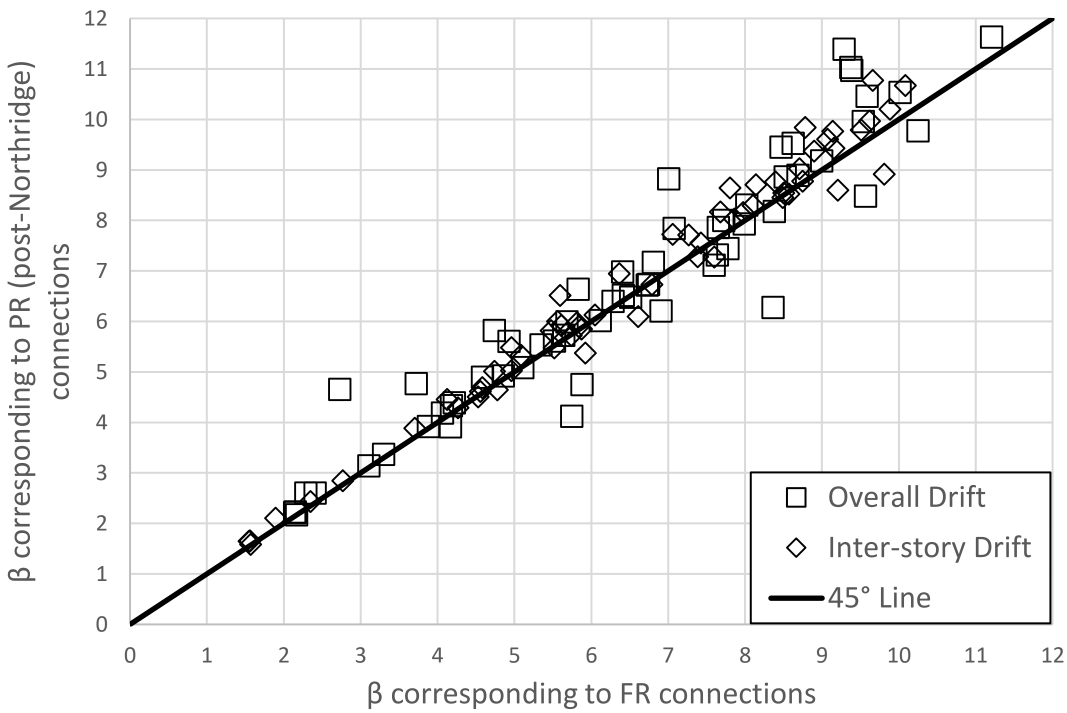

Figure 5.11 – Reliability comparison among FR and PR (post-Northridge) connections for 3-story building.

Numerical relations among reliability index (β) for the 9-story building considering FR and PR (post-Northridge) connections are shown in Figure 5.12. A strong analogy between β values can be observed using FR and PR connections. This confirms the favorable effects of using the post-Northridge connections introduced in this dissertation. Again, a little higher difference between reliability indexes is observed for overall drift with respect to inter-story drift.

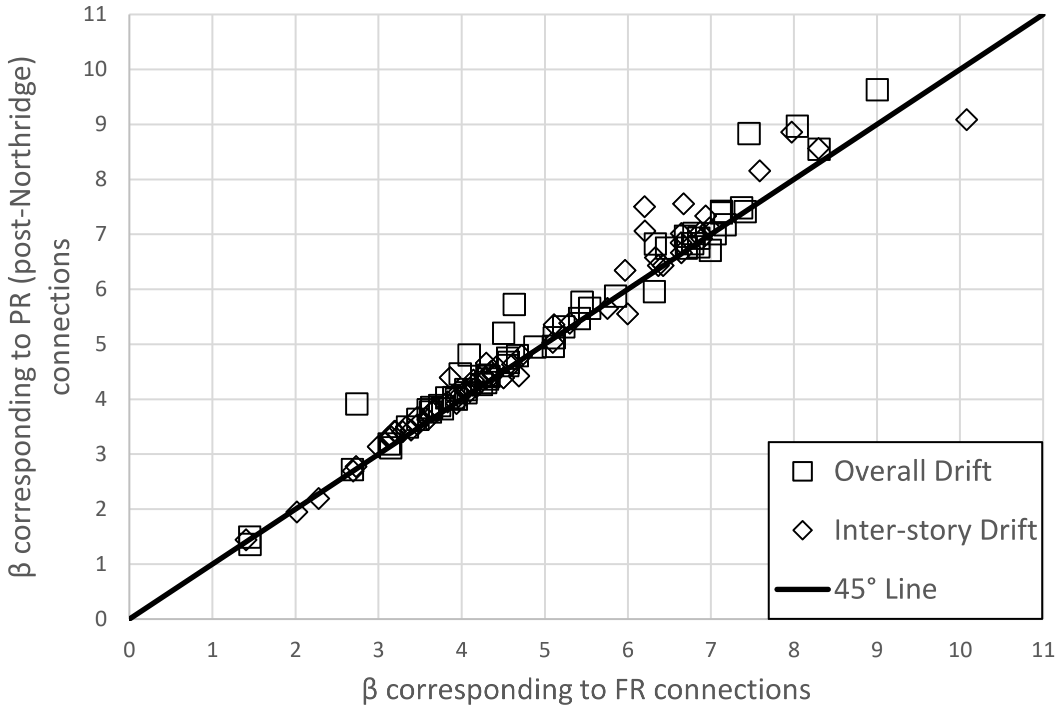

Figure 5.12 – Reliability comparison among FR and PR (post-Northridge) connections for 9-story building.

Figure 5.13 illustrates reliability indexes for overall and inter-story drift, respectively, corresponding to the 20-story building, using FR and PR (post-Northridge) connections. In addition to previous examples, a considerable positive similarity is detected between the use of FR and PR (post-Northridge) connections. Then, results illustrated in Figures 5.11, 5.12, and 5.13 demonstrate that for the 3-, 9-, and 20-story buildings the use of PR post-Northridge beam-to-column connection is beneficial. It is demonstrated to be a step in the right direction towards the design of seismic tolerant steel structures.

Hence, the accuracy and robustness of the alternative reliability approach was demonstrated, verified, and documented with the help of several numerical examples. It can be stated that post-Northridge structural design increases the possibility of achieving more earthquake-resistant steel structures.

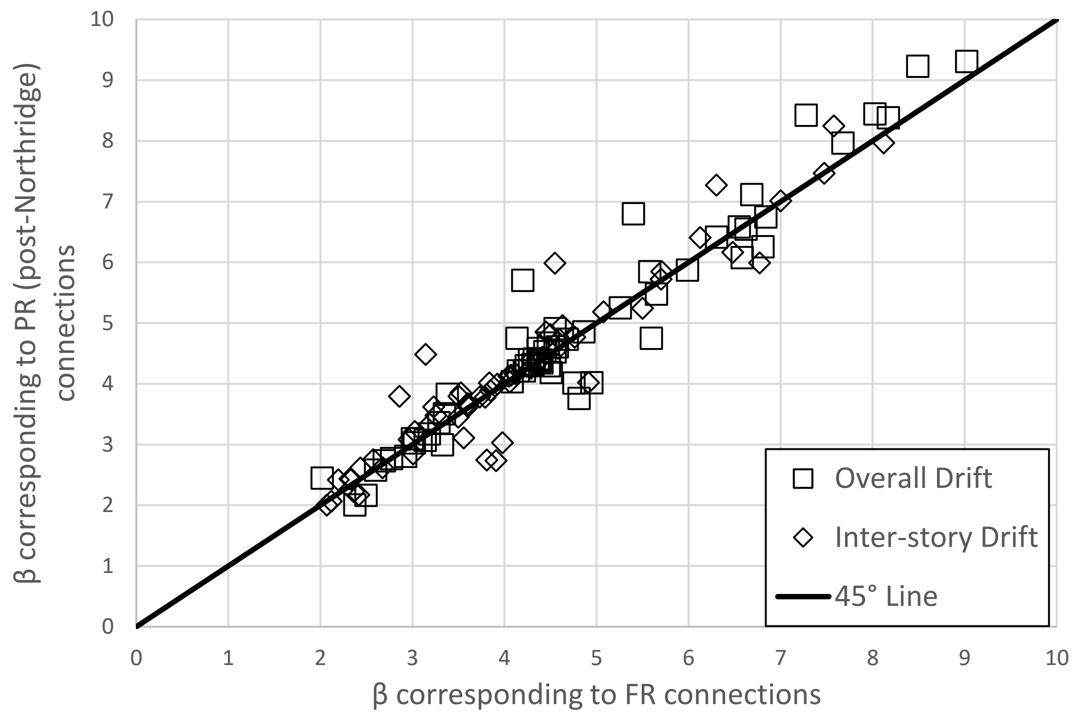

Figure 5.13 – Reliability comparison among FR and PR (post-Northridge) connections for 20-story building.

5.4 Summary and Concluding Remarks

The novel reliability technique proposed in this study was explained in this chapter. Its implementation in PBSD was properly documented in terms of IO, LS, and CP performance levels. In order to calculate β, p_f, and MPFP, an intelligent integration of RSM, FEM, FORM, SD, and CCD was precisely presented. Several issues related to uncertainties in loads and resistance parameters were addressed. At the end of this chapter, the novel reliability technique was validated with the help of a 2-story steel frame. It was demonstrated that the extracted reliability information using the proposed technique was very similar with respect to MCS. Then, in terms of accuracy, it was validated. The robustness of the novel reliability technique was documented by the risk evaluation of three steel buildings with different heights. Several beneficial characteristics were detected when post-Northridge connections are used. The importance of properly modeling structures was documented considering PR instead of FR connections. In addition, the superiority of the proposed technique was verified by computing the risk of structures performing hundreds of deterministic FE analyses, instead of thousands or millions generally required in MCS. Thus, at this point of this study, a novel reliability technique for implementation in PBSD is completely viable. However, in most cases, real ground motions were used for exciting structures, and then extracting the corresponding reliability information. An extension is proposed in the next chapter in terms of artificially simulated ground motions.

CHAPTER 6
STRUCTURAL RELIABILITY USING SIMULATED GROUND MOTIONS

6.1 Introduction

Previous discussions documented the viability of a novel reliability technique for implementation in PBSD. Verification and application potential of the novel reliability technique were demonstrated, and several steel buildings were studied considering different performance levels. However, ground motion records were obtained from previous investigations (Somerville, 1997). Generally, structural engineers face the problem of ground motion selection for a specific site. In some cases, there are not enough records representing the corresponding seismic hazard of the zone. When the availability of ground motions is not sufficient for nonlinear analyses, the ASCE building code (ASCE 7-10, 2010) recommends the use of “appropriate simulated ground motions”. Unfortunately, no further guidance is reported for the simulation of ground motions. The main problem is how to generate such ground motions representing the seismic hazard of the zone. Several investigations reported in the literature propose how to generate ground motions using appropriate simulation techniques (Burks, Zimmerman and Baker, 2015; Cacciola and Deodatis, 2011; Cacciola and Zentner, 2012; Shinozuka and Deodatis, 1988; Suarez and Montejo, 2005; Yamamoto and Baker, 2013; Shields, 2014). In this chapter, the Broadband Platform (BBP) developed by the Southern California Earthquake Center (SCEC) is used for the proper simulation of ground motions (SCEC, 2016). Validation of the BBP is performed with the help of a 2-story steel frame, it is excited using real and simulated versions of the 1994 Northridge earthquake. A comparison is made in terms of response spectrum and structural reliability. Once BBP is properly verified, an adequate set of ground motions is generated for a specific zone in the Los Angeles area. Using such a set of ground motions, 11 of them are properly selected considering a target response spectrum and dynamic properties of a 3-story steel frame. Then, reliability is calculated for the 3-story steel frame which was designed for the location under consideration. At the end of this chapter, the application of the novel reliability technique considering simulated ground motions is demonstrated.

6.2 The SCEC Broadband Platform

The BBP is an open source software developed by the SCEC for hybrid broadband simulation of ground motions (SCEC, 2016). Several researchers have developed modules of the BBP for nonlinear site effects, low and high frequency seismogram synthesis, and rupture generation (Zeng, Anderson, and Yu, 1994; Motazedian, and Atkinson, 2005; Graves, and Pitarka, 2010; Schmedes, Archuleta, and Lavallee, 2010; Mai, Imperatori, and Olsen, 2010). In order to simulate ground motions using the BBP, a single-plane fault surface should be described. A simple description of the rupture is defined by the user in terms of hypocenter location, magnitude, rupture dimensions, dip, strike, and rake. These terms will be discussed later in this research. This information is used by the BBP rupture generator module and a detailed time history of slip on the rupture surface is created. A list of stations where ground motion time histories will be simulated is also provided by the user in terms of latitude, longitude, and V_{S30} (shear wave velocity of the top 30 m of the subsurface profile) of the specific site. Both low- and high-frequency synthesis modules compute deterministically and stochastically frequency seismograms, respectively. This will be discussed later. Such seismograms are then merged together at a frequency of approximately 1 Hz. Furthermore, an empirical site amplification is applied to its Fourier spectrum depending on the corresponding target value of V_{S30}. At the end, results are reported for every station in terms of three acceleration time histories: North-South (N-S), East-West (E-W), and Vertical (V). The BBP sequential process is illustrated in Figure 6.1.

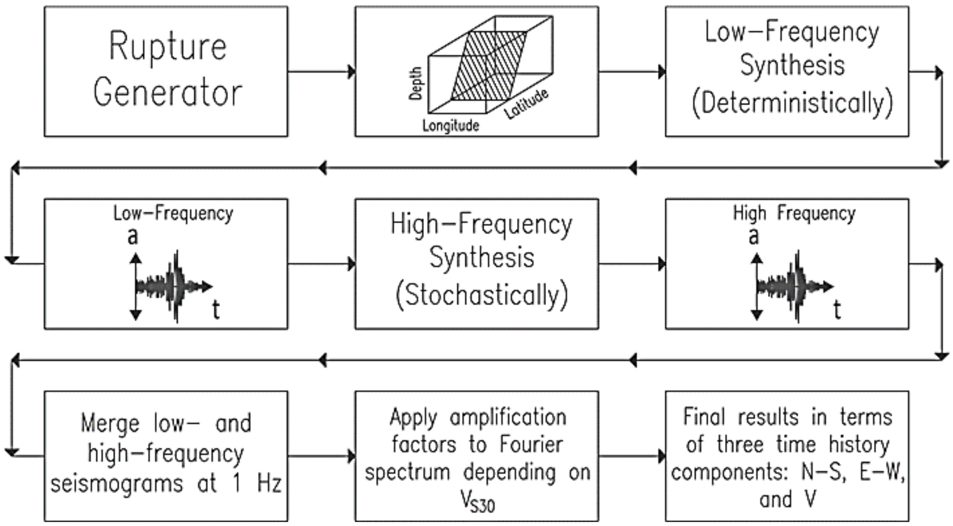

Figure 6.1 – Flowchart of the BBP process.

6.2.1 Rupture Generation, Low- and High-Frequency Seismograms, and Specific Amplification Factors

A description of the physical characteristics of the rupture is a fundamental element of the BBP. In order to properly generate the rupture, the required parameters are hypocenter (rupture initiation point), fault location (latitude and longitude), geometry (width, length, dip, and strike), rake (slip direction), and magnitude. Figure 6.2 illustrates the BBP rupture characterization. As previously mentioned, the BBP process begins computing individually the low- and high-frequency ranges, and then both are combined to produce a time history (Hartzell et al., 1999). When frequencies are smaller than 1 Hz, the approach is deterministic, containing a theoretical representation of wave propagation and fault rupture, trying to replicate recorded ground-motion amplitudes and waveforms (Graves and Pitarka, 2010). When frequencies are greater than 1 Hz, the BBP uses a stochastic representation in terms of source radiation, combining scattering effects and a simplified theoretical representation of wave propagation. Since wave propagation effects and source radiation are mainly stochastic at frequencies equal to or higher than 1 Hz, different simulation approaches for different frequency bands are used. This demonstrates the absence of information about higher frequencies of ground motions. At the final stage of the BBP process, nonlinear amplification factors are applied to the simulated time histories. They incorporate site-specific geologic conditions in the final seismograms. Nonlinear amplification factors are based on the V_{S30} of the site of interest (Walling, Silva and Abrahamson, 2008).

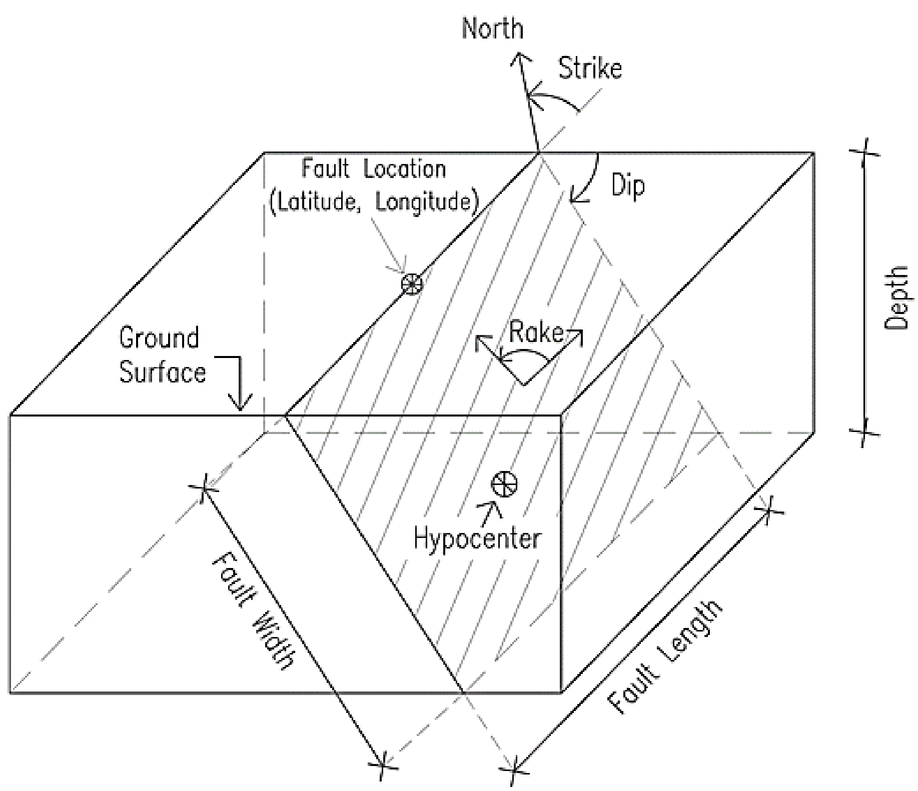

Figure 6.2 – Illustration of rupture.

In this dissertation, the BBP version v16.5.0 (SCEC, 2016) is used for ground motion simulations. As previously discussed, several methods are available in the BBP for the simulation of ground motions (Zeng, Anderson and Yu, 1994; Liu, Archuleta and Hartzell, 2006; Schmedes, Archuleta and Lavallee, 2010; Schmedes, Archuleta and Lavallee, 2013; Motazedian and Atkinson, 2005; Atkinson et al., 2009; Boore, 2009; Graves and Pitarka, 2010; Mai, Imperatori, and Olsen, 2010; Mena, et al., 2010). Among them, the method proposed by Graves and Pitarka (2010), hereafter denoted as GP method, is utilized for the simulations as discussed in the next sections.

6.3 Validation of BBP

Before the application of the BBP in the calculation of structural risk, it must be properly validated. In order to verify the accuracy of BBP, the 1994 Northridge earthquake is generated. Four locations in southern California are selected where real time histories of the 1994 Northridge earthquake are available. They are: (1) Santa Susana, (2) Alhambra – Fremont, (3) Littlerock – Brainard, and (4) Rancho Palos Verdes. Using the BBP v16.5.0 (SCEC, 2016) and GP method, simulations corresponding to the 1994 Northridge earthquake are performed for the above four stations. The rupture was generated using a magnitude of 6.7, fault length and width equal to 20 and 27 km, respectively. Strike, rake, and dip were considered as 122°, 105°, and 40°, respectively. Figure 6.3 illustrates the corresponding response spectra for real and simulated versions of the 1994 Northridge earthquake. Response spectra are plotted considering the N-S and E-W components of every station under study. It can be observed in Figure 6.3 that response spectra for simulated and real ground motions are very similar. In order to validate the BBP in terms of structural risk, the novel reliability technique presented in this dissertation is used. The 2-Story steel frame shown earlier in Figure 5.7-(a) is excited using real and simulated versions of the 1994 Northridge earthquake as illustrated in Figure 6.3. Risk is obtained using the RVs summarized earlier in Table 5.2.

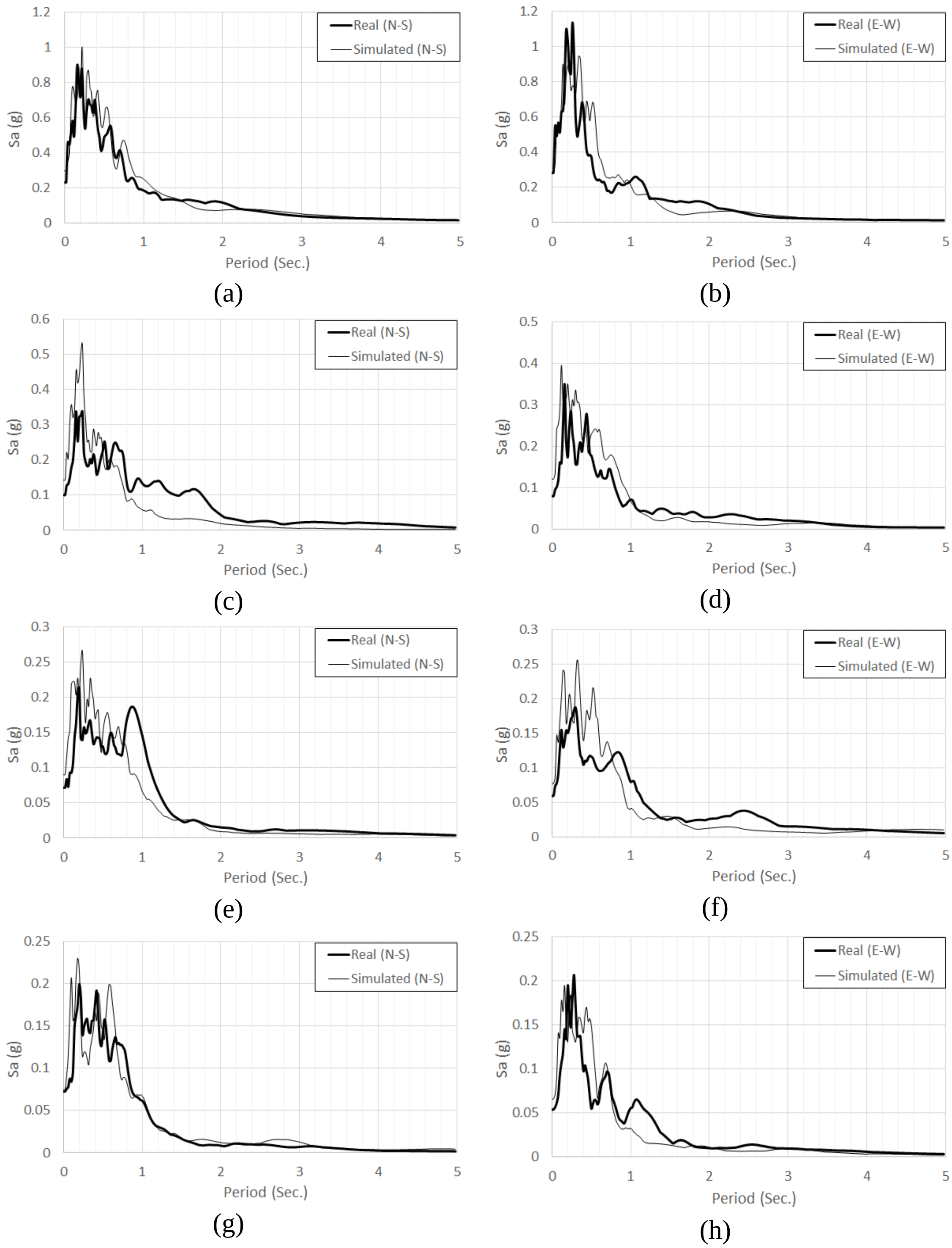

Figure 6.3 – 1994 Northridge earthquake real and simulated response spectra: (a) Santa Susana N-S, (b) Santa Susana E-W, (c) Alhambra - Fremont N-S, (d) Alhambra - Fremont E-W, (e) Littlerock – Brainard N-S, (f) Littlerock - Brainard E-W, (g) Rancho Palos Verdes N-S, and (h) Rancho Palos Verdes E-W.

Since the objective of this chapter is to demonstrate the applicability of the novel reliability technique using simulated ground motions, only FR connections are considered for the reliability analysis of the 2-story frame. Table 6.1 summarizes the results of the structural reliability of the 2-Story frame using simulated and real ground motions, respectively. It can be observed that β and p_f are very similar for simulated and real versions of ground motions. In terms of mean reliability index (β_μ), it can be observed that the performance of the building is more critical for inter-story drift conditions. Based on the results presented in this section, the accuracy calculating structural risk of the BBP version v16.5.0 (SCEC, 2016) is validated.

Table 6.1 – Structural reliability for real and simulated ground motions.

Station	Overall Lateral Drift		Inter-Story Drift	
	Real	Simulated	Real	Simulated
	β	β	β	β
Santa Susana N-S	3.6137	3.9556	3.0545	3.0810
Santa Susana E-W	3.8067	3.6250	3.4565	3.3591
Alhambra - Fremont N-S	4.2430	4.3176	4.1201	4.3594
Alhambra - Fremont E-W	5.2484	5.4095	5.4044	5.3108
Littlerock – Brainard N-S	3.8286	3.2042	3.8287	3.2146
Littlerock - Brainard E-W	4.2997	4.1296	3.8521	3.1554
Rancho Palos Verdes N-S	4.8866	4.6424	3.8442	3.3492
Rancho Palos Verdes E-W	3.5370	3.3994	3.8271	3.8622
β_μ	4.1830	4.0854	3.9235	3.7115
(p_f)	(1.4384E-05)	(2.2000E-05)	(4.3636E-05)	(1.0302E-04)

6.4 Application of BBP

As previously discussed, when nonlinear time domain analysis is required, it is common for structural engineers to face the problem of lack of ground motion records. It was verified in the previous section that the BBP v16.5.0 (SCEC, 2016) can be used for the proper generation of ground motions for a specific site. To demonstrate the applicability of the BBP, a set of ground motions is generated for a specific site in Los Angeles area. Since the 3-story steel frame presented earlier in Figure 5.8 was designed for the Los Angeles zone, it is used as a case study. Considering that an appropriate number of real ground motions are difficult to obtain for near-fault locations (Burks, Zimmerman and Baker, 2015), the Raymond Hill Fault located close to Los Angeles is considered in this study. The BBP is used for the proper simulation of ground motions at 16 stations placed around the building and fault location. Figure 6.4 illustrates the location of the building, stations, and fault.

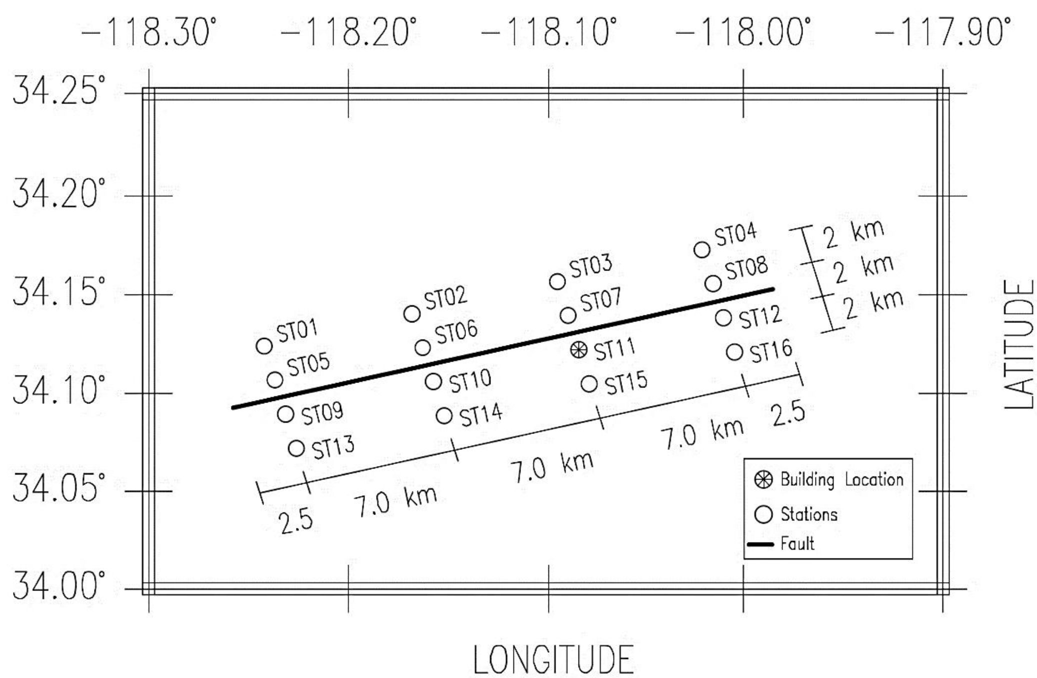

Figure 6.4 – Stations, building, and fault location.

In order to simulate ground motions using the BBP, a description of the rupture is necessary. The seismic hazard analysis for the building location yields an earthquake magnitude equal to 6.7 (USGS, 2008). In addition, fault length and width were considered to be 26 and 20 km, respectively (Wells and Coppersmith, 1994). Strike, rake, and dip are equal to 75°, 0°, and 90°, respectively. Six hypocenters were used in order to simulate the variability of their location in the rupture. Figure 6.5 illustrates the location of every hypocenter considered in this study.

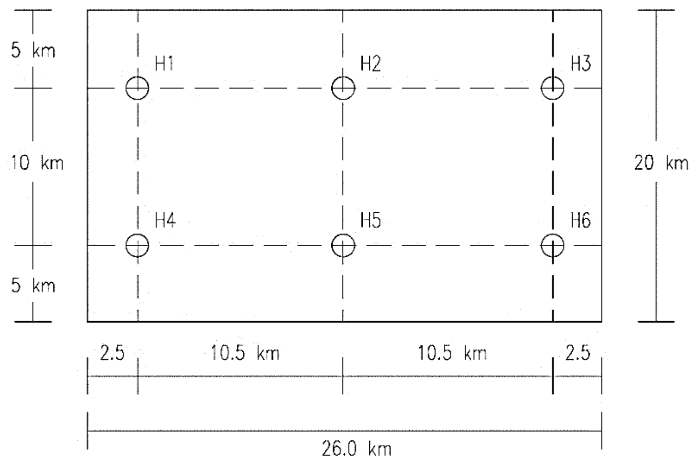

Figure 6.5 – Location of hypocenters.

Considering six hypocenters, sixteen stations, and two components (N-S and E-W) per station, a total of 192 grounds motions were generated. For the sake of clarity, the corresponding response spectra of the simulated ground motions are plotted in Figure 6.6.

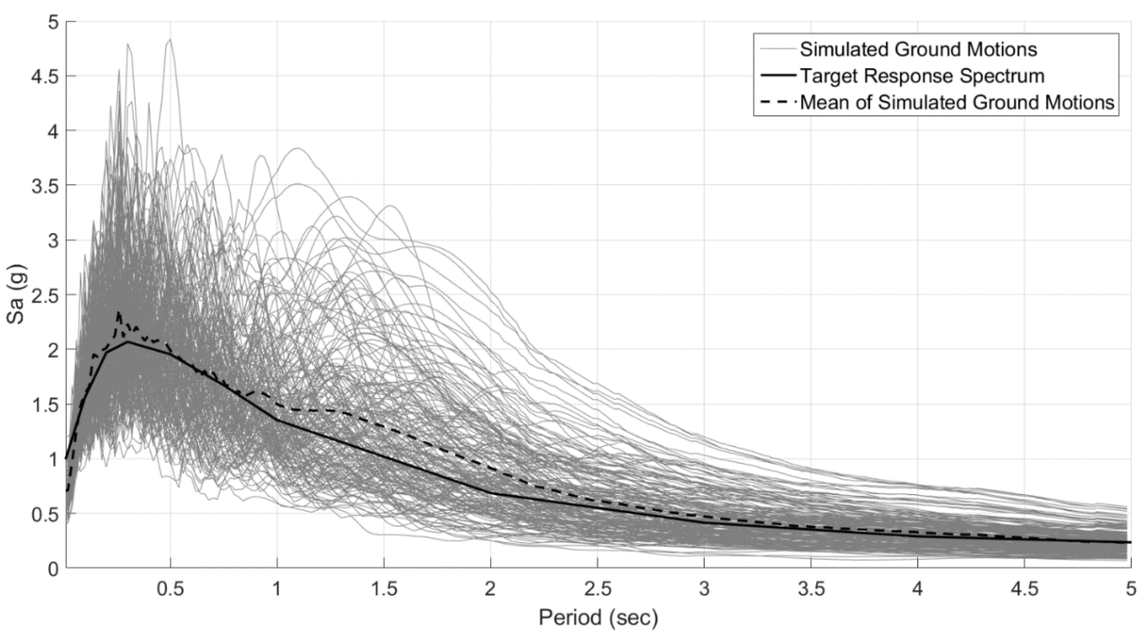

Figure 6.6 – Simulated ground motions response spectra and target response spectrum.

Using the above set of simulated ground motions, 11 ground motion time histories were selected using as a target the Uniform Hazard Spectrum (UHS) with a probability of exceedance of 2% in 50 years (Azizsoltani, Gaxiola-Camacho and Haldar, 2017). UHS has been used by the engineering community as a suitable target response spectra for seismic-resistant design over the last 20 years. It is the graphical representation of the spectral acceleration versus the period. In this sense, UHS represents the response spectrum of the site having the same rate of exceedance for the spectral acceleration at all periods. The generation of the UHS is performed using the United States Geological Survey (USGS) web application (USGS, 2008). The USGS application provides a data base for generating site-specific hazard curves in terms of spectral acceleration versus annual rate of exceedance for spectral periods of Peak Ground Acceleration (PGA) of 0.1, 0.2, 0.3, 0.5, 1.0, 2.0, 3.0, 4.0, and 5.0 seconds. Using the site-specific hazard curves generated by the USGS application, information of the spectral accelerations for each period can be obtained.

Currently, the use of at least 7 site-specific ground motions is recommended by the ASCE 7-10 (2010) construction code. However, more recent studies suggest to consider at least 11 of such site-specific ground motions (Zimmerman et al., 2015). In this study, 11 time histories scaled from the previously generated ground motion set (Figure 6.6) are selected. The scaling is generally done by matching the probabilistic ground motion response spectrum at the fundamental period of the structure (T). A Scale Factor (SF) close to 1 is generally desired (Watson-Lamprey and Abrahamson, 2006). However, SF can vary widely. Bommer and Acevedo (2004) recommended limiting the upper limit of SF up to a value of 4. The potential scaled site-specific time histories are ranked in terms of suitability in order to select only the most appropriate ones. To determine the suitability factor, *T* is considered to range between 0.2*T* and 2.0*T*. ASCE 7-10 (2010) defines this range to be between 0.2*T* and 1.5*T* in section 16.1.3.1. However, Baker (2010) noticed large sensitivity of structures to the response spectra at highly nonlinear phases at periods longer than 1.5*T*. Then, the period of the structure is considered to range between 0.2*T* and 2.0*T*. This interval is subdivided into 40 equal subintervals to consider the information on the lower and upper bounds. The matching of ground motions for higher vibration modes is based on the lower bound, while the upper bound is used for matching ground motions at highly nonlinear phases. The total error is evaluated for each ground motion as the Square Squares Errors (SSE) as recommended by Jayaram, Lin and Baker (2011). Finally, only 11 ground motions with the smallest SSE are considered for each suite of time histories, and are considered for the reliability evaluation. The eleven ground motions response spectra, mean value of them, and target response spectrum are illustrated in Figure 6.7. They were selected for the 3-story steel frame (Figure 5.8) with *T*=0.85 seconds.

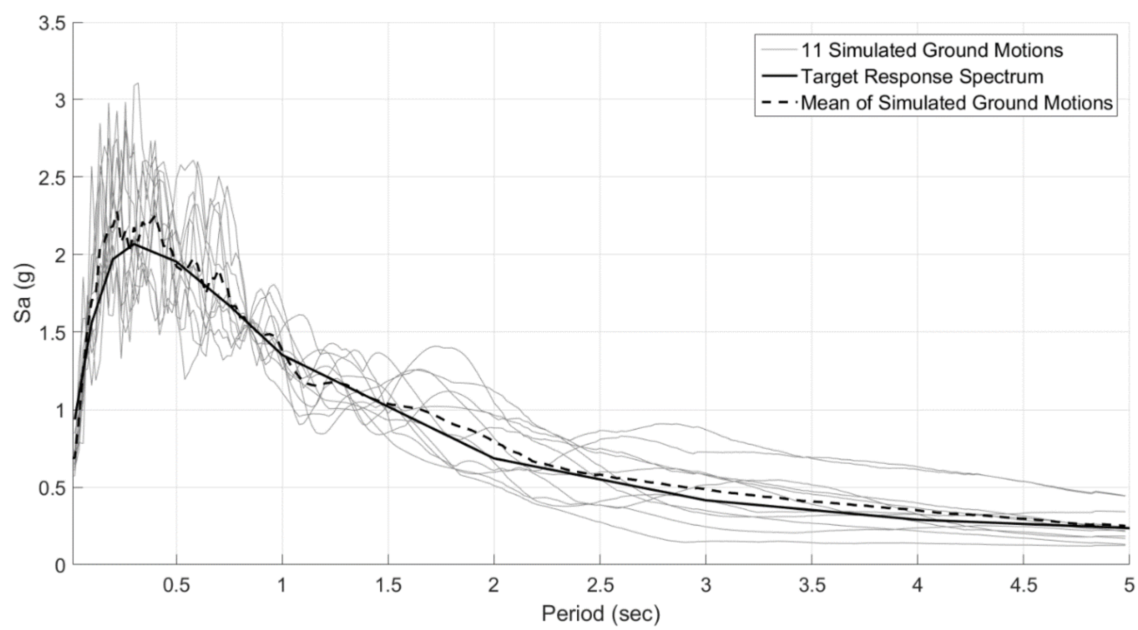

Figure 6.7 – Response spectra of eleven selected ground motions and target response spectrum.

The 3-story steel frame is excited using the 11 selected ground motions. Reliability information is extracted with the novel reliability technique considering the RVs reported earlier in Table 5.4. Results are summarized in Table 6.2. In general, it can be noted that the structural reliability in terms of β and p_f is adequate. For all cases, p_f is smaller than 10% satisfying the main intent of the code. Hence, when there are not enough real records in the zone of interest, the BBP is a reliable computational tool for the proper simulation of them.

Table 6.2 – Structural reliability of 3-story frame using 11 simulated ground motions.

EQ	Station	Scale Factor	Overall Lateral Drift	Inter-Story Drift
			β	β
1	Stat. 15 - Hyp. 01 - NS	1.16	4.5801	4.0993
2	Stat. 15 - Hyp. 02 - NS	1.17	5.7207	4.3864
3	Stat. 16 - Hyp. 04 - EW	1.31	5.6494	4.8015
4	Stat. 09 - Hyp. 06 - NS	0.92	4.4624	3.9622
5	Stat. 13 - Hyp. 04 - EW	1.01	5.0137	4.2825
6	Stat. 10 - Hyp. 03 - EW	1.30	4.7445	4.7030
7	Stat. 04 - Hyp. 06 - EW	1.12	4.7523	4.9018
8	Stat. 08 - Hyp. 03 - EW	1.02	4.9477	4.2880
9	Stat. 14 - Hyp. 02 - NS	1.06	5.2112	4.3837
10	Stat. 15 - Hyp. 06 - NS	0.84	4.5904	4.0513
11	Stat. 02 - Hyp. 06 - EW	1.15	5.9262	5.3427
		β_μ	5.0544	4.4729
		(p_f)	(2.1587E-07)	(3.8583E-06)

6.5 Summary and Concluding Remarks

The BBP version v16.5.0 (SCEC, 2016) was validated. It was demonstrated to be a viable computational tool for the simulation of ground motions. Time histories of ground motions were simulated for the 1994 Northridge earthquake. Response spectra were compared for simulated and real versions. Since response spectra were found to be very similar, the accuracy of the simulations was validated. The application of the BBP was demonstrated by generating a set of ground motions representative of the seismic hazard of the Los Angeles area. A target response spectrum was calculated following the recommendations of the code (ASCE 7-10, 2010) and USGS (USGS, 2008). Based on the structure under consideration, target response spectrum, and the set of generated ground motions, eleven time histories were selected. A 3-story steel frame was subjected to the eleven selected ground motions and its corresponding reliability information was extracted. The results verify and demonstrate the potential of BBP for the generation of ground motions.

CHAPTER 7
SUMMARY, CONCLUSIONS, AND RECOMMENDATIONS

7.1 Summary

A Performance-Based Seismic Design (PBSD) procedure for steel structures is developed, documented, and showcased in this study. Several issues related to the reliability estimation of steel structures, considering the rigidity of partially and fully restrained beam-to-column connections, subjected to seismic loading are presented. To implement the PBSD concept, a novel reliability technique is proposed by integrating the finite element method, the first-order reliability method, the response surface method, and advanced factorial design concept producing compounding beneficial effects. To consider major sources of nonlinearity and rigidities of connections, structures are represented by finite elements. Steel structures are excited by seismic loading applied in time domain, as required for the most sophisticated analysis. In addition, major sources of uncertainty are incorporated in the algorithm. The accuracy and efficiency of the novel reliability technique are verified with the help of several informative examples.

The accuracy of the novel reliability technique is established by considering a 2-story steel frame, using three acceleration time histories recorded during the 1994 Northridge earthquake considering different connection conditions used before and after the 1994 Northridge earthquake. The results are successfully verified using the Monte Carlo Simulation (MCS) technique. The novel reliability technique is documented to be accurate and efficient. The behavior of post-Northridge design is demonstrated to be superior to that of the pre-Northridge design, as expected. The robustness and implementation potential of the PBSD approach are demonstrated with the help of 3-, 9- and 20-story steel frame buildings. These structures were designed by experts for the Los Angeles area after the 1994 Northridge earthquake satisfying the post-Northridge design requirements. The frames are excited by three sets of ground motions representing three performance levels: collapse prevention, life safety, and immediate occupancy. Reliabilities of steel frame structures for the overall lateral and inter-story drift are evaluated. The importance of appropriately modeling steel structures is demonstrated to estimate reliability with these examples. On an average basis, the reliabilities of these buildings were observed to be within acceptable levels for the three performance levels. The performance criteria suggested by the Federal Emergency Management Agency (FEMA) appear to be reasonable and expected to satisfy the intent of the PBSD concept. Multiple deterministic analyses considering major sources of nonlinearity and uncertainty are required to make a structure more damage-tolerant, as documented in this study. Post-Northridge design requirements increase the possibility to achieve more resilient and damage-tolerant steel structures.

To demonstrate the applicability of the novel reliability technique for simulated ground motions, the Broadband Platform (BBP) version v16.5.0 (SCEC, 2016) developed by the Southern California Earthquake Center (SCEC) is used in this study. In order to validate the simulation of ground motions, structural reliability information related to a 2-story frame is extracted using simulated and real versions of the 1994 Northridge earthquake. Once accuracy of the BBP is validated, a set of 192 ground motions is simulated for a specific site in the Los Angeles area, and 11 of them are selected based on a target response spectrum. Then, a 3-story steel frame is exited using the selected ground motions, and its corresponding reliability information is properly calculated.

Hence, the PBSD procedure using a novel reliability technique is appropriately documented and showcased for practicing engineers, working on structural steel design and construction for everyday use.

7.2 Conclusions

Based on the results obtained in this study, several observations and conclusions can be made.

1. The novel reliability approach is found to be very efficient and accurate in implementing PBSD. Structures are represented by finite elements and seismic loading is applied in time domain. Major sources of nonlinearity and uncertainty are incorporated in the formulation.
2. Referring to the results obtained in this dissertation, the applicability of the novel reliability technique for steel structures is demonstrated. The capabilities of the technique are expected to be acceptable to all concerned parties and can be used for routine applications.
3. Using the novel reliability technique, the structural risk can be obtained using hundreds instead of several thousands of deterministic analyses. This technique represents an alternative to MCS and the classical random vibration methods.
4. If connections in steel buildings are designed considering appropriate rigidities, it may produce more economical design. A type of post-Northridge PR connection considered in this study appears to have many desirable characteristics. It may make steel structures more seismic load-tolerant and economical.

5. The study confirms that designing structures using multiple time histories, as suggested in recent design guidelines, is a step in the right direction. Multiple deterministic analyses considering major sources of nonlinearity and uncertainty are required to make a structure more damage-tolerant.
6. The BBP version v16.5.0 (SCEC, 2016) is demonstrated to be a viable option for the proper simulation of ground motions. Its accuracy in terms of structural risk is demonstrated using the novel reliability technique and several steel structures.

7.3 Recommendations for Future Studies

To advance the state-of-the-art in PBSD further, the following topics are recommended to be addressed in future investigations.

1. The conclusions made for the implementation of the novel reliability technique in PBSD were based on the seismic performance of steel moment resisting frames. More research is required to demonstrate the applicability of the proposed approach for braced and other types of steel frames.
2. In the proposed PBSD algorithm, serviceability of steel structures in terms of overall lateral and inter-story drift were considered. Requirements for the strength limit states are yet to be developed. This area needs further attention in the near future.
3. Using the BBP algorithm, several ground motions were generated for a specific site in the Los Angeles area. However, to demonstrate a broader application of the BBP algorithm in generating ground motions, simulations in others earthquake prone regions in the United States are recommended.

REFERENCES

AISC (2011), “Steel Construction Manual”, American Institute of Steel Construction (AISC).

AISC 341-10 (2010), "Seismic Provisions for Structural Steel Buildings", American Institute of Steel Construction (AISC).

Ang, A. H. S., and Cornell, C. A. (1974), “Reliability bases of structural safety and design”, *Journal of the Structural Division*, **100**(9), 1755-1769.

ASCE/SEI 41-13 (2014), “Seismic Evaluation and Retrofit of Existing Buildings”, American Society of Civil Engineers (ASCE), Reston, VA, USA.

ASCE/SEI 7-10 (2010), “Minimum design loads for buildings and other structures”, American Society of Civil Engineers (ASCE), Reston, VA, USA.

Atkinson, G. M., Assatourians, K., Boore, D. M., Campbell, K., and Motazedian, D. (2009), “A guide to differences between stochastic point-source and stochastic finite-fault simulations”, *Bulletin of the Seismological Society of America*, **99**(6), 3192-3201.

Au, S. K., and Beck, J. L. (1999), “A new adaptive importance sampling scheme for reliability calculations”, *Structural Safety*, **21**(2), 135-158.

Au, S. K., and Beck, J. L. (2001), “First excursion probabilities for linear systems by very efficient importance sampling”, *Probabilistic Engineering Mechanics*, **16**(3), 193-207.

Azizsoltani, H., Gaxiola-Camacho, J. R., and Haldar, A. (2017), “Site-Specific Seismic Safety Assessment of Nonlinear Structural Systems”, *Earthquake Engineering & Structural Dynamics* (under review).

Baker, J. W. (2010), “Conditional mean spectrum: Tool for ground-motion selection”, *Journal of Structural Engineering*, **137**(3), 322-331.

Bathe, K. J. (1982), *Finite Element Procedures in Engineering Analysis*, Prentice-Hall, Englewood Cliffs, NJ, USA.

Bertero, R. D., and Bertero, V. V. (1999), “Redundancy in earthquake-resistant design”, *Journal of Structural Engineering*, **125**(1), 81-88.

Bommer, J. J., and Acevedo, A. B. (2004), “The use of real earthquake accelerograms as input to dynamic analysis”, *Journal of Earthquake Engineering*, **8**(spec01), 43-91.

Boore, D. M. (2009), “Comparing stochastic point-source and finite-source ground-motion simulations: SMSIM and EXSIM”, *Bulletin of the Seismological Society of America*, **99**(6), 3202-3216.

Box, G. E., Hunter, W. G., and Hunter, J. S. (1978), *Statistics for Experimenters: An Introduction to Design, Data Analysis, and Model Building*, Wiley, New York, NY, USA.

Brunesi, E., Nascimbene, R., and Rassati, G. A. (2014), "Response of partially-restrained bolted beam-to-column connections under cyclic loads", *Journal of Constructional Steel Research*, **97**, 24-38.

Brunesi, E., Nascimbene, R., and Rassati, G. A. (2015), "Seismic response of MRFs with partially-restrained bolted beam-to-column connections through FE analyses", *Journal of Constructional Steel Research*, **107**, 37-49.

Bucher, C. G., and Bourgund, U. (1990), "A fast and efficient response surface approach for structural reliability problems", *Structural safety*, **7**(1), 57-66.

Burks, L. S., Zimmerman, R. B., and Baker, J. W. (2015), "Evaluation of hybrid broadband ground motion simulations for response history analysis and design", *Earthquake Spectra*, **31**(3), 1691-1710.

Cacciola, P., and Deodatis, G. (2011), "A method for generating fully non-stationary and spectrum-compatible ground motion vector processes", *Soil Dynamics and Earthquake Engineering*, **31**(3), 351-360.

Cacciola, P., and Zentner, I. (2012), "Generation of response-spectrum-compatible artificial earthquake accelerograms with random joint time–frequency distributions", *Probabilistic Engineering Mechanics*, **28**, 52-58.

Chen, W. F., and Kishi, N. (1989), "Semirigid steel beam-to-column connections: Data base and modeling", *Journal of Structural Engineering*, **115**(1), 105-119.

Chen, W. F., and Kishi, N. (1989), "Semirigid steel beam-to-column connections: Data base and modeling", *Journal of Structural Engineering*, **115**(1), 105-119.

Chen, W. F., and Lui, E. M. (1987), "Effects of joint flexibility on the behavior of steel frames", *Computers & Structures*, **26**(5), 719-732.

Chen, X., and Lind, N. C. (1982), "Fast probability integration by three-parameter normal tail approximation", *Structural Safety*, **1**(4), 269-276.

Ching, J., Au, S. K., and Beck, J. L. (2005), "Reliability estimation for dynamical systems subject to stochastic excitation using subset simulation with splitting", *Computer Methods in Applied Mechanics and Engineering*, **194**(12), 1557-1579.

Clough, R. W., and Penzien, J. (1993), *Dynamics of Structures*, McGraw-Hill, New York, NY, USA.

Colson, A. (1991), "Theoretical modeling of semirigid connections behavior", *Journal of Constructional Steel Research*, **19**(3), 213-224.

Cornell, C. A. (1969), “A probability-based structural code”, *Journal of ACI*, **66**(12), 974-985.

Cornell, C. A., Jalayer, F., Hamburger, R. O., and Foutch, D. A. (2002), “Probabilistic basis for 2000 SAC federal emergency management agency steel moment frame guidelines”, *Journal of Structural Engineering*, **128**(4), 526-533.

Der Kiureghian, A., Haukaas, T., and Fujimura, K. (2006), “Structural reliability software at the University of California, Berkeley”, *Structural Safety*, **28**(1), 44-67.

Ellingwood, B. (1980), *Development of a Probability Based Load Criterion for American National Standard A58: Building Code Requirements for Minimum Design Loads in Buildings and Other Structures*, US Department of Commerce, National Bureau of Standards, Cambridge, MA, USA.

El-Salti, M. K. (1992), “Design of frames with partially restrained connections”, PhD Dissertation, Department of Civil Engineering and Engineering Mechanics, University of Arizona, Tucson, Arizona.

Elsati, M. K., and Richard, P. (1996), “Derived moment rotation curves for partially restrained connections”, *Structural Engineering Review*, **8**(2-3), 151-158.

Engelhardt, M. D., and Sabol, T. A. (1998), “Reinforcing of steel moment connections with cover plates: benefits and limitations”, *Engineering Structures*, **20**(4-6), 510-520.

Faravelli, L. (1989), “Response-surface approach for reliability analysis”, *Journal of Engineering Mechanics*, **115**(12), 2763-2781.

FEMA P-58 (2012), “Seismic Performance Assessment of Buildings”, Federal Emergency Management Agency (FEMA).

FEMA P-751 (2012), “NEHRP Recommended Seismic Provisions: Design Examples”, Federal Emergency Management Agency (FEMA).

FEMA-273 (1997), “NEHRP Guidelines for the Seismic Rehabilitation of Buildings”, Federal Emergency Management Agency (FEMA).

FEMA-350 (2000), “Recommended seismic design criteria for new steel moment-frame buildings”, Federal Emergency Management Agency (FEMA).

FEMA-351 (2000), “Recommended Seismic Evaluation and Upgrade Criteria for Existing Welded Steel Moment-Frame Buildings”, Federal Emergency Management Agency (FEMA).

FEMA-352 (2000), “Recommended Post-earthquake Evaluation and Repair Criteria for Welded Steel Moment-Frame Buildings”, Federal Emergency Management Agency (FEMA).

FEMA-353 (2000), "Recommended Specifications and Quality Assurance Guidelines for Steel Moment-Frame Construction for Seismic Applications", Federal Emergency Management Agency (FEMA).

FEMA-355C (2000), "State of the art report on systems performance of steel moment frames subject to earthquake ground shaking", Federal Emergency Management Agency (FEMA).

FEMA-355F (2000), "State of the art report on performance prediction and evaluation of steel moment-frame buildings", Federal Emergency Management Agency (FEMA).

Foutch, D. A., and Yun, S. Y. (2002), "Modeling of steel moment frames for seismic loads", *Journal of Constructional Steel Research*, **58**(5), 529-564.

Frye, M. J., and Morris, G. A. (1975), "Analysis of flexibly connected steel frames", *Canadian Journal of Civil Engineering*, **2**(3), 280-291.

Gao, L. (1994), "Stochastic finite element method for the reliability analysis of nonlinear frames with PR connections", PhD Dissertation, Department of Civil Engineering and Engineering Mechanics, University of Arizona, Tucson, Arizona.

Gao, L., and Haldar, A. (1995), "Safety evaluation of frames with PR connections", *Journal of Structural Engineering*, **121**(7), 1101-1109.

Gaxiola-Camacho, J. R., Azizsoltani, H., Villegas-Mercado, F. J., and Haldar, A. (2017a), "A novel reliability technique for implementation of Performance-Based Seismic Design of structures", *Engineering Structures*, **142**, 137-147.

Gaxiola-Camacho, J. R., Haldar, A., and Reyes-Salazar, A. (2015, November). Riesgo Sísmico de Estructuras de Acero: Una Nueva Metodología de Confiabilidad Estructural Basada en Desempeño. *In Proceedings of 20th National Mexican Conference on Earthquake Engineering, Acapulco, Mexico. Paper* (No. 078).

Gaxiola-Camacho, J. R., Haldar, A., Azizsoltani, H., Valenzuela-Beltran, F., and Reyes-Salazar, A. (2017b), "Performance Based Seismic Design of Steel Structures Using Rigidities of Connections", *Journal of Constructional Steel Research* (under review).

Gaxiola-Camacho, J. R., Haldar, A., Villegas-Mercado, F. J., and Reyes-Salazar, A. (2017c, January). Performance-Based Seismic Design Using an Integrated Structural Reliability Evaluation Approach. *In Proceedings of 16th World Conference on Earthquake Engineering, Santiago, Chile. Paper* (No. 4968).

Ghobarah, A. (2001), "Performance-based design in earthquake engineering: state of development", *Engineering structures,* **23**(8), 878-884.

Graves, R. W., and Pitarka, A. (2010), "Broadband ground-motion simulation using a hybrid approach", *Bulletin of the Seismological Society of America*, **100**(5A), 2095-2123.

Haldar, A., and Mahadevan, S. (2000a), *Probability, Reliability, and Statistical Methods in Engineering Design*, Wiley, New York, NY, USA.

Haldar, A., and Mahadevan, S. (2000b), *Reliability Assessment using Stochastic Finite Element Analysis*, Wiley, New York, NY, USA.

Haldar, A., and Nee, K. M. (1989), "Elasto-plastic large deformation analysis of PR steel frames for LRFD", *Computers & Structures*, **31**(5), 811-823.

Hamburger, R. O., and Hooper, J. D. (2011), "Performance-based seismic design", *Modern Steel Construction*, 51(4), 36-39.

Hamburger, R. O., Foutch, D. A., and Cornell, C. A. (2003), "Translating research to practice: FEMA/SAC performance-based design procedures", *Earthquake Spectra*, **19**(2), 255-267.

Hamburger, R. O., Krawinkler, H., Malley, J. O., and Adan Scott, M. (2009), "Seismic design of steel special moment frames", *NEHRP seismic design technical brief*, (2).

Hartzell, S., Harmsen, S., Frankel, A., and Larsen, S. (1999), "Calculation of broadband time histories of ground motion: Comparison of methods and validation using strong-ground motion from the 1994 Northridge earthquake", *Bulletin of the Seismological Society of America*, **89**(6), 1484-1504.

Hasofer, A. M., and Lind, N. C. (1974), "Exact and invariant second-moment code format", *Journal of the Engineering Mechanics Division*, **100**(1), 111-121.

Haukaas, T., and Der Kiureghian, A. (2005), "Parameter sensitivity and importance measures in nonlinear finite element reliability analysis", *Journal of Engineering Mechanics*, **131**(10), 1013-1026.

Haukaas, T., and Der Kiureghian, A. (2006), "Strategies for finding the design point in non-linear finite element reliability analysis", *Probabilistic Engineering Mechanics*, **21**(2), 133-147.

Hinton, E., and Owen, D. R. J. (1986), *Finite Elements in Plasticity: Theory and Practice*, Pineridge Press, Swansea, UK.

Huh, J. (1999), "Dynamic reliability analysis for nonlinear structures using stochastic finite element method", PhD Dissertation, Department of Civil Engineering and Engineering Mechanics, University of Arizona, Tucson, Arizona.

Huh, J., and Haldar, A. (2001), "Stochastic finite-element-based seismic risk of nonlinear structures", *Journal of Structural Engineering*, **127**(3), 323-329.

IBC (2012), "International Building Code", *International Code Council*, Washington DC, United States.

Jayaram, N., Lin, T., and Baker, J. W. (2011), "A computationally efficient ground-motion selection algorithm for matching a target response spectrum mean and variance", *Earthquake Spectra*, **27**(3), 797-815.

Jones, S. W., Kirby, P. A., and Nethercot, D. A. (1980), "Effect of semi-rigid connections on steel column strength", *Journal of Constructional Steel Research*, **1**(1), 38-46.

Kanegaonkar, H. B., Haldar, A., and Ramesh, C. K. (1986), "Fatigue analysis of offshore platforms with uncertainty in foundation conditions", *Structural Safety*, **3**(2), 117-134.

Khuri, A. I., and Cornell, J. A. (1996), *Response Surfaces: Designs and Analyses*, Marcel Dekker, New York, NY, USA.

Kim, J., and Kim, T. (2009), "Assessment of progressive collapse-resisting capacity of steel moment frames", *Journal of Constructional Steel Research*, **65**(1), 169-179.

Kim, S. H., and Na, S. W. (1997), "Response surface method using vector projected sampling points", *Structural Safety*, **19**(1), 3-19.

Kondoh, K., and Atluri, S. N. (1987), "Large-deformation, elasto-plastic analysis of frames under nonconservative loading, using explicitly derived tangent stiffnesses based on assumed stresses", *Computational Mechanics*, **2**(1), 1-25.

Koo, H., Der Kiureghian, A., and Fujimura, K. (2005), "Design-point excitation for non-linear random vibrations", *Probabilistic Engineering Mechanics*, **20**(2), 136-147.

LATBSDC (2011), "An Alternative Procedure for Seismic Analysis and Design of Tall Buildings Located In the Los Angeles Region", Los Angeles Tall Buildings Structural Design Council (LATBSDC).

Lee, S. Y. (2000), "Static and dynamic reliability analysis of frame and shear wall structural systems", PhD Dissertation, Department of Civil Engineering and Engineering Mechanics, University of Arizona, Tucson, Arizona.

Lee, S. Y., and Haldar, A. (2003), "Reliability of frame and shear wall structural systems. II: Dynamic loading", *Journal of Structural Engineering*, **129**(2), 233-240.

Lee, Y. J., and Moon, D. S. (2014), "A new methodology of the development of seismic fragility curves", *Smart Structures and Systems*, **14**(5), 847-867.

Leger, P., and Dussault, S. (1992), "Seismic-energy dissipation in MDOF structures", *Journal of Structural Engineering*, **118**(5), 1251-1269.

Lin, Y. K., and Cai, G. Q. (2004), "Probabilistic structural dynamics: advanced theory and applications", *Mcgraw-hill Professional Publishing*.

Lionberger, S. R., and Weaver, W. (1969), "Dynamic Response of Frames with Nonrigid Connectors", *Journal of the Engineering Mechanics Division*, **95**(1), 95-114.

Liu, P., Archuleta, R. J., and Hartzell, S. H. (2006), "Prediction of broadband ground-motion time histories: Hybrid low/high-frequency method with correlated random source parameters", *Bulletin of the Seismological Society of America*, **96**(6), 2118-2130.

Luco, N., and Cornell, C. A. (2000), "Effects of connection fractures on SMRF seismic drift demands", *Journal of Structural Engineering*, **126**(1), 127-136.

Mai, P. M., Imperatori, W., and Olsen, K. B. (2010), "Hybrid broadband ground-motion simulations: Combining long-period deterministic synthetics with high-frequency multiple S-to-S backscattering", *Bulletin of the Seismological Society of America*, **100**(5A), 2124-2142.

Mehrabian, A. (2002), "Seismic performance of steel frames with a post-Northridge connection", PhD Dissertation, Department of Civil Engineering and Engineering Mechanics, University of Arizona, Tucson, Arizona.

Mehrabian, A., Ali, T., and Haldar, A. (2009), "Nonlinear analysis of a steel frame", *Nonlinear Analysis: Theory, Methods & Applications*, **71**(12), e616-e623.

Mehrabian, A., Haldar, A., and Reyes-Salazar, A. (2005), "Seismic response analysis of steel frames with post-North ridge connection", *Steel and Composite Structures*, **5**(4), 271-287.

Mena, B., Mai, P. M., Olsen, K. B., Purvance, M. D., and Brune, J. N. (2010), "Hybrid broadband ground-motion simulation using scattering Green's functions: Application to large-magnitude events", *Bulletin of the Seismological Society of America*, **100**(5A), 2143-2162.

Motazedian, D., and Atkinson, G. M. (2005), "Stochastic finite-fault modeling based on a dynamic corner frequency", *Bulletin of the Seismological Society of America*, **95**(3), 995-1010.

Motazedian, D., and Atkinson, G. M. (2005), "Stochastic finite-fault modeling based on a dynamic corner frequency", *Bulletin of the Seismological Society of America*, **95**(3), 995-1010.

Neuenhofer, A., and Filippou, F. C. (1997), "Evaluation of nonlinear frame finite-element models", *Journal of Structural Engineering*, **123**(7), 958-966.

Nguyen, P. C., and Kim, S. E. (2015), "Second-order spread-of-plasticity approach for nonlinear time-history analysis of space semi-rigid steel frames", *Finite Elements in Analysis and Design*, **105**, 1-15.

Nowak, A. S., and Collins, K. R. (2012), *Reliability of Structures*, CRC Press, Boca Raton, FL, USA.

Pecce, M., and Rossi, F. (2015), "The experimental behavior and simple modeling of joints in composite MRFs", Engineering Structures, **105**, 249-263.

Pirmoz, A., and Liu, M. M. (2017), "Direct displacement-based seismic design of semi-rigid steel frames", *Journal of Constructional Steel Research*, **128**, 201-209.

Popov, E. P., Yang, T. S., and Chang, S. P. (1998), "Design of steel MRF connections before and after 1994 Northridge earthquake", *Engineering Structures*, **20**(12), 1030-1038.

Rackwitz, R., and Flessler, B. (1978), "Structural reliability under combined random load sequences", *Computers & Structures*, **9**(5), 489-494.

Rajashekhar, M. R., and Ellingwood, B. R. (1993), "A new look at the response surface approach for reliability analysis", *Structural Safety*, **12**(3), 205-220.

Razavi, M., and Abolmaali, A. (2014), "Earthquake resistance frames with combination of rigid and semi-rigid connections", *Journal of Constructional Steel Research*, **98**, 1-11.

Reyes-Salazar, A. (1997), "Inelastic seismic response and ductility evaluation of steel frames with fully, partially restrained and composite connections", PhD Dissertation, Department of Civil Engineering and Engineering Mechanics, University of Arizona, Tucson, Arizona.

Reyes-Salazar, A., and Haldar, A. (2000), "Dissipation of energy in steel frames with PR connections", *Structural Engineering and Mechanics*, **9**(3), 241-256.

Reyes-Salazar, A., and Haldar, A. (2001), "Energy dissipation at PR frames under seismic loading", *Journal of Structural Engineering*, **127**(5), 588-592.

Reyes-Salazar, A., López-Barraza, A., Rivera-Leyva, J.O., Ramírez-Ramírez, J.A., and Bojorquez, E. (2008), "Seismic behavior of perimeter moment resisting steel frames", *14th World Conference on Earthquake Engineering*, Beijing, China.

Richard, R. M., Allen, C. J., and Partridge, J. E. (1997), "Proprietary slotted beam connection designs", *Modern Steel Construction*, 28-33.

Roeder, C. W., and Foutch, D. A. (1996), "Experimental results for seismic resistant steel moment frame connections", *Journal of Structural Engineering*, **122**(6), 581-588.

SCEC (2016). Broadband Platform. Southern Califorinia Earthquake Center (SCEC). URL https://scec.usc.edu/scecpedia/Broadband_Platform.

Schmedes, J., Archuleta, R. J., and Lavallee, D. (2010), "Correlation of earthquake source parameters inferred from dynamic rupture simulations", *Journal of Geophysical Research: Solid Earth*, **115**(B3).

Schmedes, J., Archuleta, R. J., and Lavallee, D. (2013), "A kinematic rupture model generator incorporating spatial interdependency of earthquake source parameters", *Geophysical Journal International*, **192**(3), 1116-1131.

Shi, G., and Atluri, S. N. (1988), "Elasto-plastic large deformation analysis of space-frames: A plastic-hinge and stress-based explicit derivation of tangent stiffnesses", *International Journal for Numerical Methods in Engineering*, **26**(3), 589-615.

Shields, M. D. (2014), "Simulation of Spatially Correlated Nonstationary Response Spectrum–Compatible Ground Motion Time Histories", *Journal of Engineering Mechanics*, **141**(6), 04014161.

Shinozuka, M. (1983), "Basic analysis of structural safety", *Journal of Structural Engineering*, **109**(3), 721-740.

Shinozuka, M., and Deodatis, G. (1988), "Stochastic process models for earthquake ground motion", *Probabilistic Engineering Mechanics*, **3**(3), 114-123.

Somerville, P. G. (1997) "Development of Ground Motion Time Histories for Phase 2 of the FEMA/SAC Steel Project", SAC Joint Venture, Federal Emergency Management Agency (FEMA).

Suarez, L. E., and Montejo, L. A. (2005), "Generation of artificial earthquakes via the wavelet transform", *International Journal of Solids and Structures*, **42**(21), 5905-5919.

Tangaramvong, S., Tin-Loi, F., Yang, C., and Gao, W. (2016), "Interval analysis of nonlinear frames with uncertain connection properties", *International Journal of Non-Linear Mechanics*, **86**, 83-95.

TBI (2010), "Guidelines for performance-based seismic design of tall buildings", Pacific Earthquake Engineering Research Center, Tall Buildings Initiative (TBI).

USGS (2008). Interactive Deaggregations (beta). United States Geological Survey (USGS). URL https://earthquake.usgs.gov/hazards/interactive.

Villegas-Mercado, F. J., Azizsoltani, H., Gaxiola-Camacho, J. R., and A. Haldar (2017), "Seismic Reliability Evaluation of Structural Systems for Different Soil Conditions", *International Journal of Geotechnical Earthquake Engineering* (under review).

Walling, M., Silva, W., and Abrahamson, N. (2008), "Nonlinear site amplification factors for constraining the NGA models", *Earthquake Spectra*, **24**(1), 243-255.

Watson-Lamprey, J., and Abrahamson, N. (2006), "Selection of ground motion time series and limits on scaling", *Soil Dynamics and Earthquake Engineering*, **26**(5), 477-482.

Wells, D. L., and Coppersmith, K. J. (1994), "New empirical relationships among magnitude, rupture length, rupture width, rupture area, and surface displacement", *Bulletin of the seismological Society of America*, **84**(4), 974-1002.

Wen, Y. K. (2001), "Reliability and performance-based design", *Structural Safety*, **23**(4), 407-428.

Yamamoto, Y., and Baker, J. W. (2013), “Stochastic model for earthquake ground motion using wavelet packets”, *Bulletin of the Seismological Society of America*, **103**(6), 3044-3056.

Yun, S. Y., Hamburger, R. O., Cornell, C. A., and Foutch, D. A. (2002), “Seismic performance evaluation for steel moment frames”, *Journal of Structural Engineering*, **128**(4), 534-545.

Zeng, Y., Anderson, J. G., and Yu, G. (1994), “A composite source model for computing realistic synthetic strong ground motions”, *Geophysical Research Letters*, **21**(8), 725-728.

Zhou, Y. (1992), “Efficient stochastic finite element method for the reliability analysis of nonlinear frame structures”, PhD Dissertation, Department of Civil Engineering and Engineering Mechanics, University of Arizona, Tucson, Arizona.

Zimmerman, R. B., Baker, J. W., Hooper, J. D., Bono, S., Haselton, C. B., Engel, A., Hamburger, R. O., Celikbas, A., and Jalalian, A. (2015), “Response History Analysis for the Design of New Buildings in the NEHRP Provisions and ASCE/SEI 7 Standard: Part III-Example Applications Illustrating the Recommended Methodology”, *Earthquake Spectra* (In-Press).